Contributions to the Development of a Water-Based Neutrino Detector for the T2K Project

by

Hiroko Nakahara

A THESIS SUBMITTED IN PARTIAL FULFILMENT OF
THE REQUIREMENTS FOR THE DEGREE OF

Bachelor of Science

in

The Faculty of Science

(Physics and Astronomy)

The University Of British Columbia

April 20, 2006

© Hiroko Nakahara 2006

Abstract

This thesis project aims to contribute to the development of a water-based neutrino detector. The detector will be one of the crucial components used in the neutrino near detector for the upcoming T2K neutrino oscillation experiments in Japan. To study the performance of the water-based liquid scintillator detector a prototype cell prototype detector was built and tested at TRIUMF. The goal of this project is to maximize the light yield of the prototype detector and to ensure that the detector performance does not degrade with time. There were three major parts to this thesis work:

1. In the first part, the amount of primary and secondary fluor in the water-based liquid scintillator solution were optimized by varying the fluor concentrations and measuring the light outputs of the various solutions. The light output was found to be maximized using the original fluor concentrations in the commercial scintillator Quicksafe-A (QSA).

2. In the second part various biological inhibitors were added to the standard liquid scintillator cocktail to prevent biological growth in the solution which can degrade the detector performance. Of the commercial products tested the biological inhibitor Germall Plus was found to be most suitable because including it in the scintillation cocktail (0.5% by volume) did not change the cloud point temperature or light output of the solution. Zinc was also added to the cocktail to inhibit fungi growth. When include at a 3000 ppm by weight concentration using either of the compounds zinc sulphate or zinc acetate the light yield of the solution is found to drop by up to 10%. Biological growth in scintillator cocktails containing these biological inhibitors has so far not been observed.

3. In the final part of this thesis a protective coating of the reflective paint Eljen-520 is applied to the inner walls of the polypropylene prototype detector cell. This protective coating was deemed necessary because one of the ingredients of the liquid scintillator QSA chemically attacks the cell wall thereby reducing the lifetime of the detector. A custom airbrush based on the Bernoulli effect was designed and built to apply the protective coating to the long narrow detector cell. The coating was found to increase the light output of the prototype detector by 20%.

Hiroko Nakahara.
nakahara_hiroko@yahoo.com

Table of Contents

List of Tables

List of Figures

Acknowledgements

First and foremost, I owe my supervisor Dr. Stanley Yen a great deal of gratitude his help, kindness and especially extreme patience during this thesis work. I also appreciate his openness to receiving my suggestions regarding this project. I must also thank Dr. Yen for encouraging me to pursue physics in the future. I am also in debt to Dr. Scott Oser for supporting my situation as an international student and allowing me the opportunity to complete this work. Dr. Oser also provided me with an exciting project in his Particle Physics course which first sparked my interest in neutrino physics.

I have also benefitted from the patience of Marieke Navin from Sheffield University in the UK. Marieke's support by e-mail has been very much appreciated. I would like to thank Dr. Lee Thompson for his help during the fluor test measurements. I have Patrick Bonnick to thank for many useful tips regarding working at TRIUMF and starting this project.

I am grateful to Dr. Rob Kiefl for providing me with the opportunity to complete the thesis course and for listening to my presentations. I would also like to extend my appreciation to Dr. Janis McKenna for first advising me to enroll in the thesis course. I must thank Dr. Walter Hardy for generously allowing me to use his lab facility and equipment. My appreciation also goes to Jeff Mottershead for strongly encouraging me to take the thesis course.

I want to thank my friend Keiko Ojima for eating out with me and helping me relax and enjoy the wide variety of food available in Vancouver. I need to send thanks to Yuna, Rika, Hide, Kinneth, for discussions regarding course work and having fun with me at my hot pot parties. I also thank Nicholas Baal for a helpful discussion regarding the airbrush and for providing me with wonderful memories of life in Canada.

I have to thank Dr. Bates, Mr. Feldman, Mr. Joensen, Mr. Krauz, Dr. Perrott, Jakkie, Tamara, Philomena, Felicity, Tom, Linda for helping me start studying in Canada and their patience and friendliness while I learned English.

Furthermore, I would like to say thank to my all family. My host family, Mom, Dad, Grandma, Joella, Niana, Karindi , for helping me start life in Canada, taking care of me in Castlegar, and always being there for me. I need to thank my Mom for her love and the tremendous amount of support she has has offered, more than I could have expected. To my Grandma and Grandpa and my Auntie and Uncle and family in Kobe thanks for the continued support and providing a welcoming environment whenever I visit. I thank my Brother for helping me convince my family to let me studying in Canada and for sincere and honest discussions about my life in a manner that nobody else could. I am comforted by the cheerfulness and humor of my sister-in-law Misa. I am all the time touched by the heart-warming atmosphere of my Auntie and Uncle in Chiba. To my Dad, thank you for

constantly taking care of me even from across the Pacific Ocean. I can't say enough about your constant encouragement, and endless love.

Most importantly, I'm honoured to thank my husband, Jake Bobowski. Without his continuous support, understanding, patience,respectfulness, generosity, kindness, and love my project could not have completed. From the bottom of my heart, thank-you Jake, for your total support.

Chapter 1

Neutrinos and Neutrino Oscillations

In this chapter a brief introduction to neutrinos is given followed by an overview of the circumstances that led Pauli to postulate their existence. In §1.3 the neutrino mass is discussed and then the history of neutrino oscillations from its initial prediction to its experimental verification is summarized in §1.4. The final two sections of this chapter discuss the relevance of nonzero neutrino masses and then the phenomenon of neutrino oscillations is revisited and given a more formal treatment.

1.1 Neutrinos

Neutrinos, written ν, are fundamental particles that carry zero charge and interact with matter only through the short range ($\approx 10^{-17}$ m) weak force and have very small interaction cross-sections. Weak interactions are mediated by the exchange of massive (>80 GeV) W^+, W^-, and Z^0 bosons. The large masses of these exchange bosons are responsible for making the weak interaction so weak. In fact, the weak force is approximately 10^5 times weaker than the strong force and 10^3 times weaker than the electromagnetic force, while the gravitational force is about 34 orders of magnitude weaker than the weak force. Because the neutrino is so weakly interacting it is able to travel great distances through dense matter. The neutrino mass is extremely small; in fact, evidence that neutrinos have a finite mass at all has come only relatively recently [2] and the absolute mass of any one of the neutrino flavours is still unknown. Because the neutrino mass is so small and the gravitational force so weak gravity can be safely neglected when considering neutrino interactions. Neutrinos are leptons making up half of the six leptons (and anti-leptons) that are currently known to exist (see fig. 1.1). The six leptons are the electron (e), muon (μ), and tau (τ) particles and their associated neutrinos labeled ν_e, ν_μ, and ν_τ respectively. [4]

1.2 Discovery of the Electron Anti-Neutrino

In 1930, Wolfgang Pauli postulated the existence of a neutral particle that could explain the missing energy observed in nuclear beta decays. This neutral particle was later termed a neutrino (meaning little neutral one) by Enrico Fermi in 1933. An example of a beta minus decay is given below followed by an example of a beta plus decay:

$$^{137}_{55}\mathrm{Cs} \rightarrow {}^{137}_{56}\mathrm{Ba} + \mathrm{e}^- + x \tag{1.1}$$

$$^{22}_{11}\mathrm{Na} \rightarrow {}^{22}_{10}\mathrm{Ne} + \mathrm{e}^+ + y \tag{1.2}$$

The missing energy in the beta minus decay was supposed to be carried by a neutral particle x which was later identified as an electron anti-neutrino (written $\bar{\nu}_\mathrm{e}$). Neutrinos were first

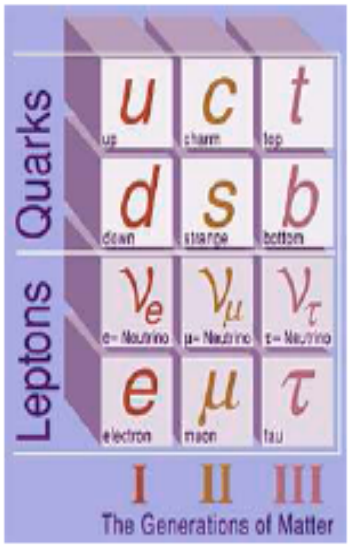

Figure 1.1: Table of the quark and lepton families. The three neutrino flavours (electron, muon, and tau) make up half of the lepton family.

observed by C.L. Cowan *et al.* in 1956. Cowan *et al.* used the Savannah River nuclear reactor as a source of anti-neutrinos to observe the inverse-beta decay: [5]

$$\bar{\nu}_{\mathrm{e}} + \mathrm{p} \rightarrow \mathrm{n} + \mathrm{e}^{+} \tag{1.3}$$

Pauli, Fermi, and F. Reines were all awarded Nobel Prizes in 1945, 1938, and 1995 respectively.

1.3 Neutrino Mass

Experimentally determining the mass of neutrinos is very difficult. Below we describe why neutrinos were initially thought to be massless and then describe a method that could in principle be used to determine the mass the electron neutrino, but in practice proves to be extremely challenging. In the next section the idea of neutrino oscillations is introduced and we see how these oscillations can be used to determine the mass difference between the neutrino flavours, but not the absolute mass of any one flavour.

From early studies of the β-decay it was known that certain radioactive atoms produced high-energy electrons (or positrons) during their decay process. If there were only 2 particles in the final state, then by conservation of energy and momentum the energy of the emitted electron is expected be fixed. Experimentally, however, the electron energy was seen to vary. These observations led Pauli to postulate the existence a third particle produced in the β-decay. This third particle was to share the energy emitted by the β-decay with the daughter nucleus and electron and was necessarily neutral by charge conservation. [1]

Because the daughter nucleus is heavy its recoil energy is almost zero and the remainder of the energy is shared between the electron and the neutrino. The way in which energy is distributed between these two particles varies. On rare occasions, nearly all the energy is

taken away by the electron, this is called the endpoint energy. At the endpoint, the electron has the maximum energy while the neutrino has the minimum energy. If the neutrino is massless the endpoint energy of the electron is nearly equal to the total energy produced in the β-decay, if however, the neutrino has finite mass the endpoint energy of the electron is limited to the energy released in the β-decay less the rest energy of the neutrino. [1]

Thus, the mass of the neutrino plays a role in determining the shape of the tail in the high energy very near the endpoint energy spectrum of the electron energy. For a massless neutrino the endpoint energy is higher and thus the tail of the spectrum extends further out, whereas a massive neutrino limits the maximum endpoint energy available to the electron. See Fig. 1.2. Determining the absolute electron neutrino mass in this way is difficult because

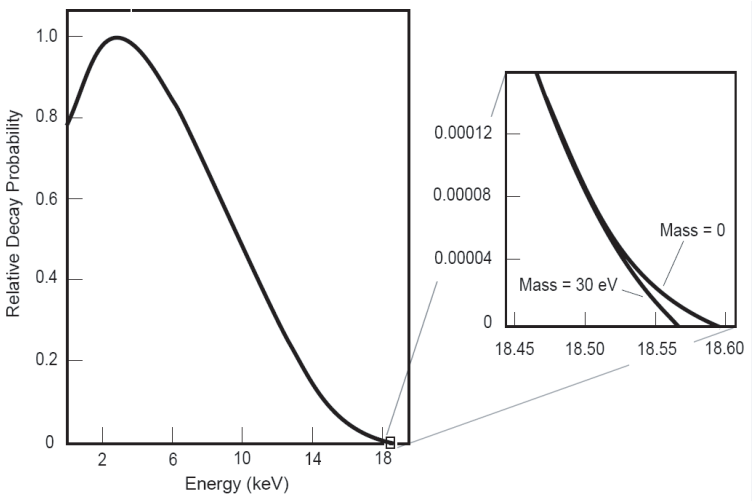

Figure 1.2: Energy spectrum of electrons emitted in β-decay. The expanded view at high energies near the endpoint energy highlights the influence of the neutrino mass in determining the shape of the spectrum at these energies. (Figure taken from reference [1])

the effect on the shape of the tail of the spectrum is very subtle requiring extreme resolution in the measurements.

In addition one needs a suitable β-decay to observe. One would like a decay that releases a small amount of energy and that has a short half-life. If the energy released is small then more decays are likely to occur near the endpoint energy where the shape of the spectrum is sensitive to the neutrino mass and a short half-life allows one to observe many decays. Experiments of this type have the further complication that one must be able to calculate the expected electron spectrum reliably in order to draw meaningful conclusions from the data. Researchers at Los Alamos favour the Tritium β-decay because it satisfies all the above criteria. The energy released is only 18.6 keV when it decays to ^{3}He, the lifetime is 12.4 years, and the molecular structure is relatively simple allowing for reliable calculations of the spectrum of the decay electron. As of this writing researches are actively trying to determine (or place upper limits) on the electron neutrino mass using these techniques[1]. [1, 4]

[1]The Katrin experiment in Germany is also studying tritium β-decay to try to measure the mass of the electron neutrino. [6]

1.4 Neutrino Oscillations

A shortcoming of the standard model of particle physics is that it does not predict whether or not neutrinos have mass. Until recently neutrinos were thought to be massless elementary particles. However, neutrino oscillation experiments have now revealed compelling evidence that suggests that neutrinos do have finite mass. [2]

Gell-Mann and Pais pointed out that the neutral kaon K^0 ($d\bar{s}$) can oscillate between its particle and antiparticle $\bar{K}^0$ ($s\bar{d}$) states. This oscillation occurs because the quark states with definite mass are a mixture of the weak states. In 1957 Pontecorvo applied this idea to neutrinos, that is neutrinos could oscillate between its particle and antiparticle states as they travel through space. Observation of these oscillations would require that neutrinos have finite mass and that the total lepton number is not conserved. If this were the case the neutrino would be a massive Majorana particle for which the particle and antiparticle states are not distinct. [2]

Around that same time Lee and Yang predicted that the parity is not conserved in the weak interaction. A key feature of their theory was that the left-handed neutrino was distinct from the right-handed antineutrino. Their prediction was promptly confirmed by Wu in the beta decay of Cobalt 60 and thus the idea of oscillations between neutrino and antineutrino states was never seriously considered. [2]

Pontecorvo's idea resurfaced in 1963 after Lederman, Steinberger, and Schwartz discovered the second type of neutrino, the muon neutrino ν_μ, which is distinct from the first type of neutrino, the electron neutrino ν_e. This time oscillations between these two neutrino families was thought to be possible provided the neutrinos families had nonzero and different masses. [2]

In 1969, the first experiment to measure ν_e's generated in the core of the sun recorded that the detected flux of ν_e's was much smaller than predicted by the standard solar model. This deficit of ν_e's was termed the "solar neutrino puzzle" and a possible explanation was that a fraction of the ν_e's were oscillating into another type of neutrino. Neutrino oscillations were proposed to explain neutrino deficits observed in other experiments, such as in atmospheric neutrino experiments. In 1998, Super Kamiokande revealed evidence for atmospheric neutrino oscillations and in 2001 SNO (Sudbury Neutrino Observatory) announced that they solved solar neutrino puzzle by observing neutrino oscillations. [2]

1.5 Implications of Neutrino Mass

If neutrinos have a small but nonzero mass there are significant consequences that must be considered in astrophysics, cosmology, and particle physics. Because neutrinos interact with matter so weakly[2] the neutrino density must be extremely high to have an impact, for example, in determining the dynamics of the universe. Physicists estimate that on average

[2] At 1 MeV neutrinos interact with matter 10^{20} times less frequently when compared to photons.

there are 300 neutrinos (100 of each family) per cubic centimeter in the universe. These neutrinos are relics of the Big Bang. [2]

The neutrino interaction cross-section is a strong function of temperature; when the universe was sufficiently hot processes involving the weak interaction were common, but as the universe expanded and cooled the cross-section for these interactions became increasingly small, effectively freezing the total number of neutrinos in the universe.

If a single neutrino has a mass on the order of a few electron volts, the total mass of all the neutrinos becomes a significant fraction of the mass of the universe. A contribution of this size to the mass of the universe , while not big enough to cause the universe to collapse back onto itself, can play an important role in determining the expansion of the universe and the formation of large scale structures like galaxies and clusters. [2]

A variety of neutrino oscillation collaborations have reported results giving experimental values for the mass difference between different families of neutrinos. Solar neutrino experiments at SNO reported that electron neutrinos oscillated to a different flavour with a mass difference of $\Delta m^2c^4 \approx 5 \times 10^{-5}$ eV^2.[3] Measurements of the neutrinos produced in the upper atmosphere by the Super-Kamiokande collaboration indicate that ν_μ's are oscillating into ν_τ's with a mass difference of $m^2c^4 \approx 3 \times 10^{-3}$ eV^2. The minimum neutrino masses consistent with these results are one type of neutrino with mass $mc^2 \approx 0.05$ eV, a second type of neutrino with mass $mc^2 \approx 0.007$ eV and the last type with mass $mc^2 << 0.007$ eV. If these estimates are accurate the total mass of all neutrinos accounts for only 0.5% of nonbaryonic dark matter believed to be present in the universe. If the dark matter in the universe is entirely composed of neutrinos then the absolute mass of neutrinos would have to be ≈ 4 eV. In this scenario the mass difference between the families of neutrinos would be very small compared to the absolute mass. [7]

There also exists the possibility that neutrino deficits measured in oscillation experiments are due to neutrinos oscillating not into one of the known lepton family neutrinos, but in to a new exotic neutrino termed the sterile neutrino. Sterile neutrinos are right-handed and their antiparticles are left-handed. In addition, if they exist, sterile neutrinos are even more weakly interacting than the lepton-type neutrinos and interact with matter only through the gravitational force. As of this writing there has been no compelling experimental evidence to suggest that these sterile neutrinos exist. [2]

Because neutrino oscillation experiments seem to confirm nonzero mass neutrinos, the description of neutrinos in the standard model needs to be modified. In standard model, all neutrinos are lefthanded and all antineutrinos are righthanded. Due to the existence of a nonzero neutrino mass, righthanded neutrinos and lefthanded antineutrinos also have to be included in the standard model.

Neutrino oscillations may offer some insight to more exotic questions. For example it is not currently understood why there is a difference between the mass states and weak states of neutrinos. Massive neutrinos that can oscillate between families may also contribute to the development of a complete grand unified theory (GUT) such as superstring theory. [2]

[3]Note that $\Delta m^2c^4 \equiv m_2^2c^4 - m_1^2c^4$, where m_1 and m_2 are the masses of two different flavours of neutrinos.

1.6 Neutrino Oscillation Theory

Neutrino oscillation is a process in which a neutrino can change from one flavour into another. This discussion will be limited to the case of mixing between two kinds of leptons. If mixing among all three lepton families is considered a mixing matrix analogous to the CKM mixing matrix for quarks would be needed. (CKM matrix is a mixing matrix between the mass states and quark weak states among the three quarks families. The first family is u and d, the second is c and s, and the third is t and b).

The neutrino mass eigenstates labeled ν_1 and ν_2 and the weak eigenstates labeled ν_e and ν_μ are used to describe two families of neutrinos (see Fig. 1.3). These sets of states are like the

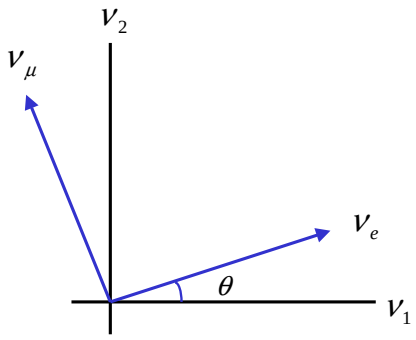

Figure 1.3: Neutrino mass states and neutrino weak states. In this figure the neutrino weak states ν_e and ν_μ are rotated by an angle θ with respect to the neutrino mass states ν_1 and ν_2.

two independent orthogonal sets of unit vectors in a plane that differ by the rotation angle θ, known as the mixing angle. A mixing matrix rotates the mass coordinates into the weak coordinates. [2] and the inverse of the mixing matrix takes the weak coordinates into the mass coordinates. A neutrino produced by the weak interaction such as in a muon decay is expressed by the linear superposition of the two mass states. It will be shown that the two mass states are constructively or destructively added as the neutrino passes through space. The interference allows the pure states (i.e. weak states) to appear and disappear with time and causes the neutrino oscillate between the two weak states as in Fig. 1.4. Moreover, if there is no mass difference in the two mass states the interference does not occur and there is no neutrino oscillation. [2, 8] Consider a muon neutrino that is described as a linear combination of two mass states $|\nu_1\rangle$ and $|\nu_2\rangle$ at $t = 0$:

$$|\nu_\mu\rangle = -|\nu_1\rangle \sin\theta + |\nu_2\rangle \cos\theta. \tag{1.4}$$

The relative phase shift at $t = 0$ is π. At a later time the two mass states evolve in time determined by their energies E_1 and E_2. The energy difference between E_1 and E_2 is caused by the mass difference of the two mass states $m_1 \neq m_2$. They make up a pure ν_μ every time the interference pattern of the two matter waves return to the initial state, that is, the relative phase shift moves ahead by 2π. Otherwise, the muon state becomes a mixture of ν_1 and ν_2. [8]

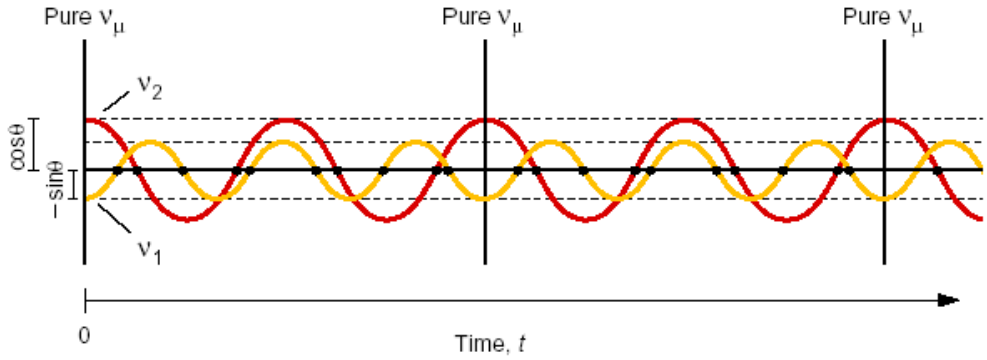

Figure 1.4: Cartoon diagram of neutrino oscillations. (Figure taken from reference [2]).

Neutrino weak states $|\nu_e\rangle$ and $|\nu_\mu\rangle$ are expressed as linear combinations of the neutrino mass states with mass eigenvalues m_1 and m_2. Quantum mechanically this linear combination, which is related to the mixing matrix with the mixing angle θ described above, is given by:

$$|\nu_e\rangle = \cos\theta|\nu_1\rangle + \sin\theta|\nu_2\rangle, \tag{1.5}$$
$$|\nu_\mu\rangle = -\sin\theta|\nu_1\rangle + \cos\theta|\nu_2\rangle. \tag{1.6}$$

The angle θ determines the amount of the mixing of the mass eigenstates in the weak states. If θ is close to 0, $\cos\theta \approx 1$ and ν_e is composed almost entirely of ν_1 while ν_μ is almost purely made of the m_2 state. When $\theta = \pi/4$ (so-called maximal mixing), $\cos\theta = \sin\theta = 1/\sqrt{2}$ and ν_1 and ν_2 are 180° out of phase and contribute equally to both ν_e and ν_μ. [8]

Putting the correct quantum mechanical time dependence for the $|\nu_\mu(t)\rangle$ state gives:

$$|\nu_\mu(t)\rangle = -\mathrm{e}^{-iE_1 t}\sin\theta|\nu_1\rangle + \mathrm{e}^{-iE_2 t}\cos\theta|\nu_2\rangle, \tag{1.7}$$

where t is time and E_1 and E_2 are the energies of mass eigenstates $|\nu_1\rangle$ and $|\nu_2\rangle$ respectively and $\hbar$ has been set to one (the speed of light c will also be set to one). Neutrinos are highly relativistic so that $E, p \gg m$ and hence:

$$E_k = \sqrt{p^2 + m_k^2} \approx p + \frac{m_k^2}{2p}, \tag{1.8}$$

where p is the neutrino momentum, and the index $k = 1, 2$ (note that the two mass eigenstates are assumed to have the same momentum p). Substituting this result in to eq. 1.7 and simplifying leads to:

$$|\nu_\mu(t)\rangle = -\mathrm{e}^{-i\left(p+\frac{m_1^2}{2E_\nu}\right)t}\sin\theta|\nu_1\rangle + \mathrm{e}^{-i\left(p+\frac{m_2^2}{2E_\nu}\right)t}\cos\theta|\nu_2\rangle, \tag{1.9}$$
$$= \mathrm{e}^{-i\left(p+\frac{m_1^2}{2E_\nu}\right)t}\left[-\sin\theta|\nu_1\rangle + \mathrm{e}^{i\frac{\Delta m^2}{2E_\nu}t}\cos\theta|\nu_2\rangle\right], \tag{1.10}$$

where $E_1 \approx E_2 \approx p \equiv E_\nu$ and $\Delta m^2 \equiv m_2^2 - m_1^2$. Neutrinos travel at approximately the speed of light and with $c = 1$, t can simply be replaced by L the distance traveled by the neutrino. Then, starting with a muon neutrino at $t = 0$, probability of observing an electron

neutrino at distance L is given by $|\langle\nu_e|\nu_\mu(t)\rangle|^2$, and hence after some simple rearrangement and application of trigonometric identities:

$$P(\nu_\mu \to \nu_e) = \sin^2 2\theta \sin^2\left(\frac{1.27\Delta m^2(\text{eV})L(\text{km})}{E_\nu(\text{GeV})}\right), \quad (1.11)$$

$$= \sin^2 2\theta \sin^2\left(\frac{\pi L}{\lambda_{osc}}\right), \quad (1.12)$$

where the factor of 1.27 arises due to the choices of units made above and λ_{osc} is an oscillation length defined by $\lambda_{osc} = \pi E_\nu / 1.27\Delta m^2$. The probability that muon neutrino produced at t = 0 will remain a muon neutrino as time passes decreases from 1 to a minimum of $1 - \sin^2\theta$ and then returns to 1 with period given by $2\lambda_{osc}$ which is inversely proportional to Δm^2 (see fig 1.5). [2, 9] Thus the amplitude of the oscillation given by $\sin^2(2\theta)$ is a

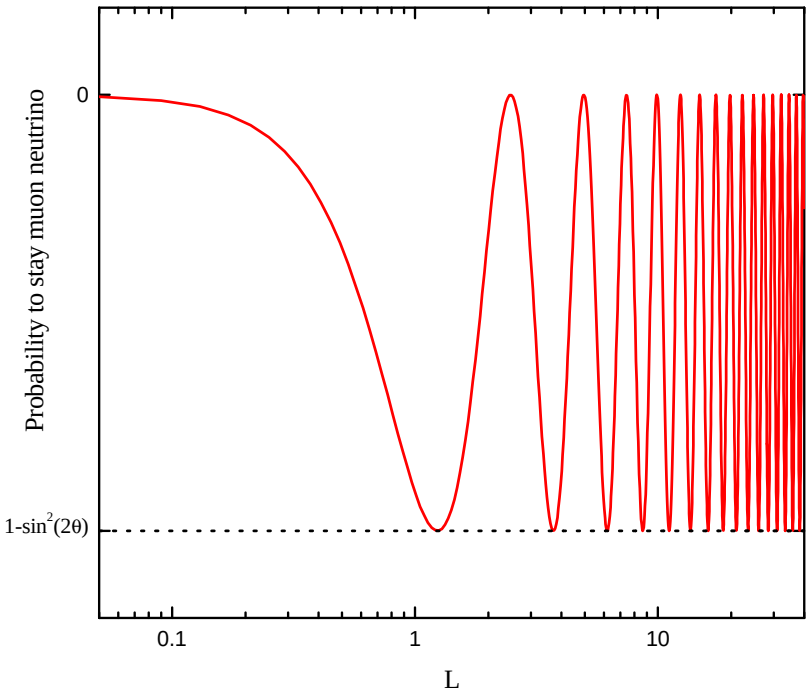

Figure 1.5: Probability that a muon neutrino created at $t = 0 (L = 0)$ remains a muon neutrino as a function of time (or flight distance L).

measure of the mixing angle θ and the oscillation length is a measure of Δm^2.

Chapter 2

Super-Kamiokande, T2K, and the Near Detector

The aim of this chapter is to discuss the neutrino detector Super-Kamiokande (SK) in Japan and the Tokai-to-Kamioka (T2K) neutrino oscillation experiments planned to start in 2009. The T2K experiments will compare neutrino events at a near detector in Tokai to events at the far detector SK. The near detector is discussed in some detail in §2.3. One component of the near detector is a water-based fine grain detector (FGD). This thesis focuses on improving the performance of the FGD detector in three separate ways. These possible improvements are introduced in the final section of this chapter.

2.1 Super-Kamiokande

The SK neutrino detector is a large water Cherenkov detector located 1000 m underground at the Kamioka mine in the Japanese Alps. The detector is a stainless steel cylinder with dimensions of 41.4 m (height) x 39.3 m (diameter). The detector is filled with 50 ktons of ultra pure water and is lined with photomultiplier tubes (PMTs).

The detector is separated into two regions. First, the inner volume contains 32 ktons of water and is lined with 11,200 PMTs facing inward. The outer region is a two meter thick shell of water surrounding the inner region. There are 1800 PMTs facing outward from the inner surface of the outer region. Optically opaque sheets separate the two regions of the detector and the surfaces of the outer detector are coated with reflective white DuPont Tyvek material. [10] The SK detector is the successor to the Kamiokande detector and has ten times the volume and twice the PMT density. See Fig. 2.1. There are three main requirements for the Super-K detector:

- It must be big. The rate that neutrinos interact with nuclei in the water is very low. In fact the vast majority of the neutrinos will pass through the detector leaving behind no trace of their presence. Thus the larger the detector is the more events one will detect.
- The detector should be deep underground to limit the number of cosmic ray muons which cause undesirable signals from impinging on the detector.
- The water should be ultra-pure to eliminate radioactive sources from the water which produce an excess of charged particles that also contribute to undesirable signals.

The SK detector can reconstruct the energy, starting position, and direction of charged particles passing through the detector by using the PMTs to measure the Cherenkov light produced by the charged particles. The outer layer of the detector is used as a filter to

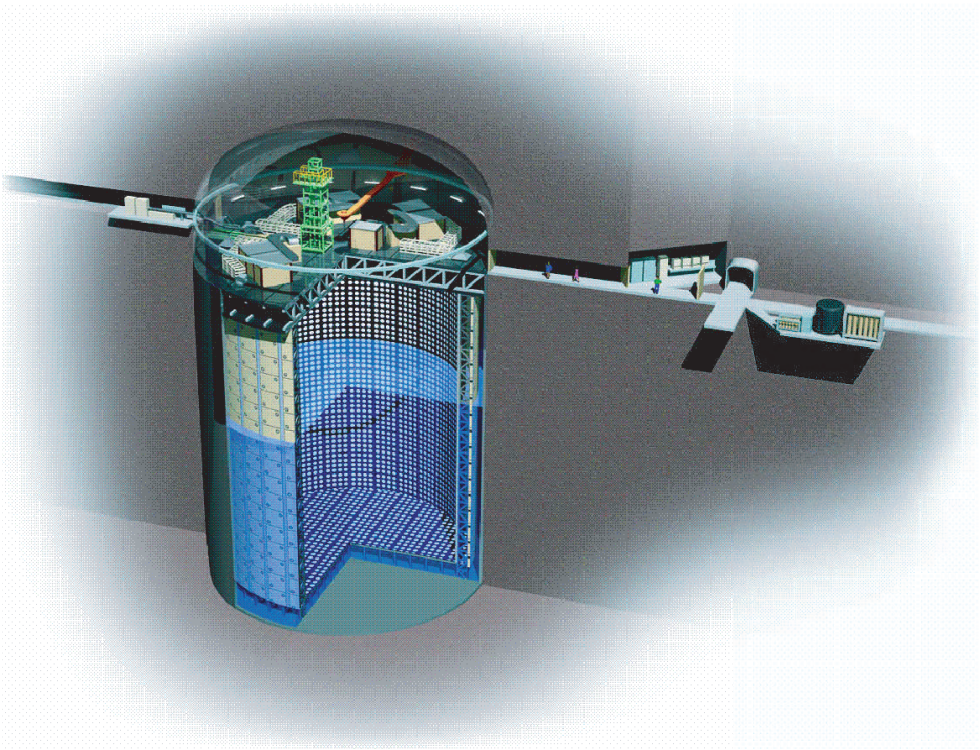

Figure 2.1: The Super-Kamiokande neutrino detector.

remove spurious signals. When a neutrino enters the detector and interacts with a nucleus in the water a charged lepton is produced. This charged lepton then produces Cherenkov light that originates from within detector. Conversely if a charged particle from a cosmic ray (muon) or from reactions within the surrounding rock enter the detector the resulting Cherenkov light will first appear at the outside surface of the outer layer of the detector. Thus the outward facing PMTs will detect these events and can be used to substantially reduce the contamination of these incoming charged particles. In fact only events that originate greater than 2 m from the surface of the inner detector wall are accepted making the effective target volume 22.5 ktons. [11, 12]

2.1.1 How Super-Kamiokande Detects Neutrinos

Because neutrinos are neutral weakly interacting particles detecting them is extremely challenging. Neutrinos cannot be detected directly; one must detect secondary particles generated in neutrino interactions. For example, in the experiment that first discovered neutrinos Cowan et al. detected positrons produced when neutrinos interacted with the protons in their detector. Similarly, secondary particles are used to detect neutrinos in the Super-K detector. The detector is a large tank of water and the neutrinos entering the SK water tank interact with the nuclei in the water via the process: [5, 13]

$$\nu + N \rightarrow l + X, \tag{2.1}$$

where N is some nucleus present in the water tank, l is a produced lepton, and X is a new nucleus different from N. The charged leptons are detected and from this information neutrino events are deduced.

If the neutrino that causes the interaction is an electron neutrino (antineutrino) the lepton produced is an electron (positron) and if the neutrino is a muon neutrino (antineutrino) the lepton is a muon (anti-muon). Tau leptons are not produced because the energies of atmospheric neutrinos are insufficient to produce these massive particles.

In their 1998 publication the SK collaboration concluded that their data was consistent with atmospheric ν_μ's oscillating to ν_τ's. The SK data were shown in three distinct ways all giving strong evidence that neutrino oscillations have been observed. First the ratio of e-like to μ-like events were compared to simulated data. This comparison showed that the SK data were better represented by models that included oscillations. Second was the asymmetry of the number of upward going neutrinos versus the number of downward going events was measured as a function of energy. Upward going atmospheric neutrinos necessarily pass through the earth and hence travel much farther en route to the SK detector than downward going atmospheric neutrinos and therefore are more likely to have changed flavour. This asymmetry was observed for muon neutrinos but not electron neutrinos. Finally, the zenith angle dependence of the number of electron and muon neutrinos was measured. Again the data were best fit using models that include oscillations. [13]

2.2 The T2K Project

Pioneering experiments like SK [13] and SNO [14] used naturally occurring neutrinos as a source. The energy and direction of these neutrinos cannot be controlled. To produce the most accurate data one wants a tunable neutrino source with high statistics (lots of events).

Aiming for the more accurate measurement of neutrino behavior the K2K project arose in 1999. The K2K (KEK to Kamiokande) was the first long base-line neutrino oscillation experiment that reproduces the neutrino deficit by using a manmade neutrino beam generated from the 12 GeV proton synchrotron at KEK (High Energy Accelerator Research Organization) in Tsukuba prefecture. There are two detectors prepared for K2K; one is located at KEK to measure the muon neutrino flux produced by the KEK synchrotron. The other is the Super Kamiokande detector 295 kilometers away.

In 1995, a powerful proton synchrotron (50 GeV) was suggested to be used as a controllable source of neutrinos for measuring neutrino mixing angles and mass differences more accurately. This project has been named T2K. The T2K experiment will observe muon neutrinos oscillating to electron neutrinos. From these observations, the mixing angle θ_{13} and the mass difference $\Delta m^2 = m_3^2 - m_1^2$ will be determined. Also, by comparing neutrino oscillations to antineutrino oscillations T2K may also be able to test CP violation which could help explain why the universe seems to be dominated by matter rather than by an antimatter. [3]

A 50 GeV accelerator to be used as the neutrino source for T2K is now under construction at the JPARC laboratory in Tokai. The circular synchrotron is 1568 m in circumference,

accelerates proton energy up to 50 GeV, and will produce the world's highest beam power. The high intensity proton beam will be shot at carbon nuclei in a 0.9 m long graphite cylinder cooled by water or helium producing a shower of the π-mesons and kaons. This shower of particles is focused into a parallel beam by a magnetic device called a "horn". The negative π^--mesons are filtered out using the horn and the remaining positive π-mesons and kaons enter a 100 m long tunnel. The kaon reactions are less frequent and the beam is only 5-10% kaons. In the tunnel the positive π-mesons decay into the secondary particles such as muons and muon neutrinos:

$$\pi^+ \rightarrow \mu^+ + \nu_\mu. \tag{2.2}$$

A 4 m thick wall made of graphite and copper will filter out the muons and the ν_μ's will pass through. The beam will also have a small component of ν_e's produced by kaon decays. In this way, the most intense neutrino beam in the world will be produced before reaching a near detector 280 m away. At this near detector, the position and energy of muon neutrinos are determined as well as the composition of the neutrino beam. The neutrino beam then travels 295 km before reaching the SK detector. Here an excess of electron neutrinos and a deficit of muon neutrinos will be observed and studied in great detail. [3]

2.3 The Near Detector

A near detector (diameter 17.5 m) will be located 280 m from the graphite target. The performance goal of the near detector is to predict neutrino events at the far detector 295 km away. This task requires the near detector to identify the beam's neutrino energy flux, energy spectrum, flavor content, and cross section before it reaches the far detector. The are several different types of events in the near detector that allow the neutrino beam to be characterized. [3]

Charged Current Quasi Elastic (CCQE) Events

In this type of event the neutrino energy flux, energy spectrum, and flavour content will be measured. The most likely type of neutrino interaction at T2K is categorized as this type of event:

$$\nu + n \rightarrow l + p. \tag{2.3}$$

For this process the neutrino's energy can be calculated from the lepton's energy and direction. [3]

Charged Current Pion Production (CC-1π) Events

These events proceed as follows:

$$\nu_l + N \rightarrow l + N' + \pi. \tag{2.4}$$

At SK only the final charged lepton is observed because the π is below the Cerenkov threshold. As a result these events are not distinguished from CCQE events. The near detector being a scintillator, can detect both the lepton and the pion, and can thus distinguish these events and allow for an improved determination of the neutrino beam energy spectrum and improved predictions of the neutrino event distribution at SK. [3]

Neutral Current Pion Production

In this case the interaction is given by:

$$\nu_l + N \rightarrow \nu_l + N + \pi^0. \tag{2.5}$$

The gamma ray produced from the neutral pion decay is the only observable in this process. These events provide a background signal at SK because e^- and e^+ produced by gamma rays from neutral pion decay can be falsely identified as electrons made by ν_e's interacting with the water. The near detector will determine the cross section of these events. [3]

Antineutrino contamination in the beam can be determined at the near detector by looking for opposite sign leptons.

Fig. 2.2 shows a cutaway view of the near detector highlighting the various components. The detector is surrounded by a 0.2 T magnet used to measure the momenta of the charged

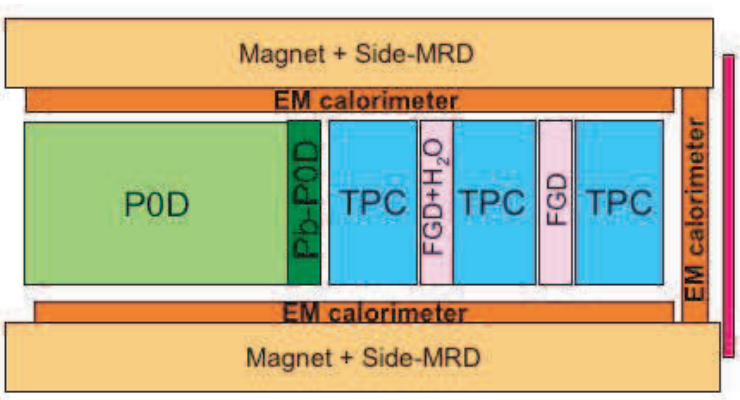

Figure 2.2: Schematic drawing of the near detector design. (Figure taken from reference [3]).

particles produced in the detector. When neutrinos first enter the near detector they encounter the Pi-Zero Detector (P0D). The details of the detector are not given here, we only mention that gamma-rays produced by π^0 decays are converted to charged particles and tracked. After traversing the P0D detector neutrinos enter the tracker which is designed to measure the momenta of electron and muon from the CCQE and CC-1π events. The tracker contains two important components: Time Projection Chambers (TPC) and Fine-Grained Detectors (FGD). [3]

Three TPCs measure the 3 components of muon momenta and provides the most accurate determination of the energy spectrum of the neutrinos. The TPC will also identify the type of charged particle produced (muon, electron, or pion) and the sign of its charge.

The FGDs are responsible for measuring the direction and the range of the recoil proton from the charged current (CC) neutrino interaction with nuclei and tagging CCQE and CC-non QE events. The FGD plays the role of a massive target in which neutrino interactions occur and TPC observe the events. There are two FGDs and each is located between two

TPCs. The first FGD is a plastic (i.e. carbon-based) scintillator and the second is a water-based scintillator. Having two FGD will allow experimenters to separate the cross sections of neutrino interactions with carbon and oxygen nuclei. The ability to separate these cross-sections is important because the far detector at SK is a water based detector. To reliably predict neutrino interaction rates at SK rates at the near detector must be measured using a water-based detector. In the next section the water-based FGD is discussed. [3]

2.4 The Fine-Grained Detector (FGD)

The water FGD will contain 30 (200 cm $\times$ 200 cm $\times$ 1 cm) sheets each with $\sim$ 200 extruded square tubes (1 cm $\times$ 1 cm). The sheets (known as Matraplast) are 1 cm thick boards made of polypropylene. Matraplast is an inexpensive commercially available material commonly used for signs at urban construction sites. The sheets will be glued in alternating x and y layers using Cemedine PM-200 epoxy resin. See Fig. 2.3. These $x-y$ layers provide

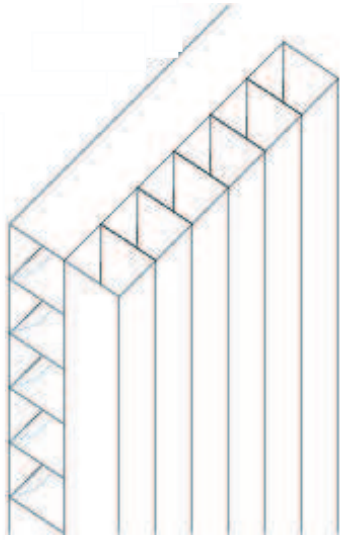

Figure 2.3: Schematic drawing of the $x-y$ assembly of two sheets of Matraplast.

mechanical stability and produce enough granularity to reconstruct the neutrino interaction vertex. The FGD is to measure the interaction vertex and record the final directions and momenta produced by all charged particles passing through the detector. [3]

Each of the detector cells is filled with a water-based scintillation cocktail and equipped with a Kuraray Y11 1.5 mm diameter wave-shifting fiber that runs along the center of the cell. When neutrinos enter the detector a small fraction of them interact with the oxygen nuclei in the water molecules. When a ν_μ interacts with a neutron in the oxygen nucleus a muon and proton are emitted:

$$\nu_\mu + n \rightarrow \mu^- + p. \tag{2.6}$$

Occasionally protons are reabsorbed in the nucleus and therefore go undetected. If the near detector is made of different nuclei than the far detector the amount of proton reabsorption will differ between the two detectors. To minimize the difference of proton absorption rate

between the near and far detector, a high content of water is used at the water-based near detector. [3]

2.5 Improvements and Development of the Water-Based FGD

To analyze the performance of the water based scintillator single cell prototype detectors (1 cm × 1 cm × 50 cm) are constructed and tested at the Tri-University Meson Facility (TRIUMF). TRIUMF supplies a 120 MeV/c mixed beam of pions, electrons and muons. When these charged particles enter the scintillation solution light is created. Because the particles have the same momentum but different masses they travel at different speeds. Their individual contribution to the light output can be easily separated by software cuts on the time of flight between two plastic scintillators placed on either side to the prototype detector, and separated by a distance 4.42 m.

2.5.1 The Prototype Detector

The prototype detector tube is filled with scintillation solution and sealed at both ends with feed-throughs for the fibre. The feed-through is sealed at the bottom using RTV silicone rubber. One end of the fiber has a reflective mylar mirror attached and the opposite end is connected to a photomultiplier tube (PMT). See Fig. 2.4. A crucial design criteria is to maximize the light output of these single cell detectors and to ensure that the performance does not degenerate with time. In Appendix A the various components of the prototype detector (scintillators, wavelength shifting fibres, ...) are discussed.

The current scintillation cocktail consists of 70% boiled distilled water, 25% Quicksafe A (QSA), and 5% TX-100 (percentages are by volume). QSA is a commercial liquid scintillator supplied by Zinsser Analytic, whose active ingredient is di-isopropylnaphthalene. Triton X-100 is a surfactant used to help dissolve the QSA in the water. High water content in the scintillator solution is required in FGD design as discussed above. Increasing the amount of water further has the undesirable effect of reducing the light output. At present, the amounts of the three ingredients given above is thought to be the best compromise between having a high water content and a high light output. The wave-shifting fibre serves two purposes. First once light enters the fibre it is guided to the PMT for detection to signify an event and second, the wavelength of the light entering the fibre is shifted to a wavelength for which the PMT detector is particularly sensitive thereby maximizing the light output. [3]

The purpose of my project is to optimize the prototype of a single detector cell by focusing on the three issues. First issue is regarding optimizing liquid scintillator. One of the ingredients of QSA contains a fluorescent material that absorbs the light produced by a charged particle passing through a scintillator and re-emits the light at the new wavelength which is sensitive to PMT that usually detects the light output. By changing the amount of the fluor in QSA, the liquid scintillator is optimized. The second issue in this project is biological growth in the scintillation solution. Mold or fungi will reduce the light output of the detector. This growth must be minimized if the detector is to perform reliably over long periods of time. We have to explore the use of biological inhibitors with the standard cocktail. Again the addition of these inhibitors must not significantly affect the light output

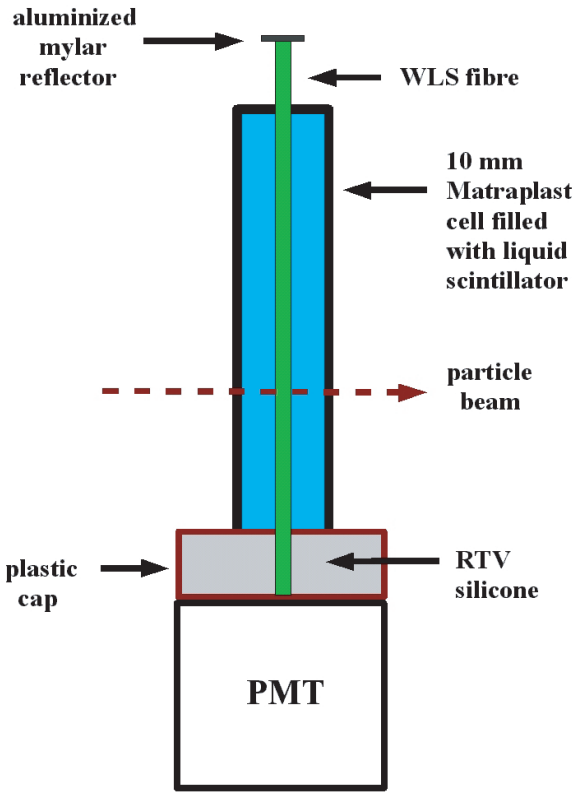

Figure 2.4: Schematic drawing of the single cell used to test the performance of the water-based FGD design. (Figure taken from reference [3]).

of the detector. The third issue with the water-based FGD is that the standard cocktail chemically attacks the cell walls of the detector. A yellow discolouring of the walls has been observed when the cocktail is left inside the cell for extended periods of time. A solution to this problem is to apply a protective coating to the inner walls of the cell. There is a commercially available reflective paint called Eljen-520 that resists chemical attack by the scintillation cocktail. A highly reflective coating has the additional advantage that the light output of the cell is maximized and "cross-talk" between adjacent cells will be minimized. Techniques to spray a uniform coating of this paint to the interior walls of the cells need to be developed. Finally a reliable way to analyze light output data is needed and this thesis project will devote significant time to developing a robust data fitting procedure.

Chapter 3

Experiment 1: Fluor Test

The aim of this experiment is to optimize the light output of the standard liquid scintillator cocktail to be used in the water-based neutrino near detector. This goal will be achieved by measuring the light output of cocktails that have varying amounts of the primary and secondary fluor in the commercially available liquid scintillator Quicksafe A (QSA), which is one component of the standard cocktail. Fluor is the ingredient that absorbs light emitted by a scintillating substance and then re-emits the light at a wavelength for which the detector (photomultiplier tube) is particularly sensitive.

3.1 Introduction

As mentioned above the T2K project will have two detectors: a far detector and a near detector. The purpose of the near detector is to measure the energy spectrum, angular spread, and flavour composition of the neutrino beam near the source and thereby predict neutrino events that will occur at the far detector 295 km away. The far detector is the water Cherenkov detector Super-Kamiokande (SK). Because the far detector is water based it is essential to have a water-based near detector to reliably predict neutrino interaction rates at SK. The near detector will have two components, a plastic scintillator and a water-based scintillator. With both these scintillators in place it will be possible for experimenters to separate the cross-sections of neutrino interactions with carbon nuclei (i.e. plastic scintillator) and oxygen nuclei (i.e. water-based scintillator). The ability to make this separation is important because SK is water based and will experience only neutrino-oxygen interactions.

Thus, it is important to develop a water-based liquid scintillator with the highest possible water content. The standard cocktail used in these tests are solutions of boiled distilled water, Quicksafe A (QSA), and Triton X-100 mixed in the ratios 70:25:5 by percent volume. QSA is a commercially available liquid scintillator supplied by Zinsser Analytic [15] and Triton X-100 is a surfactant (ethoxylated octylphenol) used to help QSA dissolve in the water. The 70:25:5 recipe given above has previously been optimized to yield a large light output while maintaining a high water concentration.

QSA has many advantages: it is inexpensive, has a flash point (temperature at which the substance's surface become ignitable) over 150°C, does not contain hazardous materials or fumes, and it is biologically degradable. [15] QSA uses Di-isopropyl naphthalane as its primary scintillator. A scintillator absorbs incident radiation and releases the energy gained in the form of light of a particular wavelength. QSA also contains a surfactant to help mix the solvents giving a uniform solution. Mineral oil is used to increase the volume of QSA. Finally, QSA has fluorescent material, called fluor. Fluor is a material that absorbs light at a certain wavelength and re-emits the light at a different wavelength that is generally sensitive to a photomultiplier tube (PMT). In QSA, the active scintillator emits light as

radiation penetrates the solution and the wavelength of the emitted light is shifted by the fluor material. QSA contains two fluorescent ingredients: a primary fluor and a secondary fluor. The primary fluor shifts the wavelength of the light emitted by the scintillator and the secondary flour shifts the wavelength of the light emitted by the primary fluor to a wavelength appropriate for the PMT. A summary of the QSA content is given below (percentages are given by volume). [16]

QSA:

- 47% Di-isopropyl naphthalane (DIN), (Primary scintillator)
- 43% Surfactant (ethoxylated nonylphenol)
- 8% Mineral Oil
- 1% Primary Fluor (PPO)
- 0.1% Secondary Fluor (bis-MSB)

In this report the amount of flour in the 70:25:5 standard cocktail will be varied and the optimum flour concentrations determined by finding that which maximizes the light output of the scintillating cocktail.

3.2 Apparatus/Set up

The apparatus used in this report are the following:

- Photomultiplier tube (PMT)——Photonis XP2262, 2-inch diameter PMT "Jenna" + Base "Jenna"
  High voltage used for PMT was -2180 V and attenuator was set to × 0.7
- MIDAS data acquisition software
- Particle beam (electrons, muons, and pions) of momentum 120 MeV/C
- Prototype detector cell
  - 1.5 mm diameter wavelength shifting fiber with aluminized mylar reflector
  - 50 cm long painted Matraplast cell, inside dimension 8.5 mm×8.5 mm
- Standard liquid scintillator cocktail
  - 70% by volume Boiled distilled water
  - 25% Quicksafe A
  - 5% Triton X-110

- Standard liquid scintillator cocktail made with QSA without fluor (prepared by the team at Sheffield University)

In these tests a PMT was used to detect the scintillation light collected by the wavelength shifting (WLS) fibre (refer to the figure 2.4). Mineral oil was used to improve the optical coupling between the WLS fiber and the PMT. After each measurement it was important to make sure that the mineral oil is filled high enough to make good optical contact between WLS fiber and PMT. The MIDAS data acquisition system was used for processing and recording signals from the PMT.

The prototype detector used in this measurement was assembled by Patrick Bonnick (a previous co-op student). For the procedure for building the detector refer to Patrick's report. A single cell detector consists of a single tube and WLS fiber with aluminized mylar reflector adhered to one end of the fiber. The single cell is made of polypropylene and is cut from a sheet called Matraplast. This board is an inexpensive commercially available material commonly used for signs at urban construction sites. The interior of the detector tube was coated with a specialty Eljen EJ-520 reflective paint which resists chemical attack by QSA. The paint was applied by pulling a sponge soaked in the paint through the tube using a wire.[4] The detector cell is sealed with RTV silicone at the bottom and is threaded by a WLS fiber. The standard cocktail was made in the way describe below in §4.1.1. QSA without fluor was mixed from the raw ingredients and is called "home-made QSA".

3.3 Experiment Description

To measure the light output a computer data acquisition (DAQ) system controlled by MIDAS computer software is used. The DAQ uses a CAMAC system using several types of electronic modules. The light output measurement uses four main modules: fan-out, time to digital converter (TDC), discriminator, and analog to digital converter (ADC). The Fan-out copies and sends off signals when they come in. The TDC is like an electronic stop watch, that can tell the time interval between start and stop signals. The ADC integrates the total charge in the analog input signal pulse while the ADC gate signal is in the "ON" or "TRUE" state, and outputs the integrated charge as a digital value. The discriminator outputs a logic "TRUE" when its analog input exceeds a threshold value set by the user. The schematic of the experimental setup is shown in Fig. 3.1. [3, 17] The visual scalar shown in the diagram is simply and indicator that the particle beam is on. This device is essentially counting the number of coincidences.

There are two plastic scintillators (denoted $S1$ and $S2$) connected to discriminators that lead to an electronic component called a *coincidence unit*. If a charged particle passes through the first scintillator $S1$ with an energy above a certain threshold, the signal sent from $S1$ passes through the discriminator. Meanwhile, the charged particle moves on and enters the second scintillator $S2$. If the particle still maintains an energy above the threshold, then the signal from $S2$ can go through the second discriminator. The two signals sent from the discriminators go to the coincidence unit. When the two signals from $S1$ and $S2$ cause a

[4]Note that the more recent prototype detectors have the interior of the tube coated by a spraying a fine mist using a custom airbrush.

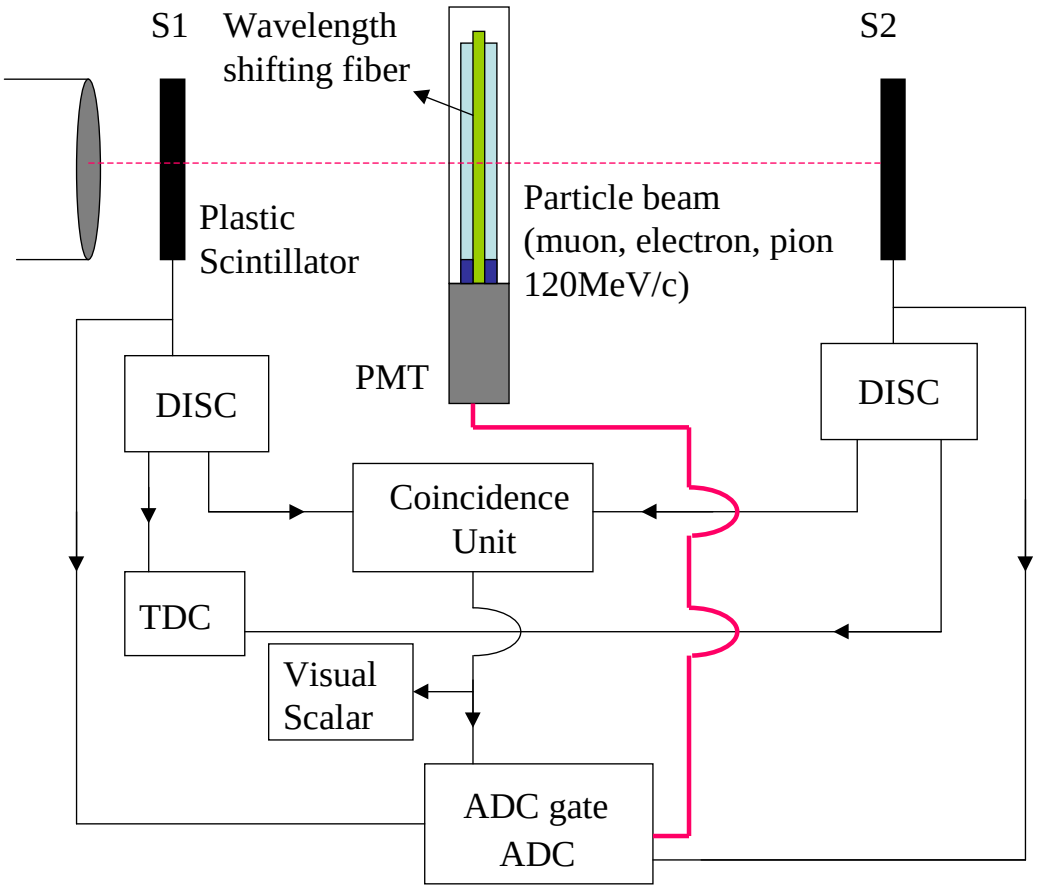

Figure 3.1: Schematic drawing of the data acquisition system using DAMAC to measure the light output of the liquid scintillator in the prototype detector placed in between two plastic scintillators $S1$ and $S2$. When high energy charged particles pass through $S1$ and $S2$ the discriminators allow the signals to pass through and go on to cause a "coincidence" in a coincidence unit. The coincidence unit will then open the ADC gate which will accept the analog signal to from the PMT detecting the light generated in the prototype detector.

so-called *coincidence* the coincidence unit opens the ADC gate for recording signals from the PMT which is coupled to the prototype detector's WLS fibre. If the beam does not reach $S2$ because of misalignment or energy loss in the beam, the coincidence unit obtains only one signal from $S1$ and does not open the ADC gate and signals from the PMT will not be recorded.

Generally each data set is shown as a histogram with three peaks: *pedestal peak*, *1 photo-electron peak*, and *centroid peak*. Note that the graph of each data set is a histogram (counts verses energy) not a graph of voltage verses time.

The first pedestal peak is produced by charged particles that hit the two trigger scintillators and cause a coincidence, but miss the detector. In this case the ADC gate is opened and noise from the PMT and electronics is recorded. If, on the other hand, the charged particles cause a coincidence and also pass through the detector, then the scintillation solution will

produce light that is collected by the WLS fibre and then detected by the PMT. These events contribute to third peak called the centroid peak. [3]

The source of the second peak (1 photoelectron peak) has not yet been clearly identified and needs to be further explored. One possible source that has been suggested is thermal noise in the PMT. There may be enough thermal energy in the PMT to free a photoelectron from its cathode thereby producing a spurious signal. Until recently Cherenkov light was thought to be a possible cause of the one photoelectron peak. Cherenkov radiation is observed when a charged particle travels through a medium faster than the speed of light. Charged particles can travel at super-luminous speeds in some media because the speed of light is reduced from its vacuum speed c according to $v = c/n$, where n is the index of refraction of the medium. For water $n = 1.33$ so the speed of light in water is $\approx 0.75c$. Because the liquid scintillator we have been using contains large amounts of water, Cherenkov radiation was considered as a possible cause of the one photoelectron peak. The one photoelectron peak, however, was still observed even for detectors that do not contain any liquid, therefore eliminating Cherenkov radiation from the liquid as a possible source. Cherenkov radiation caused by the particle directly hitting the fiber could be a cause.

The ADC integrates the area under the voltage verses time curve of the signal within the allowed time interval, called the gate. The integrated areas are sorted into bins and plotted as a histogram. The x-axis of histogram is energy of the signal (integrated area under the curve) and the y-axis is the number of times that an area between E and $E + \Delta E$ was found where ΔE defines the bin size of the histogram. [3]

The TRIUMF M11 beam used in this study is a mixture of three types of charged particles. The beam reaching the PMT consists of about 60% muons, 30% electrons, and 10% pions. The centroid peak is different for each of these particles. Each particle has a different rate of energy loss when passing through the scintillator which is inversely proportional to velocity of the particle:

$$\text{Rate of energy loss} = -\frac{\partial E}{\partial x} \propto \frac{z^2}{v^2}\rho, \tag{3.1}$$

where z = charge of the particle, v = velocity of the particle, and ρ = density of the scintillator. This is the Bethe-Bloch equation, whose derivation my be found in many nuclear physics books. So the total energy lost when passing a distance Δx through the scintillator is:

$$\text{Energy loss} = \Delta E = \frac{\partial E}{\partial x}\Delta x. \tag{3.2}$$

Thus slow particles lose more energy when passing through the scintillator and fast particles lose less energy. Because of the fixed momentum of the TRIUMF beam from the M11 channel, the heaviest particle (pion) is the slowest and the lightest particle (electron) is the fastest. Pions create largest the pulse (volts verses time) output from the PMT. In the histogram of ADC, the centroid peak of the pion has the largest x value the largest and the centroid from electron has the smallest value. [3]

It is necessary to identify the type of particle producing each detected event in order to quantify how much light output each particle of the beam produces under the particular condition. The TDC allows us to differentiate each signal as coming from either an electron, muon, or pion by recording the flight time of each particle between $S1$ and $S2$. The TDC

creates a histogram of the flight time of the particles and contains three peaks. Each peak in the histogram can be identified as electron, muon, or pion due to the difference in the flight time. The flight time between $S1$ and $S2$ can be deduced from the mass of the particles and the fixed momentum of the beam at M11[5]. Three peaks are observed; the first peak is due to electrons, the second peak muons, and the third peak pions. Fig. 3.2 shows a typical TDC histogram. This is the histogram from run #773 for the light output measurements in the biological inhibitor test of §4.2. The three peaks due to the three types a particles are clearly separated. [3] From the TDC data, the measured light output of the beam in ADC

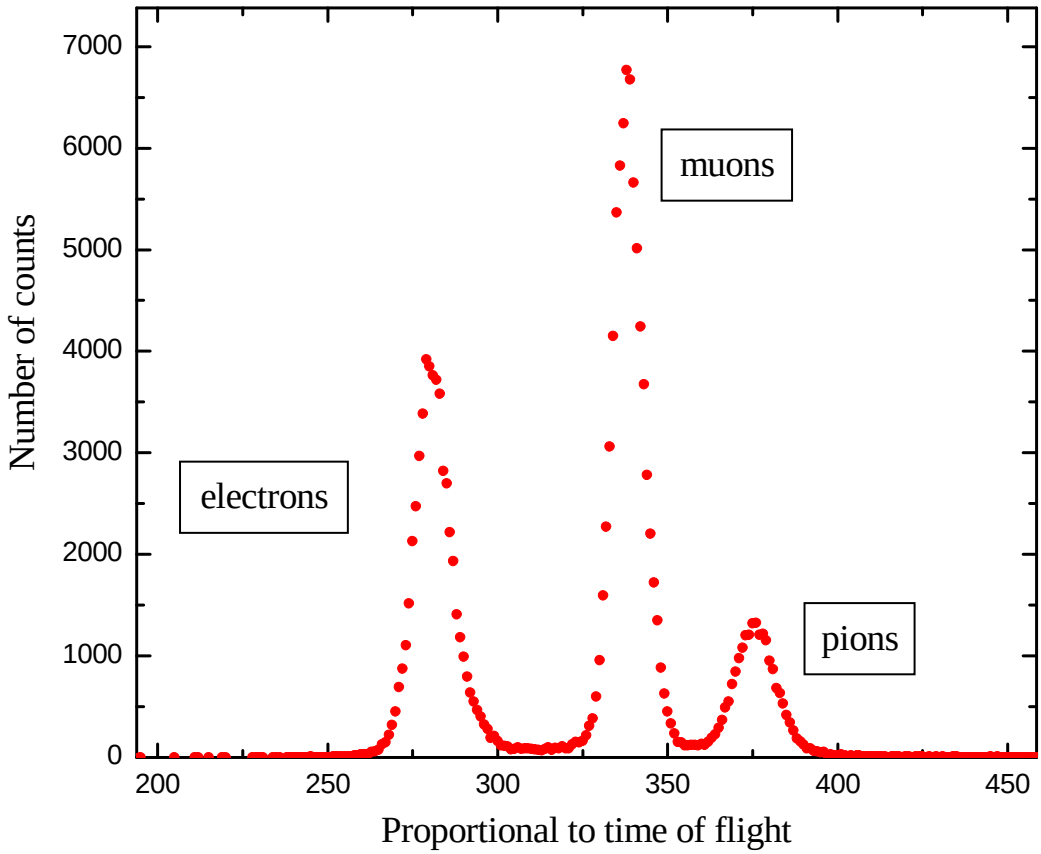

Figure 3.2: TDC histogram for 120 MeV/c. The first peak is due to electrons, the second peak muons, and the third peak pions.

is sorted into three separate data sets each corresponding to one of three particle types. Figure 3.3 shows a typical light output data set with a muon centroid peak. This data set is run #713 from the light output measurements discussed in §3.6. The error bars have been omitted from this figure for clarity, but as in all counting experiments each data point has an associated error equal to the square root of the number of counts.

[5]A beam momentum of 120 Mev/c was used for the measurements presented in this report.

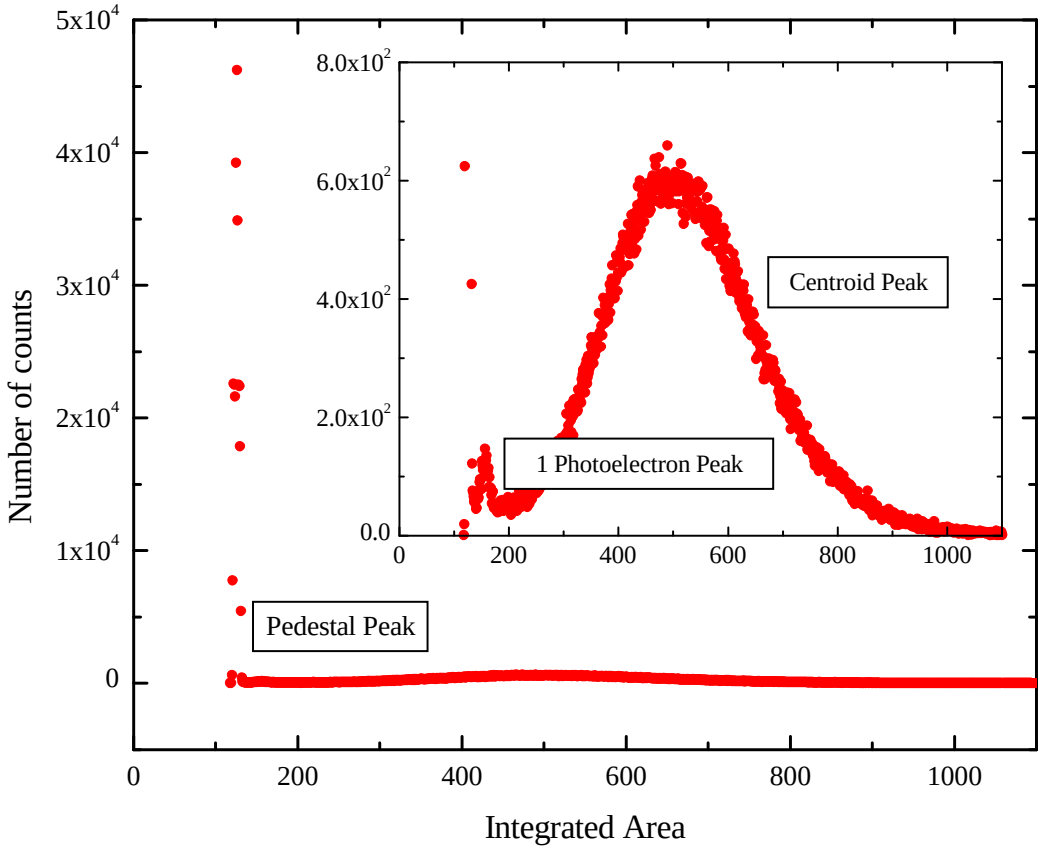

Figure 3.3: Typical ADC light output histogram. These data are from muon events. The inset displays the same data as in the main graph, the only difference is that the scale has been adjusted to emphasize the 1 photoelectron and muon centroid peaks.

3.4 Procedure

A standard cocktail with commercial QSA and a standard cocktail with home-made QSA (without primary and secondary fluors) were prepared using the standard 70:25:5 recipe. Mixing the two different standard cocktails can produce a cocktail containing different concentration of fluor in the QSA. The amount of fluor in the original QSA is defined to be 100% (100% is the maximum amount of fluor that can be made by mixing two different standard cocktails). If we measure the light output of cocktail made by mixing 50% of the cocktail made with commercial QSA and 50% of the cocktail made with home-made QSA, then that cocktail has, by definition 50% fluor. More than 100% fluor can be made by adding primary (PPO) and secondary fluor (bis-MSB) to a standard cocktail made with commercial QSA. In this way, we measured the light output of standard cocktails with a wide range of fluor concentrations.

Note that the procedure above changes the concentrations of both the primary and secondary fluors by equal amounts. The concentration of the secondary flour bis-MSB can be changed independently by adding bis-MSB to standard cocktail with the commercial QSA.

3.5 Data Analysis

A technique for fitting data sets of the kind shown in Fig. 3.3 has been developed and implemented using Mathematica 4.0. The strategy has been to fit each of the three peaks to a Gaussian line shape:

$$P(x) = \sqrt{\frac{2}{\pi}}\frac{A}{w}\exp\left[\frac{2(x-x_c)^2}{w^2}\right], \tag{3.3}$$

where A is the area under the curve, w describes the width, and x_c locates the centre of the distribution. A Gaussian distribution is generally applicable when each random measurement is independently performed. Gaussian distributions are applied to many experimental phenomena, however, for random processes that give discrete values, such as counting experiments when the average rate of arrival is constant, the resulting distribution is a Poisson distribution. Generally the beam test measurements performed in this report follow a Poisson distribution. Nevertheless, in the limit of large values of the centroid, the Poisson distributions is well approximated by a Gaussian. The Gaussian distribution fits the line shapes very well, is easy to use, and directly yields the centre position of the three distributions in Fig. 3.3 which are need to quantify the light output of each individual run (see below). [18, 19]

In the first attempt to analyze the data Mathematica was used to do a weighted fit of the data to a model that was simply a sum of three Gaussians:

$$model = \sqrt{\frac{2}{\pi}}\frac{A_1}{w_1}\exp\left[\frac{2(x-x_{c1})^2}{w_1^2}\right] + \sqrt{\frac{2}{\pi}}\frac{A_2}{w_2}\exp\left[\frac{2(x-x_{c2})^2}{w_2^2}\right] + \sqrt{\frac{2}{\pi}}\frac{A_3}{w_3}\exp\left[\frac{2(x-x_{c3})^2}{w_3^2}\right]. \tag{3.4}$$

Naively, this model is a good choice, however, as can be seen in Fig. 3.3, the first pedestal peak statistically dominates the other two peaks. This fitting routine would then preferentially do the best possible fit to the pedestal peak at the expense of the remaining two peaks. It is better to cut the data into three separate data sets and fit the peaks individually. The pedestal peak is easily separated because it is very sharp (narrow). Separating the 1 photoelectron peak from the centroid peak is less trivial and special care needs to be taken.

There is considerable overlap of the 1 photoelectron and centroid peaks and hence choosing a place to separate the data is difficult. Even after cutting the data the 1 photoelectron peak cannot be analyzed as a pure Gaussian because it is sitting on the tail of the centroid peak. The fitting procedure that has been adopted is the following:

1. Separate the pedestal peak and perform a single weighted Gaussian fit.

2. Separate the 1 photoelectron peak from the centroid peak and fit the centroid to a Gaussian.

3. Using the fit parameters obtained from the centroid peak subtract the tail of the centroid distribution from the 1 photoelectron peak. Be sure to take care of error propagation.

4. Now that we have a 1 photoelectron peak that is approximately a pure Gaussian do a weighted fit to a Gaussian distribution.

This procedure will yield three parameters (A, w, and x_c) with error estimates for all three peaks shown in Fig. 3.3. A print out of the Mathematica notebook used to analyze the data shown in Fig. 3.3 has been included in Appendix D.

After fitting the three peaks shown in Fig. 3.3 how can we use the fit parameters to extract the number of photoelectrons needed to produce the observed centroid peak? Suppose one muon passes through the detector and x photoelectrons are counted. If this experiment is repeated we will in general measure a different number of photoelectrons. Each measurement can be thought of as a point in a histogram. If the experiment is repeated many times on average we will measure $\bar{x}$ photoelectrons and the histogram will approach a continuous distribution. The resulting distribution is a Poisson distribution with mean $\mu = \bar{x}$ and standard deviation $\sigma = \sqrt{\bar{x}}$ [6]. For $\mu > 10$ the Poisson distribution is approximated extremely well by a Gaussian distribution with the same mean and standard deviation.

This Gaussian distribution, which we are using to approximate a Poisson distribution, will satisfy:

$$\frac{\sigma}{\mu} = \frac{1}{\sqrt{\bar{x}}}. \tag{3.5}$$

This equation provides us with a means for estimating the number of photoelectrons from the data like that shown in Fig. 3.3. We assume that the sharp pedestal peak which is due to noise in the PMT is low in energy compared to the energy of a photoelectron and hence define the position of the pedestal peak to be zero photoelectrons. Then setting μ to be the separation between the centres of the pedestal and centroid peaks and σ to be the width of the centroid peak Eq. 3.5 can be used to solve for the average number of photoelectrons needed to produce the centroid. Dividing μ by the number of photoelectrons and adding this to the position of the pedestal peak we can estimate where a one photoelectron peak should fall. Comparing this value to the location of the centre of the second peak in Fig. 3.3 we find that these two numbers fall in roughly the same range. It is for this reason that we refer to the second peak as the one photoelectron peak. As an example consider analysis of the data in Fig. 3.3. From Appendix D the centre of the pedestal and centroid peaks are 126 and 515 respectively. Therefore $\mu = 515 - 126 = 389$ and σ of the centroid peak is 133. Hence the number of photoelectrons is given by $N = (389/133)^2 = 8.55$ and so we would expect a one photoelectron peak to be found at $389/8.55 + 126 = 171$. From the Mathematica analysis we find the so-called one photoelectron peak centred at 156. These numbers agree to within 10%. The discrepancy could be due to sources of broadening of the centroid peak other than statistical.

Having established the second peak in the data set as the one photoelectron peak an easy way to crudely estimate the number of photoelectrons using the fit parameters from the Mathematica analysis is by using the following equation:

$$\text{number of photoelectrons} = \frac{\text{centroid} - \text{pedestal}}{\text{1 p.e.} - \text{pedestal}}, \tag{3.6}$$

[6] Note that the width w in the expression for the Gaussian in Eq. 3.3 corresponds to 2σ.

Run #	Amount of Fluor (%) (Standard QSA = 100)	Pedestal (ch)	1 p.e.peak (ch)	1 p.e peak (ch/p.e)	Muon centroid (ch)	Unconrrected Muon (p.e.#)	Conrrected Muon (p.e.#)
711	100	125.9	153	27	589	15.1	15.1
712	~	~	~	~	~	~	~
713	50	126.0	155.9	29.9	517.8	12.76	12.80
714	80	126.0	160.6	34.5	572	14.5	14.5
715	90	125.9	153	27	464	11.0	14.7
716	unknown						
717	90	108.9	155	46	428	10.39	13.9
718	~	~	~	~	~	~	~
719	100	110.5	141	31	462	11.5	15.3
720	100	110.8	144	33	451	11.1	14.8
721	80	112.6	143.1	30.5	417.9	9.95	13.3
722	90	112.7	143.2	30.5	429.1	10.31	13.8
723	150	113.3	144.1	30.8	455.0	11.13	14.9
724	125	112.9	145	31.6	457	11.20	14.9
725	100 (H.M. QSA)	112.8	144.9	32.0	370.9	8.41	11.2
726	nanosuspension	~	~	~	~	~	~
727	200	113.5	147.6	34.1	446	10.85	14.5
728	100 (H.M. QSA)	113.2	142	29	454	11.11	14.8
730	90	112.4	144	32	447	10.90	14.6

Table 3.1: Measured number of photoelectrons from muon centroid peaks for standard (70/25/5) cocktail solutions with varying concentrations of fluor. The solutions tested in this table were prepared by mixing standard cocktails of homemade QSA (no fluor) with standard cocktails made with commercial QSA. For solutions with greater than 100% fluor appropriate amounts of primary and secondary fluor were added to the cocktail made with commercial QSA.

where centroid, pedestal, and 1 p.e. all represent the centres of the peaks. Using the numbers for the analysis presented in Appendix D yields 12.8 ± 0.3 photoelectrons.

3.6 Results

This section presents the results of the measured number of photoelectrons for scintillation cocktails containing various concentrations of primary and secondary fluor. In this report only data with muon centroids are analyzed because these data have the most statistics (60% of the charged particles reaching the detector are muons). The relative merits of the different concentrations of fluors in not expected to be sensitive to the type of particle responsible for producing the photoelectrons.

First, data in which both the primary and secondary fluor concentrations are changed by the same fractions are presented (i.e. if the primary fluor concentration is doubled, then the secondary fluor concentration is doubled). Table 3.1 summarizes the main results. The first column in the table is the run number as recorded in the data log book and the second column gives the fluor concentration for that run. The third, fourth, fifth, and sixth columns are the centroid of the pedestal peak, the centroid of the one photoelectron peak,

the difference in the centroids of these two peaks, and the centroid of the muon centroid peak respectively. Column seven is the number of photoelectrons as calculated from Eq. 3.6 and the final column is the corrected number of photoelectrons and further explanation is given below. Errors have been omitted from this table due to a lack of space, however the full table with errors has been included in Appendix B.

Accurately measuring the centroid of the one photoelectron peak is difficult because this peak is so small. The position of the one photoelectron peak relative to the pedestal peak (the fifth column in table 3.1) should not change from run to run. This quantity is used to determine the number of photoelectrons (denominator of Eq. 3.6) so accurately determining its value is important. Excluding run #717 which is anomalously high, the data in column five average to 31 and have a standard deviation of 2. This quantity can be more accurately determined using only data that have high statistics and therefore allows one to more clearly resolve the one photoelectron peak. Data sets #713, 721, 723, and 731 are overnight runs and therefore have the best statistics. Using the one photoelectric peak data from these runs gives an average position of 30.8 and a standard deviation of 0.7. This average value was used in the calculation of the number of photoelectrons produced by muons shown in column 7 of table 3.1.

Looking at column 7 of table 3.1, from runs #713, 714, and 711 the number of photoelectrons is seen to increase as the fluor concentration is increased from 50 to 80 and finally to 100%. Then the number of photoelectrons is seen to suddenly drop in run #715 which has a fluor concentration of 90%. One would have expected the number of photoelectrons measured in this run to fall between the number found for the 80 and 100% runs. After run #721 the detector was opened up and mylar reflector that is supposed to be fixed to the free end of the WLS fibre was found to be missing. It is speculated that the reflector came off between runs #714 and 715 and is the cause of the consistently low number of photoelectrons from run 715 onwards. To correct the data with no reflector to match the data with the reflector runs #719 and 720 were compared to run #711 (all 100% QSA data sets). Taking the ratio of the number of photoelectrons detected in run #711 to that of run #719 yields a factor of 1.31. The ratio of runs #711 and 720 gives 1.36. After properly accounting for errors in all quantities the average of the two correction factors is 1.34±0.011. The final column of Fig. 3.1 corrects the number of photoelectrons for the absence of the mylar reflector (all runs after #714) by multiplying the number of photoelectrons in column 6 by this correction factor. The corrected number of photoelectrons is plotted as a function of fluor concentration in Fig. 3.4.

From this plot it is clear that the optimum fluor concentration is found by using standard cocktails made with 100% commercial QSA. Using lower concentrations of fluor causes the number of photoelectrons to drop rapidly and using higher concentrations does not increase the light output.

Now the results of the light output tests for increasing only the concentration of the secondary fluor are presented in table 3.2. Again errors have been omitted from this table, the complete table can be found in Appendix B. High concentrations of secondary fluor were made by adding appropriate amounts of the secondary fluor to standard cocktails made using commercial QSA. The results are shown graphically in Fig. 3.5. Within experimental

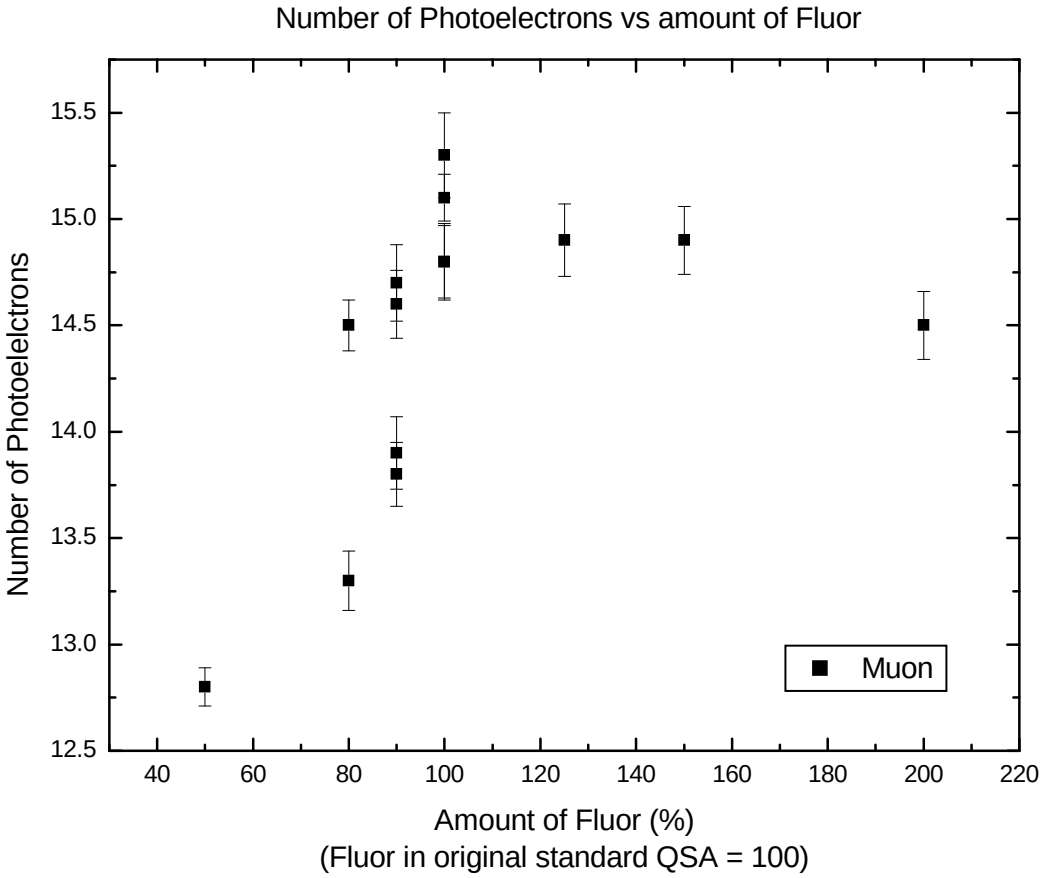

Figure 3.4: Plot of the corrected number of photoelectrons verses fluor concentration. These data are taken from Fig. 3.1.

Run #	amount of bis-MSB (the amount of MSB in Standard QSA = normal bis-MSB)	Pedestal (ch)	1 p.e.peak (ch)	1 p.e peak (ch/p.e)	Muon centroid (ch)	Uncorrected Muon (p.e.#)	Corrected Muon (p.e.#)
711	1 x normal bis-MSB	125.9	153.2	27.4	588.5	15.07	15.1
729	2 x normal bis-MSB	112.9	144.9	32.0	461.2	11.35	15.1
731	3 x normal bis-MSB	113.1	144.6	31.5	464.3	11.44	15.3

Table 3.2: Muon light output measurements of standard 70/25/5 cocktails with increasing concentrations of secondary fluor (bis-MSB).

error increasing the concentration of secondary fluor does not affect the light output of the scintillation cocktail.

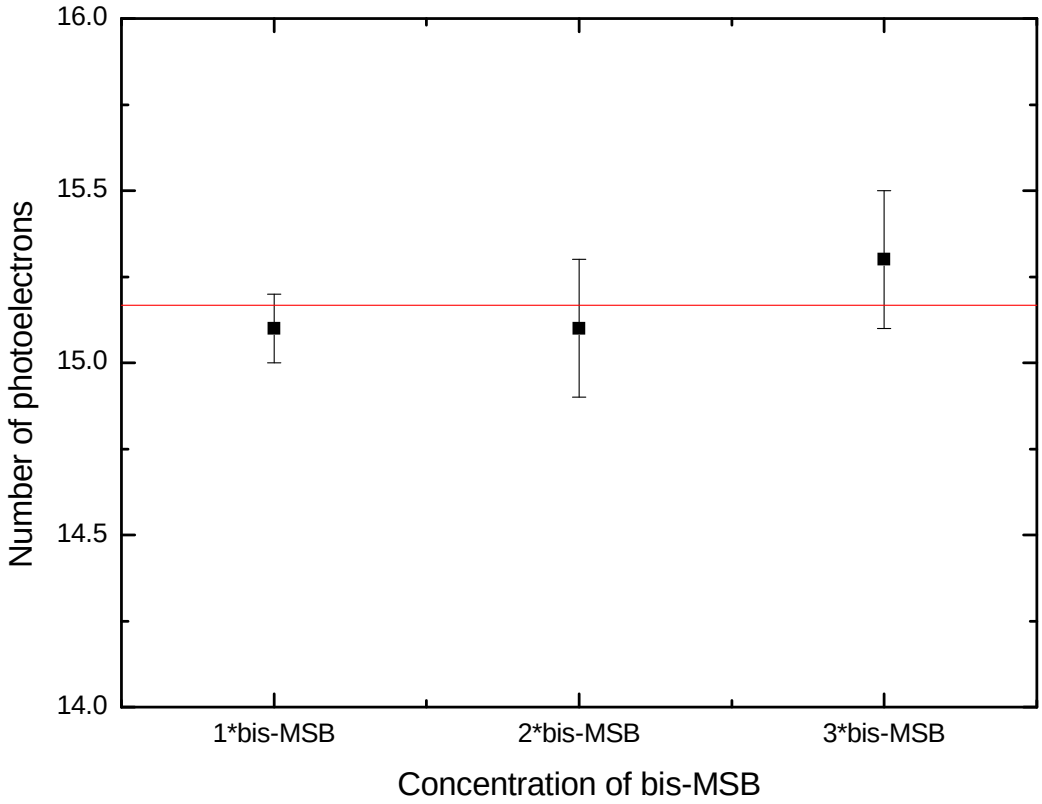

Figure 3.5: The number of photoelectrons in standard (70/25/5) cocktails with various concentrations of secondary fluor bis-MSB. 1 × bis-MSB means the same concentration of bis-MSB found in commercial QSA. 2 × bis-MSB means twice the concentration of secondary fluor found in commercial QSA and so on.

3.7 Conclusion

The primary (PPO) and secondary (bsi-MSB) fluor concentrations found in the commercial QSA was found to yield the highest light output. Changing the concentration of only the secondary fluor did not affect the light output.

Chapter 4

Experiment 2: Biological Inhibitor Test

The T2K neutrino oscillation experiment will have a near detector composed of a water-bearing liquid scintillator cocktail. Ultimately in the final version the neutrino near detector the scintillation cocktail will be stored inside the detector tubes for extended periods of time and some means of discouraging the growth of mold and mildew is necessary. In fact mold has already been seen to form in some scintillation cocktails during the detector development phase. It is for these reasons that we are exploring the possibility of adding biological inhibitors to the scintillator cocktails.

4.1 Cloud Point Test

A series of four measurements of cloud point temperatures of various liquid scintillator solutions were made. The description of measurement A gives the motivation of the measurements and includes a detailed description of the apparatus, experimental setup, and the measurement procedure. These details are not repeated in descriptions of measurements B, C, or D. In measurement A the cloud point temperatures of standard cocktail containing five different commercially available biological inhibitors designed to deter bacteria growth are tested. In measurement B low concentrations of zinc are added to the standard cocktail and to standard cocktail + the biological inhibitor Germall Plus using three different zinc compounds. Zinc is a known fungicide. Measurement C repeats the zinc tests for the standard cocktail using high concentrations of zinc that are required for zinc to act as an effective fungicide. Finally, in measurement D the high zinc concentrations are tested in solutions of standard cocktail + Germall Plus.

4.1.1 Cloud Point Test A - Biological Inhibitors

In the cloud point test the scintillation cocktails (which are clear at room temperature) are heated slowly. Over a small range of temperatures ($\sim 1°$C) the solution will turn from transparent (T) $\rightarrow$ cloudy (C) $\rightarrow$ opaque (O). The temperature where this transition occurs is the cloud point temperature. Because the detector is a scintillation type detector the solution inside the detector must remain clear in order to avoid undesirable light absorption which would severely compromise the sensitivity of the detector. In the best case scenario adding a biological inhibitor to the cocktail would not decrease the cloud point temperature of the solution below that of the control cocktail ($\sim 33°$C). We will determine the most suitable biological inhibitor by comparing the maximum temperatures at which the standard liquid scintillator mixed with biological inhibitor remains clear.

Apparatus/Setup

The following equipment are required to carry out these measurements:

- Mercury Thermometer
- Hotplate "Fisher Thermix R stirring hot plate model 610 T"
- Stir bar
- 8 glass vials
- Circular plastic box with sides partially cut away (used to raise vials away from the surface of the hotplate)
- Retort stand
- Glass container
- Bleach (65 ml per 1 litre of distilled water)
- Standard liquid scintillator cocktail
    - Boiled distilled water
    - Quicksafe A
    - Triton X-110
- Biological Inhibitors
    - Germaben 2
    - Germaben 2E
    - Liquipar Optima
    - Phenonip
    - Germall Plus
- Spore water (contaminants collected from a furnace and vacuum cleaner and mixed with water)

Figure 4.1 is a digital photograph of the assembled apparatus. The various scintillation solutions are placed in the vials and sit on top of the filter case in a water bath. The water bath is heated and stirred using the hot plate and stir bar. A mercury thermometer is used to monitor the temperature and is held in place using a retort stand as shown.

Procedure

The following recipe makes 404 ml of standard cocktail:

- 70% by volume boiled distilled water (283 ml)
- 25% by volume QSA (101 ml)
- 5% by volume TX-100 (20.2 ml)

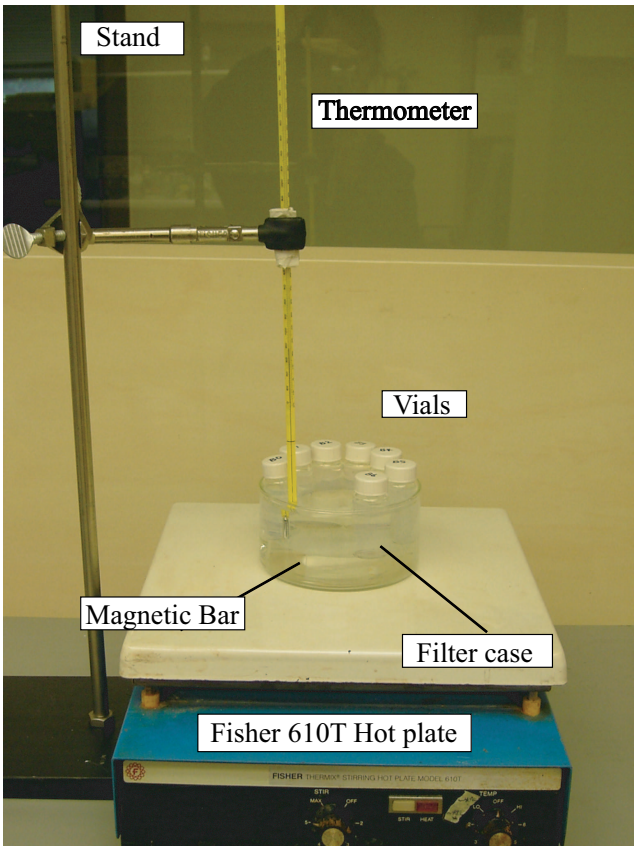

Figure 4.1: Digital photograph of apparatus.

The following is a list of the solutions whose cloud point temperatures we determined (all percentages are by volume):

- B0. Standard cocktail
- B1. Control - Standard cocktail + spore water (5%)
- B2. [Standard cocktail + Germaben2 (1%)] + spore water (5%) [7]
- B3. [Standard cocktail + Germaben2E (1%)] + spore water (5%)
- B4. [Standard cocktail + Liquipar Optima (1%)] + spore water (5%)
- B5. [Standard cocktail + Phenonip (1%)] + spore water (5%)
- B6. [Standard cocktail + Germall Plus (0.5%)] + spore water (5%)
- B7. [Standard cocktail + Liquipar Optima (1%) + Germall Plus (0.5%)] + spore water (5%)

[7]Here, and for B3 through B7, first the standard cocktail and the biological inhibitor are mixed (1% inhibitor by volume of the standard cocktail and inhibitor), then the spore water is added (5% by total volume of the combined standard cocktail, inhibitor, and spore water)

Quicksafe A, abbreviated QSA, is a commercial liquid scintillator supplied by Zinsser Analytic, whose active ingredient is di-isoprophlnaphthalene. Triton X-100 is a surfactant used to help dissolve the QSA in the water. The spore water was prepared by mixing water with many biological contaminants (dirt, dust, hair, ...) obtained from a furnace filter and a vacuum cleaner bag and allowing the solution to ferment.

Before preparing solutions all containers and items that could potentially come into contact with the test solutions must be carefully sterilized. The following is a description of the sterilizing procedure. First all items are prepared by washing with detergent and rinsed with tap-water. Then they are sterilized by immersing in a dilute bleach solution (65 ml bleach per 1 L of distilled water) for at least 5 minutes and rinsed thoroughly three times with distilled water.

Eight of each of 20 ml vials, vial lids, 125 ml jam jars, and jam jar lids were sterilized and labeled B0-B7. These jam jars are used for storing excess amounts of each cocktail and can be used at a later time, for example in light output tests.

To make 404 ml of standard cocktail, we boil 500 ml distilled water vigorously for at least 20 minutes and then allow the water to cool to room temperature. The beaker used to boil the distilled water must be sterilized beforehand. The standard cocktail mixture is prepared using the recipe given at the being of the section and needs to be heated to about 40 °C while mixing with a sterilized magnetic bar. To help the Triton X-100 dissolve, the “LO” setting on the heater knob of the hot plate sets the temperature to about around 40°C. The ”max” setting on the knob that controls the magnetic stirring speed will easily dissolve the TX-100 in the cocktail. Generally the speed of the magnetic stirring bar depends on the amount of the cocktail to be stirred. If we stir a small amount of any kind of solution, it is a good idea to choose a medium stirring speed to prevent the solution from splashing. Once the cocktail becomes hot enough, the colour changes to an opaque white. This usually takes about 15 minutes. Once the ingredients are completely dissolved, the cocktail is allowed to cool to room temperature, whereupon it turns clear again.

To prepare the test solutions put 19 ml of the cooled solution (404 ml) into B0 vial and 55 ml into each of the eight jam jars. The quantities of biological inhibitors indicated above (B1-B7) were added to the corresponding jam jars and stirred thoroughly using the stir bar. Then 19 ml of cocktail from each jar were put into vials the vials labeled B1 through B7. The solutions in these 8 vials were originally used a for biological challenge test to see how well these inhibitors suppress the growth of mold and mildew in the cocktail, so that 1 ml of the spore water was added to B1-B7. Because the mold growth in the cocktail was not observed, these cocktails were used for the cloud point test.

These vials were placed upon a circular plastic box in a water bath such that the water level reached to the shoulder of the vials (just below the lid). A magnetic stirring bar was placed beneath the plastic box in the water bath to improve the water circulation and maintain temperature homogeneity in the water bath. The water bath was slowly heated using the hotplate. Slow heating is necessary to ensure that the solutions in the vials remained at the same temperature as the water bath. The slow heating also allowed us to make a thorough observation of each vial at each temperature. Consequently, the heater knob was initially

Temperature (°C)	B0	B1	B2	B3	B4	B5	B6	B7
20	T	T	T	T	T	T	T	T
21	T	T	T	T	T	T	T	T
22	T	T	T	T	T	T	T	T
23	T	T	T	T	T	T	T	T
24	T	T	T	T	C/O	C/O	T	C
25	T	T	T	T	O	O	T	O
26	T	T	T	T	O	O	T	O
27	T	T	T/C	T/C	O	O	T	O
28	T	T	T/C	T/C	O	O	T	O
29	T	T	C/O	C/O	O	O	T	O
30	T	T	O	O	O	O	T	O
31	T	T	O	O	O	O	T	O
32	T	T/C	O	O	O	O	T	O
33	O	O	O	O	O	O	O	O
34	O	O	O	O	O	O	O	O

Table 4.1: Cloud point test results (T = transparent C = cloudy O = opaque white)

set to be "LO". At the "LO" setting the temperature stopped increasing at 26 °C. The heat control was gradually increased every 2-3 °C. At each 1°C interval from 20 °C to 40°C, each vial was observed for clarity and a record of the observations was maintained.

Results

The observed results for each vial at all temperatures are shown in the Table 4.1. Solutions B4, B5, and B7 were the first to become white opaque at 24-25 °C, which is not too surprising considering that Liquipar Optima and Phenonip have similar chemical properties. The cloud points of B2 and B3 were at 29-30°C. The standard cocktail with Germall Plus was the only biological inhibitor that remained transparent at 33 °C. In fact the cocktail with Germall Plus had a cloud point temperature equal to the cloud point temperatures of the standard cocktail and control solution which makes it a good candidate for use as a biological inhibitor in the scintillation solution of the neutrino near detector.

Conclusions

Five different biological inhibitors were tested for suitability for use in the scintillation solution of the neutrino near detector. The solution with Germall Plus was the only cocktail whose cloud point temperature remained unaffected by the addition of the biological inhibitor. This result makes Germall Plus the best candidate for use with the neutrino detector as of this writing.

4.1.2 Cloud Point Test B - Low Zinc Concentrations

Objective

Magnesium and zinc ions, when added to solutions in appropriate concentrations, have been known to inhibit biological growth. In this section we will study how adding various

zinc compounds to the liquid scintillator cocktail affects the cloud point temperature. Zinc acetate dihydrate, zinc chloride, and zinc sulfate heptahydrate are the compounds we will investigate. These compounds were added to the standard cocktail and to mixtures of the standard cocktail + Germall Plus (0.5% by volume) such that a zinc concentration of 100 parts per million (ppm) by weight was achieved.

Zinc compounds are used as fungicides in agriculture and low concentrations of the zinc ions are commonly used to inhibit moss growth on the rooftops. We want to investigate whether adding zinc in concentrations of 100 ppm to the scintillation cocktails using various zinc compounds significantly reduces the cloud point temperatures of the solutions compared to that of a control solution (standard cocktail) [8]

Cadmium is another possible biological inhibitor, however, due to its high toxicity it has been banned for use as a fungicide. If cadmium were to be used as a biological inhibitor in the water scintillator detector special procedures would need to be adapted for the handling and discarding of cadmium and cadmium contaminated materials. At the time of this writing the possibility of using cadmium as a biological inhibitor in the scintillation cocktail is not being pursued.

Procedure

Below is the procedure for adding 100 ppm by weight of zinc ions to the scintillator solutions, but first an important note of caution. The zinc compounds used in this study are potentially hazardous to human health and precautions should be taken to prevent inhaling or coming into direct contact with these compounds. When handling the compounds one should wear a lab coat, gloves, goggles, and a mask. It is also advisable to read the appropriate Workplace Hazardous Materials Information System (WHMIS) data sheets before handling these compounds.

The three zinc compounds used in this study are:

1. zinc acetate dihydrate: $Zn(CH_3COO)_2{\cdot}2H_2O$
   molecular weight = 219.49 amu

2. zinc chloride: $ZnCl_2$
   molecular weight = 136.28 amu

3. zinc sulfate heptahydrate: $ZnSO_4{\cdot}7H_2O$
   molecular weight = 269.52 amu

Now we proceed with the calculation to determine the amount of $Zn(CH_3COO)_2{\cdot}2H_2O$ needed to add 100 ppm by weight zinc ions to the liquid scintillator solution. If we start with 100 ml of scintillator solution and assume it weighs 100 g (this is only approximate,

[8] Note that the control in this cloud point test refers to just the standard cocktail (water + QSA + surfactant) whereas in cloud point test A the control used was the standard cocktail + spore water.

but close since the scintillator solution is 75% water, the actual density of the standard cocktail is 1.001±0.008 g/ml) then we require $(100/10^6) \times 10^5$ mg = 10 mg of zinc. The molecular weight of zinc acetate is 219.49 amu and the atomic weight of zinc is 65.37 amu, therefore to get 10 mg of zinc ions we require (219.49/65.37) × 10 mg = 33.58 mg of $Zn(CH_3COO)_2 \cdot 2H_2O$.

Calculations to get the required weights of the two remaining compounds are done in the same way. To add 100 ppm by weight of zinc to 100 ml of liquid scintillator solution the following amounts of the zinc compounds are required:

1. $Zn(CH_3COO)_2 \cdot 2H_2O$ ..... 33.58 mg

2. $ZnCl_2$ ..... 20.85 mg

3. $ZnSO_4 \cdot 7H_2O$ ..... 41.23 mg.

The above amounts of zinc compounds were weighed out and then placed into three separate sterilized jam jars (the sterilizing procedure is given in §4.1.1). Next 100 ml of standard cocktail (70% boiled distilled water, 25% QSA, and 5% TX-100) was added to each jam jars and the jars were labeled "control (standard cocktail) + zinc acetate", "control + zinc chloride", and "control + zinc sulphate". Each solution was heated to 40°C while being stirred by a magnetic bar in order to completely dissolve the zinc compounds. Next the solutions were allowed to cool to room temperature.

After the zinc compound solutions were made, 35 ml of the control + zinc acetate solution was poured to a liquid scintillator prototype detector to measure the light output of the zinc acetate solution. The light output measurement was part of a different series of tests and is not part of the cloud point test, however this part of the procedure is mentioned for completeness. After the light output measurements were completed the 35 ml of zinc acetate solution was poured from the detector into a sterilized beaker. Then 0.5% of Germall Plus by volume (0.005 × 35 ml = 0.175 ml) was added to the solution and stirred with a magnetic bar. A medium stirring speed was required to avoid making bubbles.

The control + zinc acetate + Germall Plus solution was transferred back into the prototype detector and the light output was again measured. A sterilized jam jar was prepared and labeled "control + zinc acetate + Germall Plus (0.5%)" to store the cocktail from the detector after the light output measurement was completed.

The same procedure was used for making control + zinc chloride + Germall Plus and control+ zinc sulfate + Germall Plus solutions. In total we had seven different solutions stored in jam jars. For the cloud point test 20 ml of solution was transferred into seven separate vials labeled 1-7. The following list gives the labeling convention that was adopted:

1. Control (standard cocktail)
2. Control + zinc acetate

Temperature (°C)	1	2	3	4	5	6	7
20	T	T	T	T	T	T	T
21	T	T	T	T	T	T	T
22	T	T	T	T	T	T	T
22	T	T	T	T	T	T	T
23	T	T	T	T	T	T	T
24	T	T	T	T	T	T	T
25	T	T	T	T	T	T	T
26	T	T	T	T	T	T	T
27	T	T	T	T	T	T	T
28	T	T/C	T	T	T	T	T
29	T	T/C	T	T	T	T	T
30	T/C	T/C	T	T/C	T/C	T/C	T
31	C	C	C	C	C	C	C
32	O	O	O	O	O	O	O

Table 4.2: Cloud Point Test (T = transparent C = cloudy O = opaque white)

3. Control + zinc acetate + Germall Plus
4. Control + zinc chloride
5. Control + zinc chloride + Germall Plus
6. Control + zinc sulfate
7. Control + zinc sulfate + Germall Plus.

To measure the cloud points of these seven solutions the vials were heated gently in a water bath and the clarity of the solutions was visually inspected at 1°C intervals. The details of the setup are the same as in §4.1.1.

Results

Table 4.2 summarizes the results of this cloud point test.

Conclusions

Adding the zinc compounds ($Zn(CH_3COO)_2{\cdot}2H_2O$, $ZnCl_2$, and $ZnSO_4{\cdot}7H_2O$) to the standard cocktail and to the standard cocktail + 0.5% Germall Plus to achieve a concentration of 100 ppm by weight of zinc does not significantly lower the cloud point temperature when compared to that of the standard cocktail. The zinc sulfate compound did, however, perform the best and has a cloud point temperature of 31°C which equals that of the control solution.

	Zinc Sulfate	Zinc Acetate
1000 ppm	0.412 g	0.336 g
3000 ppm	1.237 g	1.007 g

Table 4.3: Required weight of zinc compounds to make zinc concentrations of 1000 and 3000 ppm by weight.

4.1.3 Cloud Point Test C - High Zinc Concentrations

Objective

The purpose of this report is to see if adding high concentrations of $Zn(CH_3COO)_2{\cdot}2H_2O$, $ZnCl_2$, and $ZnSO_4{\cdot}7H_2O$ to the standard cocktail lowers the cloud point temperature. The previous study (report B) it was found that adding zinc to the standard cocktail in concentrations of 100 ppm by weight did not significantly lower the cloud point temperature ($ZnSO_47H_2O$, in particular, showed no change in the cloud point temperature). It is thought that to effectively work as a fungicide the zinc concentration must be much higher - in the range of 1000 - 3000 ppm by weight. [20] This report will measure the cloud point temperatures of solutions with high zinc concentrations.

Introduction

Zinc is known to be an inhibitor of fungi. The effectiveness of zinc as a fungicide has a strong dependence on the concentration of zinc according to a report by Joanna Duniewska [20]. While low concentrations of zinc ions such as 50, 100, 200, and 300 ppm do not inhibit fungi growth, higher concentrations of 1000 and 3000 ppm are much more effective. In this study we wish to investigate whether higher zinc concentrations can be used in the liquid scintillator cocktail. We must address questions such as: Can high concentrations of zinc compounds be dissolved in the scintillation cocktail?, Is the cloud point temperature significantly altered?, and Is the light output of the detector affected? This report will address the first two questions and the third will be the topic of a separate investigation.

Procedure

Before preparing the scintillator solutions with zinc we first tested how well large amounts of the three zinc compounds dissolve in water. By introducing equal scoops of each compound into separate vials containing 18 ml of water. It was found that both $Zn(CH_3COO)_2{\cdot}2H_2O$ and $ZnSO_4{\cdot}7H_2O$ completely dissolve, but $ZnCl_2$ did not. For this reason $ZnCl_2$ was eliminated as a possible source of zinc in the liquid scintillator solution.

The high concentrations we will test in this report are 1000 and 3000 ppm by weight of zinc. We will use two zinc compounds as sources of zinc, namely $Zn(CH_3COO)_2{\cdot}2H_2O$ and $ZnSO_4{\cdot}7H_2O$. The required amounts of zinc sulfate and zinc acetate for these concentrations can be calculated by following the calculation used for low concentrations done in §4.1.2. The calculated weights are given in Table 4.3.

To make the zinc sulfate solutions the required amount of compound was added to a sterilized 125 ml jam jar. Rather than mixing the zinc sulfate directly with 100 ml of standard

cocktail (70% water, 25% QSA, 5% Triton X-100 [9]) the compound was first mixed with 70 ml of boiled distilled water. This was done for a couple of reasons. First, if the zinc compound does not completely dissolve in the water then it is not necessary to add the QSA and Triton X-100 and time and solution can be saved. Second and more important, it is easier to see if all of the compound has dissolved in the clear water than it is in the comparatively opaque standard cocktail.

The zinc sulphate compound dissolved completely in the water at both 1000 and 3000 ppm concentrations so 25 ml of QSA and 5 ml of Triton X-100 were added to the each mixture. The solutions were stirred and heated in a manner described in cloud point test B. Both of the final zinc sulphate solutions seemed less clear than the previous 100 ppm concentration tested in cloud point test B, however there was no undissolved material at the bottom of a jam jar.

Next a solution of standard cocktail mixed with 3000 ppm of zinc from the compound $Zn(CH_3COO)_2{\cdot}2H_2O$ was made using the same steps as for the $ZnSO_4{\cdot}7H_2O$ solution. This solution was transparent so a 1000 ppm solution was not made. A higher concentration of zinc is desirable because it will be a stronger fungicide, so if the 3000 ppm concentration is clear it would always be chosen over the 1000 ppm concentration.

In this study we will measure the cloud point temperatures of the following solutions:

1000 ppm zinc from $ZnSO_4{\cdot}7H_2O$

3000 ppm zinc from $ZnSO_4{\cdot}7H_2O$

3000 ppm zinc from $Zn(CH_3COO)_2{\cdot}2H_2O$.

Next 20 ml of each solution was transferred into three separate sterilized vials and the apparatus for the cloud point test was setup as described in cloud point test A. In these measurements the control cocktail was taken from a portion of the standard cocktail prepared in cloud point test A.

Results

The result of 1°C interval observations of the four scintillator solutions is given in Table 4.4.

Conclusions

Among all zinc solutions, the standard cocktail/zinc sulfate mixture with a 1000 ppm concentration has the highest cloud point temperature very nearly equal to that of the control solution. However, there is not much variation in the cloud point temperatures among all four of the solutions tested (see Table 4.5). In fact the zinc acetate solution with 3000 ppm zinc has a cloud point temperature that is only 1-2°C lower than than of the control solution. We will do further cloud point tests with 0.5% by volume of Germall Plus added to these solutions. Germall Plus is the biological inhibitor that had the highest cloud

[9] Percentages are by volume.

Temperature (°C)	Zn Acetate 3000 ppm	Zn Sulfate 3000 ppm	Zn Sulfate 1000 ppm	Standard 70/27/5
20	T	T	T	T
21	T	T	T	T
22	T	T	T	T
23	T	T	T	T
24	T	T	T	T
25	T	T	T	T
26	T	T	T	T
27	T	T	T	T
28	T	T	T	T
29	T	C/O	T	T
30	C/O	O	T	T
31	O	O	C	C
32	O	O	O	C/O
33	O	O	O	O
34	O	O	O	O

Table 4.4: Observation of the clarity of scintillation solutions containing high concentrations of zinc compared to the clarity of the standard cocktail as a function of temperature. (T = transparent C = cloudy O = opaque white)

	Zn Acetate 3000 ppm	Zn Sulfate 3000 ppm	Zn Sulfate 1000 ppm	Standard 70/27/5
Cloud point (°C)	30-31	29-30	32	32.5

Table 4.5: Cloud point temperatures of the solutions tested.

point temperature of all inhibitors tested in cloud point test A. The biological inhibitor Germall Plus is for deterring bacteria growth and fungi whereas zinc deters fungi growth only.

The fine grained detector will be kept at around room temperature, thus a difference in cloud point temperatures of a few °C is tolerable. However, fungi growth is a serious problem because it could significantly reduce the light output of the liquid scintillator. Therefore solution with a slightly lower cloud point temperature but a significantly a higher concentration of zinc is preferred over a solution with the highest possible cloud point temperature but lower zinc concentration. Also the zinc acetate solution seems to be inherently clearer than the zinc sulfate solution even at room temperature. For these reasons the $Zn(CH_3COO)_2{\cdot}2H_2O$ solution with 3000 ppm zinc concentration is the best candidate for the liquid scintillator solution at the time of this writing.

4.1.4 Cloud Point Test D - High Zinc + Germall Plus

In this section high concentrations (1000 and 3000 ppm by weight) of zinc are added to solutions of standard cocktail + 0.5% by volume Germall Plus. The zinc is introduced using one of two compounds - $Zn(CH_3COO)_2{\cdot}2H_2O$ or $ZnSO_4{\cdot}7H_2O$. In cloud point test C we found that adding these high concentrations of zinc to the standard cocktail did not significantly reduce the cloud point temperature of the solution. In this measurement we will test the cloud point temperature of solutions into which both Germall Plus and high concentrations of zinc have been added.

Procedure

The three solutions examined in cloud point test C were saved and stored in sterilized 125 ml jam jars and 20 ml vials. The solutions stored in the vials will be used again in this study. They are:

1. 20 ml standard cocktail (70/25/5)+
   3000 ppm zinc from zinc acetate

2. 20 ml standard cocktail (70/25/5) +
   3000 ppm zinc from zinc sulfate

3. 20 ml standard cocktail (70/25/5) +
   1000 ppm zinc from zinc sulfate

To each solution 0.5% by volume (0.1 ml) of Germall Plus was added and the mixture was shaken vigorously. The cloud point test apparatus was set up and the vials were heated and observed at 1°C intervals (see §4.1.1). These measurements were compared to a control sample (70/25/5 standard cocktail).

Results

Table 4.6 gives the results of the cloud point test for each of the four solutions tested.

Conclusions

Table 4.7 summarizes the results of the cloud point test. Adding 0.5% Germall Plus to the solutions of cloud point test C did not change the cloud point temperatures of the solutions. As stated in the conclusions of §4.1.3 a difference of a few °C in the cloud point temperatures is not critical since the liquid scintillator detector will be kept at room temperatures. Solutions with higher zinc concentrations are favoured. Because the zinc acetate solution is visually clearer than the zinc sulfate solution the $Zn(CH_3COO)_2{\cdot}2H_2O$ compound is preferred as a source of zinc in the liquid scintillator solutions.

Temp (°C)	Zn Acetate 3000 ppm + Germall Plus 0.5%	Zn Sulfate 3000 ppm + Germall Plus 0.5%	Zn Sulfate 1000 ppm + Germall Plus 0.5%	Standard 70/27/5
20	T	T	T	T
21	T	T	T	T
22	T	T	T	T
23	T	T	T	T
24	T	T	T	T
25	T	T	T	T
26	T	T	T	T
27	T	T	T	T
28	T	T	T	T
29	T	T	T	T
30	C	O	T	T
31	C/O	O	T	C
32	O	O	O	C/O
33	O	O	O	O
34	O	O	O	O

Table 4.6: Observed clarity of the four tested solutions as a function of temperature. (T = transparent C = cloudy O = opaque white)

	Zn Acetate 3000 ppm + 0.5% GP	Zn Sulfate 3000 ppm + 0.5% GP	Zn Sulfate 1000 ppm + 0.5% GP	Standard 70/27/5
Cloud point (°C)	30-31	30	31-32	32.5

Table 4.7: Measured cloud point temperatures. These results do not differ from those of cloud point test C (GP is short for Germall Plus.).

4.2 Light output measurement of Biological Inhibitor Test

To prevent mold growth in the liquid scintillator cocktail biological inhibitors are added to the cocktail mix. The cloud points of eight different scintillator cocktails have been measured. Each of the six solutions contained a different combination of commercially available biological inhibitors added to the standard cocktail. The cloud points of these solutions have been to those measured using the standard cocktail with no biological inhibitors added. It was found that the biological inhibitor Germall Plus (0.5% by volume) was the most suitable biological inhibitor because its addition to the standard cocktail did not reduce the cloud point temperature.

Biological growth in the scintillator cocktail may include both bacteria and fungi. The

biological inhibitor Germall Plus is advertised to inhibit both bacteria and fungi. Zinc is a well known fungicide and in a previous report zinc was added to the scintillator solution at the 100 ppm (parts per million) level using three different zinc compounds (Zinc acetate dihydrate, Zinc chloride, and Zinc sulfate heptahydrate). Zinc compounds were added to standard cocktails with and without 0.5% by volume Germall Plus. The cloud point temperatures of the scintillator cocktails were not reduced by the addition of zinc. In this section of the thesis the light output of solutions containing (1) 0.5% by volume Germall Plus, (2) 100 ppm zinc, and (3) 0.5% Germall Plus and 100 ppm zinc are measured and compared to the light output of the standard scintillator solution. If the light output of the scintillator cocktail is not reduced, addition of Germall Plus and zinc may significantly extend the lifetime of the water-based neutrino near detector by inhibiting biological growth of in the scintillator solution.

4.2.1 Apparatus/Setup

The following apparatus was in this measurement:

- Photomultiplier tube (PMT)——PMT "Patrick" + Base "PAT2"
  High voltage used for PMT is -2300V and attenuator was × 1.0
- MIDAS data acquisition software
- TRIUMF Beam
- Detector cell
  - 1.5 mm diameter wavelength shifting fiber (WLS)with aluminized mylar reflector on top of the WLS glued by 5 min. epoxy
  - 50 cm long painted Matraplast cell
- Standard liquid scintillator cocktail
  - 70% of Boiled distilled water
  - 25% of Quicksafe A
  - 5% of Triton X-110

The experimental setup of this beam test is identical to that reported in §3.3.

4.2.2 Procedure

The seven different solutions for the beam test were prepared and measured in the way described in §4.1.2. Each light output measurement was performed using the same prototype detector. Each time the solution in the detector was changed the detector cell was first rinsed using methyl alcohol. Using the same detector for all measurements eliminates any systematic errors that can be caused by using different detectors. For example, the efficiency of the WSF (wavelength shifting fibre) likely varies from detector to detector.

Run #	Type of Solution	Cell	Reflector	Comment
756	Control (no inhibitor)	Painted	On	Beam stopped around 3 am.
757	Control + Germall Plus(0.5%)	Painted	On	M11 VA1 was closed.
758	Control + Germall Plus(0.5%)	Painted	On	After 758, paint got blistered during rinsing the painted matraplast cell.
759	Control	Unpainted	On	Used unpainted Matraplast cell, TWIST Magnet started.
760	Control	Unpainted	On	TWIST Magnet on.
761	Control	Unpainted	On	TWIST Magnet on.
762	Control	Unpainted	On	TWIST Magnet stable at maximum
763	Control + Germall Plus(0.5%)	Unpainted	On	
764	Control + ZnAc	Unpainted	On	
765	Control + ZnAc + Germall Plus(0.5%)	Unpainted	On	After 765, the reflector came off during rinsing the cell with reflector.
766	Control + ZnAc + Germall Plus(0.5%)	Unpainted	Off	Poor statistics even though this run was an over-night run because run00766.root file was deleted and then data acquistion was stopped.
767	Control + ZnAc + Germall Plus(0.5%)	Unpainted	Off	
768	Control + ZnCl2	Unpainted	Off	
769	Control + ZnCl2 + Germall Plus(0.5%)	Unpainted	Off	
770	Control + ZnSO4	Unpainted	Off	
771	Control + ZnSO4 + Germall Plus(0.5%)	Unpainted	Off	A lit bit lower than expected
772	Distilled water	Unpainted	Off	Measure the amount of cherencov light. 1 pe peak is obvious. No muon or electron peak visisble
773	Control	Unpainted	Off	Slightly lower than expected
774	Control	Unpainted	Off	Added 1.0ml of mineral oil
775	Control + ZnSO4	Unpainted	Off	
776	Control + ZnSO4 + Germall Plus(0.5%)	Unpainted	Off	

Table 4.8: This table contains comments for each of the light output measurements of the various liquid scintillator solutions with or without Germall Plus and zinc.

4.2.3 Results

Table 4.8 contains relevant comments regarding the various light output measurements made. In runs 756, 757, and 758 a detector cell painted using the "sponge technique" was used for the light output measurements. During the methyl alcohol rinsing process after run 758 the paint layer inside the detector cell became completely blistered. This blistering was likely caused by the alcohol penetrating into the region between the paint layer and the detector wall and subsequently evaporating. Because there were no more available painted cells all runs after 758 were done using an unpainted prototype detector. The first step was to retake the light output measurements of runs 756-758 using the new unpainted detector.

During runs 759-762 a large magnet on a neighbouring experiment TWIST was turned on. During these runs the light output of the control solution (no Germall Plus, no zinc) was repeatedly measured to ensure that the field from the TWIST experiment did not influence the light output results. After run 762 the TWIST magnet was turned off. Comparing the light output of the control solution in the presence of the TWIST magnet (runs 760-762) to the light output with no field (runs 773 and 774) shows that within experimental error the TWIST magnet does not affect the light output measurements, see Table 4.9.

After run 765 the mylar reflector located at the end of the WSF came off. Rather than try to reattach the reflector, a correction factor was applied the to light outputs measured after the reflector was lost. The measured light output is expected to drop due to the light

lost out of the end of the WSF when no reflector is in place. Runs 765 (with reflector) and 766 (no reflector) were done on the same solution and so would be expected to give the same light output. The light output of run 765 was found to be 18.6 ± 0.3 photoelectrons while the light output of run 766 was 12.2 ± 0.2 photoelectrons. Applying the correction factor $(18.6 \pm 0.3)/(12.2 \pm 0.2) = 1.52 \pm 0.04$ to 12.2 ± 0.2 photoelectrons yields 18.6 ± 0.6 photoelectrons which agrees with the measurement made with the mylar reflector in place. This correction factor was applied to the light output measurements of all runs after 765.

The light output is found by dividing the difference between the center of the centroid and the pedestal peak by the difference between the one photoelectron peak and the pedestal peak as describe in §3.5. Thus it is essential to have reliable estimates of the positions of all peaks. The distance between the pedestal and one photoelectron peaks should not vary from measurement to measurement. However, the position of the one photoelectron peak can be hard to determine because the peak size is very small compared to the other two peaks. Moreover, the tail of the centroid peak often overlaps with the one photoelectron peak making it awkward to fit the one photoelectron peak to a Gaussian. To get a good measure of the one photoelectron peak run 772 was done with the detector cell filled only 100% distilled water. This run did not produce a centroid peak because there was no scintillator in the detector making it easy to find the center of the one photoelectron peak. The one photoelectron peak center position found in run 772 was used when calculating the light output for all runs performed. Table 4.9 summarizes the light output results for all the runs listed in Table 4.8.

Figure 4.2 is a plot of the light output measured versus the solution type. When the light output of a solution was measured more than once the average light output is plotted in the graph and the error bar represents that standard deviation of the measurements. From the plot it is clear that within the error bars the light output is not varying from solution to solution. This observation indicates that adding the biological inhibitors 0.5% by volume Germall Plus and/or 100 ppm zinc to the standard cocktail (70% distilled water, 25% QSA, and 5% Triton X-110) does not reduce the light output of the solution.

4.2.4 Conclusions

Comparing the light output of the standard (70/25/5) cocktail to solutions with and without 0.5% Germall Plus and/or 100 ppm zinc (by adding the compounds $Zn(CH_3COO)_2{\cdot}2H_2O$, $ZnCl_2$, and $ZnSO_4{\cdot}7H_2O$)) shows that adding these biological inhibitors does not reduce the light output. Including these biological inhibitors in the scintillator cocktails could potentially increase the lifetime of the water-based neutrino detector by deterring biological growth in the cocktail which could reduce the light output of the detector.

After performing these measurements it was realized that to effectively inhibit fungi growth zinc needs to be present in the liquid scintillator solution at the 1000-3000 ppm level (put reference here). The cloud point and light output tests will have to be redone in order to see if it is possible to introduce zinc into the scintillator cocktail at these higher concentrations without significantly compromising the detector performance.

Run #	Type of Solution	Cell	Reflector	Pedestal (ch)	1 p.e. peak (ch)	1 p.e. peak (ch/p.e.)	Muon centroid (ch)	Uncorrected Muon (p.e. #)	Correced Muon (p.e. #)
756	C	Painted	On	103.1	128.5	25.4	457.6	14.0	14.0
757	C + G	Painted	On						
758	C + G	Painted	On	102.6	125.9	23.3	443.5	14.6	14.6
759	C	Unpainted	On	102.5	125.0	22.5	501.9	18.6	18.6
760	C	Unpainted	On	102.7	125.6	23.0	491.3	18.1	18.1
761	C	Unpainted	On	102.7	124.9	22.2	485.7	17.8	17.8
762	C	Unpainted	On	102.6	125.5	22.9	486.9	17.9	17.9
763	C + G	Unpainted	On	102.3	127.5	25.2	501.5	18.6	18.6
764	C + ZA	Unpainted	On	101.9	124.6	22.7	496.3	18.3	18.3
765	C + ZA + G	Unpainted	On	102.3	126.2	23.8	502.9	18.6	18.6
766	C + ZA + G	Unpainted	Off	102.5	128.1	25.6	365.6	12.2	18.6
767	C + ZA + G	Unpainted	Off	101.7	125.1	23.3	358.6	11.9	18.2
768	C + ZC	Unpainted	Off	103.0	125.1	22.1	371.4	12.5	19.0
769	C + ZC + G	Unpainted	Off	102.7	123.7	21.0	364.4	12.2	18.5
770	C + ZS	Unpainted	Off	102.5	123.6	21.1	375.0	12.7	19.3
771	C + ZS + G	Unpainted	Off	102.5	123.2	20.6	354.9	11.7	17.9
772	Distilled water	Unpainted	Off	102.0	123.5	21.5			
773	C	Unpainted	Off	102.0	122.6	20.5	348.4	11.5	17.4
774	C	Unpainted	Off	101.9	123.1	21.2	354.2	11.7	17.9
775	C + ZS	Unpainted	Off	101.5	125.0	23.6	355.5	11.8	18.0
776	C + ZS + G	Unpainted	Off	101.5	123.1	21.5	353.6	11.7	17.8

Table 4.9: This table summarizes the results of the light output measurements the a standard 70/25/5 cocktail without or with zinc compounds (100 ppm) and Germall Plus (0.5%) (G) as biological inhibitors. The zinc compounds added into this standard 70/25/5 cocktail, used as a control solution (C), are zinc acetate(ZA), zinc chloride (ZC), and zinc sulfate(ZS). To conserve space error estimates have been omitted from this table. The full table with errors has been printed in Appendix C

4.3 Light output measurement of Biological Inhibitor Test (High Concentrations of Zinc)

After finding that adding 100 ppm by weight of zinc to the standard liquid scintillator cocktail containing 0.5% by volume Germall Plus did not reduce the light output of the solution it was discovered that this rather low concentration of zinc is not effective for inhibiting fungi growth. A report by Joanna Duniewska [20] indicates that a much higher concentration of 1000-3000 ppm is needed to inhibit fungi growth. In the cloud point test of solutions with high zinc concentrations it was found that of the three zinc compounds tested zinc sulfate heptahydrate ($ZnSO_4 \cdot 7H_2O$) and zinc acetate dihydrate ($Zn(CH_3COO)_2 \cdot 2H_2O$) were both possible candidates for fungi inhibitors in the liquid scintillator solution. When large amounts of the other zinc compound, zinc chloride ($ZnCl_2$), were added to water it did not completely dissolve and therefore was deemed unsuitable for the liquid scintillator. In this report the light outputs of solutions to which this high concentrations (1000 ppm and 3000 ppm) of zinc have been added are measured. The compounds zinc sulphate and zinc acetate are added to the standard (70/25/5) solution and solutions contain 0.5% by volume Germall Plus.

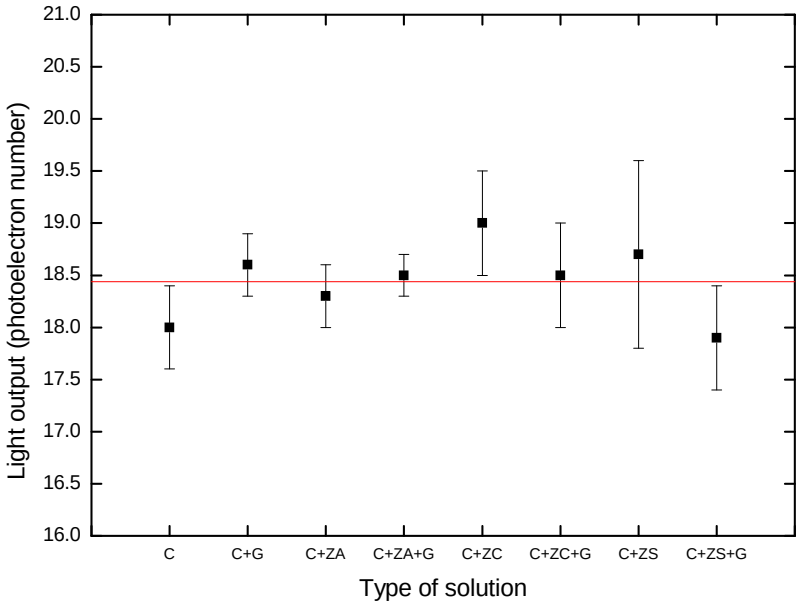

Figure 4.2: The graph illustrates the number photoelectrons produced by a standard 70/25/5 cocktail as a control solution (C) without or with zinc acetate(ZA), zinc chloride (ZC), and zinc sulfate(ZS) and Germall Plus(0.5%) (G) as biological inhibitors. The zinc compounds work as a fungicide and Germall Plus inhibits both fungal and bacterial growth in the liquid scintillator.

4.3.1 Procedure

The following solutions were prepared for light output measurements using the procedure outlined in cloud point test C.

- Standard cocktail + Zinc acetate (3000 ppm) + Germall Plus (0.5%)
- Standard cocktail + Zinc sulfate (1000 ppm) + Germall Plus (0.5%)
- Standard cocktail + Zinc sulfate (3000 ppm) + Germall Plus (0.5%)

The light output measurements were performed as described in §3.3

4.3.2 Results and Discussion

Table 4.10 summarizes relevant comments concerning each run (873-897) performed in these measurements. Runs 873-882 were not useful because the wrong prototype detector was used to perform these measurements. This detector produces a noticeably low light output and was used for in different measurements not directly related to this thesis. Runs 883-897 were performed using the same detector, called "B10" used in the previous biological inhibitor light output measurements.

Before run 888 1 ml of mineral oil used to couple the prototype detector to the PMT was added. In runs 888 and 889 the light output of the standard cocktail was measured and compared to run 883 to confirm that adding the mineral oil did not change the light output

Run #	Type of Soluton	description
873	standard70/25/5+ZnSO4(1000ppm)	TWIST magnet on. broad pedestal. Note that the "NANO" detector was used for run873-879, which was used for nonosuspension tests. We did not use "B10" detecotor for biological inhibitor tests. The result from run 873-882 cannot be compared with the light output from run 759-776 (biological inhibitor test). wrong detector.
874	standard70/25/5+ZnSO4(1000ppm)	repeat of run 873. Wrong detector.
875	standard70/25/5	Wrong detector (NANO detector).
876	empty run	
877	empty run	
878	standard70/25/5+ZnSO4(3000ppm)	Wrong detector (NANO detector).
879	standard70/25/5+ZnAcetate(3000ppm)	Wrong detector (NANO detector).
880	empty run	
881	distilled water	Wrong detector (NANO detector). TWIST magnet on. This run is to establish a prominent 1 p.e. peak. Stopped run and replaced one questionable cable because pedestal dropped to ~140ch from ~190ch.
882	distilled water	Wrong detector (NANO detector).constant with 1 p.e. from run 772.
883	standard70/25/5	Put in "B10" detector.
884	standard70/25/5+ZnSO4(1000ppm)	"B10" detector
885	standard70/25/5+ZnSO4(3000ppm)	"B10" detector
886	standard70/25/5+Germall Plus(0.5%)+ZnSO4(1000ppm)	"B10" detector
887	standard70/25/5+Germall Plus(0.5%)+ZnSO4(3000ppm)	"B10" detector
888	standard70/25/5	Before loading a cocktail, washed detector with water, then ethanol, let it dry. When removed detector, a small amount of mineral oil was left. Added 1ml of mineral oil.
889	standard70/25/5	
890	empty run	
891	distilled water	This run is to establish 1 p.e. peak by using "B10" detector.
892	standard70/25/5+ZnAcetate(3000ppm)	Before this run, put the foam rubber in the area around PMT and is going to be used as extra light seal from now on.
893	standard70/25/5+Germall Plus(0.5%)+ZnAcetate(3000ppm)	
894	standard70/25/5	Before this run, washed detector with water, ethanol. Power went down. All beam line magnets off.
895	standard70/25/5	
896	standard70/25/5+ZnAcetate(3000ppm)	repeat of run 892
897	standard70/25/5+Germall Plus(0.5%)+ZnAcetate(3000ppm)	

Table 4.10: This table contains comments for each of the light output measurements of the various liquid scintillator solutions with or without Germall Plus and high concentrations of zinc.

of the detector assembly. As in the previous biological inhibitor test a distilled water run (891) was done to establish the center position of the one photoelectron peak. Prior to run 892 a gray foam light shield was placed around the PMT. Run 895 on the standard cocktail confirms that introducing this foam shield did not disturb the measured light outputs. During run 894 there was a loss of power. Run 896 is a repeat of run 892 to confirm that the light output before and after the power loss did not change. Table 4.11 summarizes the measured light outputs of the scintillator solutions tested.

Figure 4.3 is a plot of the measured light output as a function of the solution type. When a solution was measured more than once the weighted mean of the measurements is plotted and the error bar is determined from the error in the weighted mean. Note that the light output of the control solution ($\approx$ 10.7 photoelectrons) is lower than control light output from the previous measurements done with the low concentrations of zinc ($\approx$ 18.0 photoelectrons). Because the same detector was used in both measurements one would expect to measure the same light output for the control solutions. However, recall that the first set of measurements were done with a mylar reflector on the WSF and when the reflector fell off the light outputs were corrected by multiplying by a factor of 1.52. In the set of measurements reported here the mylar reflector was not in place and no correction factor has been applied. Correcting the light output of the control from these measurements yields 16.3 photoelectrons which is in better agreement with the previous results.

Run #	Type of Soluton	Pedestal(ch)	error	1 p.e. peak (ch)	error	1 p.e. peak (ch/p.e.)	error	Muon centroid (ch)	error	Muon (p.e. #)	error
883	standard70/25/5	146.3	0.1	167.4	1.0	21.0	1.0	385.0	0.5	10.5	0.2
884	standard70/25/5+ZnSO4(1000ppm)	148.2	0.1	170.2	0.4	22.0	0.5	381.8	0.4	10.3	0.2
885	standard70/25/5+ZnSO4(3000ppm)	153.5	0.2	177.4	0.2	23.9	0.3	379.3	0.7	9.9	0.2
886	standard70/25/5+Germall Plus(0.5%)+ZnSO4(1000ppm)	154.5	0.1	180.2	0.5	25.7	0.5	372.1	0.4	9.6	0.2
887	standard70/25/5+Germall Plus(0.5%)+ZnSO4(3000ppm)	154.8	0.1	176.5	0.7	21.7	0.7	399.0	0.6	10.7	0.2
888	standard70/25/5	154.6	0.1	177.0	0.4	22.4	0.4	410.4	0.4	11.2	0.2
889	standard70/25/5	155.8	0.2	181.2	0.8	25.4	0.8	397.0	0.6	10.6	0.2
891	distilled water	155.8	0.1	178.5	0.5	22.8	0.5				
892	standard70/25/5+ZnAcetate(3000ppm)	157.7	0.1	182.0	0.3	24.3	0.4	359.4	0.5	8.9	0.2
893	standard70/25/5+Germall Plus(0.5%)+ZnAcetate(3000ppm)	158.3	0.1	182.5	0.5	24.2	0.5	375.0	0.4	9.5	0.2
895	standard70/25/5	158.9	0.2	182.0	0.4	23.0	0.4	393.1	0.4	10.3	0.2
896	standard70/25/5+ZnAcetate(3000ppm)	159.4	0.1	182.1	0.4	22.7	0.4	381.7	0.3	9.8	0.2
897	standard70/25/5+Germall Plus(0.5%)+ZnAcetate(3000ppm)	159.6	0.1	181.8	0.7	22.2	0.7	379.2	0.5	9.6	0.2

Table 4.11: This table shows light outputs of the standard (70/25/5) cocktail with and without zinc compounds at concentrations of 1000 and 3000 ppm of zinc sulfate ($ZnSO_4$) and 3000 ppm of zinc acetate and Germall Plus(0.5%). The one photoelectron peak of run 891 was used to calculate the number of photoelectrons for each run listed above.

Figure 4.3 shows a clear reduction in the light output for these high concentrations of zinc. The red line represents the light output of the standard cocktail and points with high concentrations of zinc clearly fall below this line by up to 10%. There is one surprising exception. The solution containing 0.5% Germall Plus and 3000 ppm zinc sulphate seems have a light output equal to that of the control solution. One could imagine that using the one photoelectron peak result from the water run to calculate the number of photoelectrons for the this zinc acetate run may lead to a larger than expected result. However, using the one photoelectron peak data from the zinc acetate run itself one calculates 11.3 photoelectrons which is even higher. This particular solution was measured only once and it would be instructive to measure its light output several more times in the future. At this point it is unclear why this solution appears to have an anomalously high light output.

4.3.3 Conclusions

Adding high concentrations of zinc (1000-3000 ppm by weight) to the scintillator solution using the compounds $Zn(CH_3COO)_2{\cdot}2H_2O$ and $ZnSO_4{\cdot}7H_2O$ can reduce the light output of the solution by up to 10%. If the addition of high concentrations of zinc into the solution effectively inhibits the growth of fungi in the scintillator solution thereby extending the lifetime of the detector a 10% reduction in light output may be tolerable. Long term tests of the light output of detectors with high concentrations of zinc are needed.

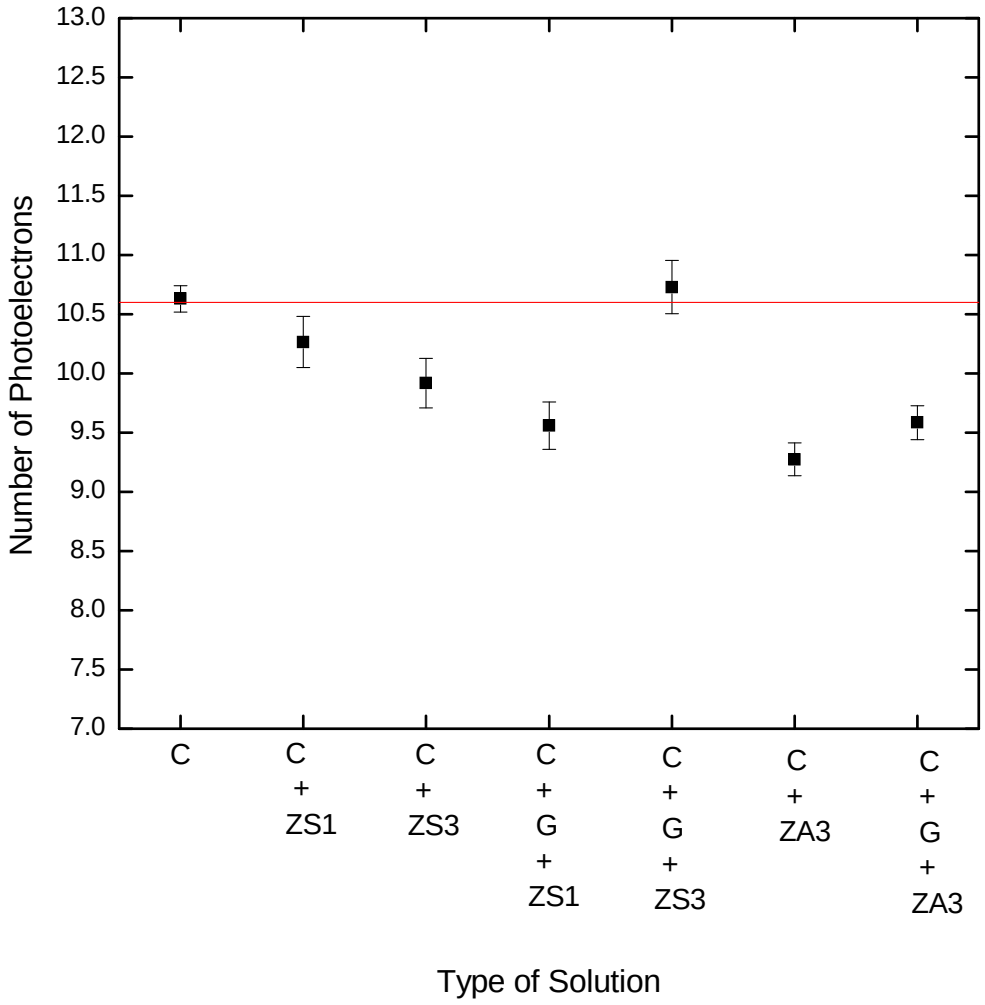

Figure 4.3: This graph illustrates the number of photoelectrons produced by the standard (70/25/5) cocktail (control solution (C)) and solutions with zinc acetate with concentrations of 3000 ppm (ZA3), zinc sulfate with concentrations of 1000 ppm (ZS1) and 3000 ppm (ZS3). These same zinc concentrations were tested in solutions with 0.5% by volume Germall Plus (G). The zinc compounds work as a fungicide and Germall Plus inhibits fungal and bacterial growth in the liquid scintillator. The red line is the light output of standard cocktail.

Chapter 5

Experiment 3: Coat of Reflective Paint

The water-based liquid scintillator solution to be used in FGD contains a liquid scintillator called QSA. It has been observed that QSA chemically attacks the polypropylene detector cell used to build the prototype detectors. Over time the chemical reaction between the QSA and detector cell causes the initially clear scintillator solution to turn a yellowish colour and consequently reduces the light output of the detector. To protect the detector cell from chemical attack, the inner wall of the detector cell has to be coated with a commercially available highly reflective white paint called Eljen-520. Eljen-520 has been engineered such that it does not react with the ingredients that make up the liquid scintillator. In fact, Eljen-520 was originally designed for painting the inner walls of metal cells containing liquid scintillator solutions. Eljen-520, does however, attack many plastics materials such as acrylics. Fortunately, Eljen-520 does not attack polypropylene and hence is be a suitable coating for the inner walls of the detector cell used in this work. [21]

5.1 Introduction

Applying this paint to the inside of the prototype detector cell is a challenging task because the cell is a long and narrow tube. The detector cell is square in cross-section with inner dimensions of 8.5 mm $\times$ 8.5 mm. The prototype detectors studied in this thesis are 50 cm long, however the FGD to be used in the T2K project will contain cells that are 2 m in length. Coating the inner wall of the cell is made even more difficult because Eljen-520 does not stick well to the walls of the polypropylene detector cell. The original method used to coat the inner walls of the cell involved pulling a square sponge soaked with paint through the detector cell using a long wire. Several small pieces of sponge, cut to match the dimensions of the polypropylene tube, were threaded onto a length of wire and then inserted into one end of the cell. Eljen-520 was then poured into the detector cell from the opposite end. The pool of the paint formed on top of the sponges was then smeared onto the sides of the detector cell by using the wire to pull the sponges through the tube. This method produced a relatively uniform and thin coat of paint. However, it is difficult to obtain a complete layer of paint without holes due to the fact that the paint does not adhere to the polypropylene cell. It is also difficult to cut the sponges to exactly match the dimensions of the cell. In addition it is easy to misalign the sponges when loading them into the detector cell to start the painting process. All three of these factors can lead to holes developing in the paint coating, especially near the corners of the cell. [22]

To make Eljen-520 stick to the polypropylene wall, a commercially available plastic paint, Krylon Fusion, was used as a primer. After a coating of primer was applied to the detector cell using the sponge method, three layers of Eljen-520 were painted. Even though Krylon

helped Eljen-520 stick to the cell, the resulting layers were fragile and weak. It was often found that if after painting a cell a short ($\sim$ 1 cm) was cut from it the "tube" of paint could be easily separated from the cell. So this painting technique effectively results in a tube of paint "floating" inside the detector cell. If there are any holes in this tube of paint the liquid scintillator could penetrate into the region between the paint and the cell. In this case the QSA in the scintillator solution will react with the polypropylene walls. The coating of paint will also be severely weakened. Both of these events will dramatically reduce the lifetime of the detector. Finally, this painting method requires a lot of time and patience and the coating produced will likely vary slightly from detector to detector due to difficulties in standardizing the technique (such how much paint to use and how quickly to pull the sponge through the detector cell). It is also hard to imagine painting the thousands of 2 m long cells that are required for the T2K FGD detector using this technique.

5.2 Airbrush Motivation

To improve the painting process and coating quality a custom airbrush was designed and built to paint the inside of the detector cell. There are several reasons that make an airbrush design appealing. First, an airbrush is a common commercially available painting tool. The mechanism (the Bernoulli effect) that makes airbrushes work is well understood and it was thought that an airbrush design could be modified to allow one to paint long narrow tubes. An airbrush is also appealing because spraying a fine mist of paint onto the inner surfaces of the polypropylene detector may encourage the Eljen-520 to stick better. An airbrush will also allow the painting procedure to be standardized. In principle an airbrush will spray paint at a constant rate so that nearly identical and uniform coatings can be applied by simply pulling the tip of the airbrush through the tube at a constant speed. In principle either the airbrush of detector cell could be mounted on a motorized linear stage moves at a constant rate. Also, if the airbrush is capable of painting 2 m long tubes one could imagine painting a panel of 200 tubes all to once using 200 identical airbrushes in parallel. The T2K FGD detector will be made of approximately 30 of these panels.

The first attempt to build a device to spray the inner walls of the detector cell was made by connecting a long brass tube to a paint reservoir. The brass tube could be inserted into the detector cell. The tip of the brass tube gradually tapered down into a fine point with a very small opening. The opposite end of the paint reservoir was connected to high pressure compressed air. The compressed air forces the paint down the brass tube and through the fine tip. When this design was tested using water the spray out of the tip was fine mist. However, when Eljen-520 was tested it was found that, because of its high viscosity, the paint either dripped or squirted out of the tip. During this testing phase the painting tool was supplied with compressed nitrogen gas from a cylinder with a regulator. The maximum pressure that could be obtained with the regulator was 60 psi (pounds per square inch). It is possible that with higher pressures this design could work even with Eljen-520, however an alternative and improved design was pursued. After many trials an airbrush based on Bernoulli's effect was designed and built.

5.2.1 Bernoulli's effect

Bernoulli's effect governs the behavior of flowing (laminar flow) fluids. Bernoulli's equation will be found to be a consequence of energy conservation. Pressure (a force per unit area) can be thought of as an energy density (energy per unit volume). Conservation of energy requires that the sum of the work per unit volume done on the fluid (i.e. the pressure), the kinetic energy per unit volume of the fluid, and potential energy per unit volume of the fluid be constant. Figure 5.1 shows a fluid flowing from region 1 to region 2. Conservation

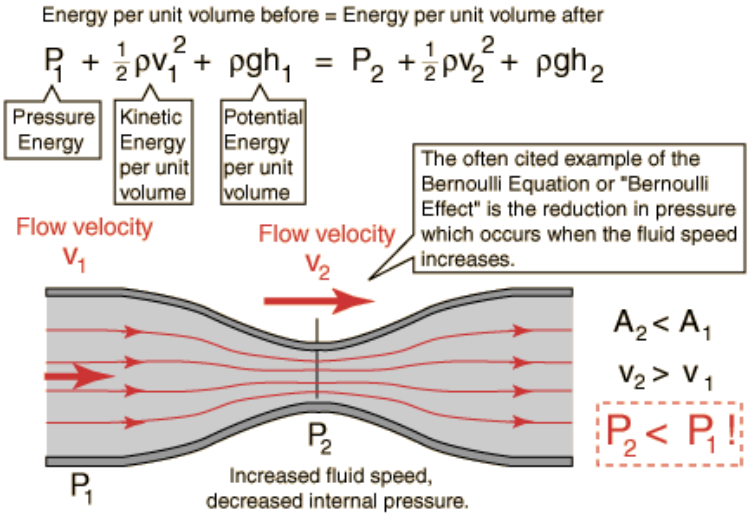

Figure 5.1: Fluid flow and Bernoulli's effect.

of energy leads to Bernoulli's equation:

$$p_1 + \frac{1}{2}\rho v_1^2 + \rho g h_1 = p_2 + \frac{1}{2}\rho v_2^2 + \rho g h_2, \tag{5.1}$$

where p is pressure, ρ is density, v is velocity, $g = 9.8\ \mathrm{ms}^{-2}$ is the acceleration due to gravity, and h is height. The subscripts "1" and "2" denote two regions of interest. If a fluid is flowing horizontally such that $h_1 = h_2$ then eq. 5.2 reduces to:

$$p_1 + \frac{1}{2}\rho v_1^2 = p_2 + \frac{1}{2}\rho v_2^2, \tag{5.2}$$

which implies that if $v_1 > v_2$, then necessarily $p_1 < p_2$. Suppose that air above a horizontal surface flows faster than the air below it, this difference in airspeed causes the pressure above the surface to be lower than the pressure below it producing lift. [23]

5.3 Airbrush Design

A cross-section of the airbrush design based on this Bernoulli's effect is shown in the Fig. 5.2. At the tip of the airbrush pictured fast air flows horizontally through a brass tube over a tip connected to a long teflon tube whose other end is immersed in paint in the paint can. The air in the teflon tube is stationary and as a result a low pressure region is created directly

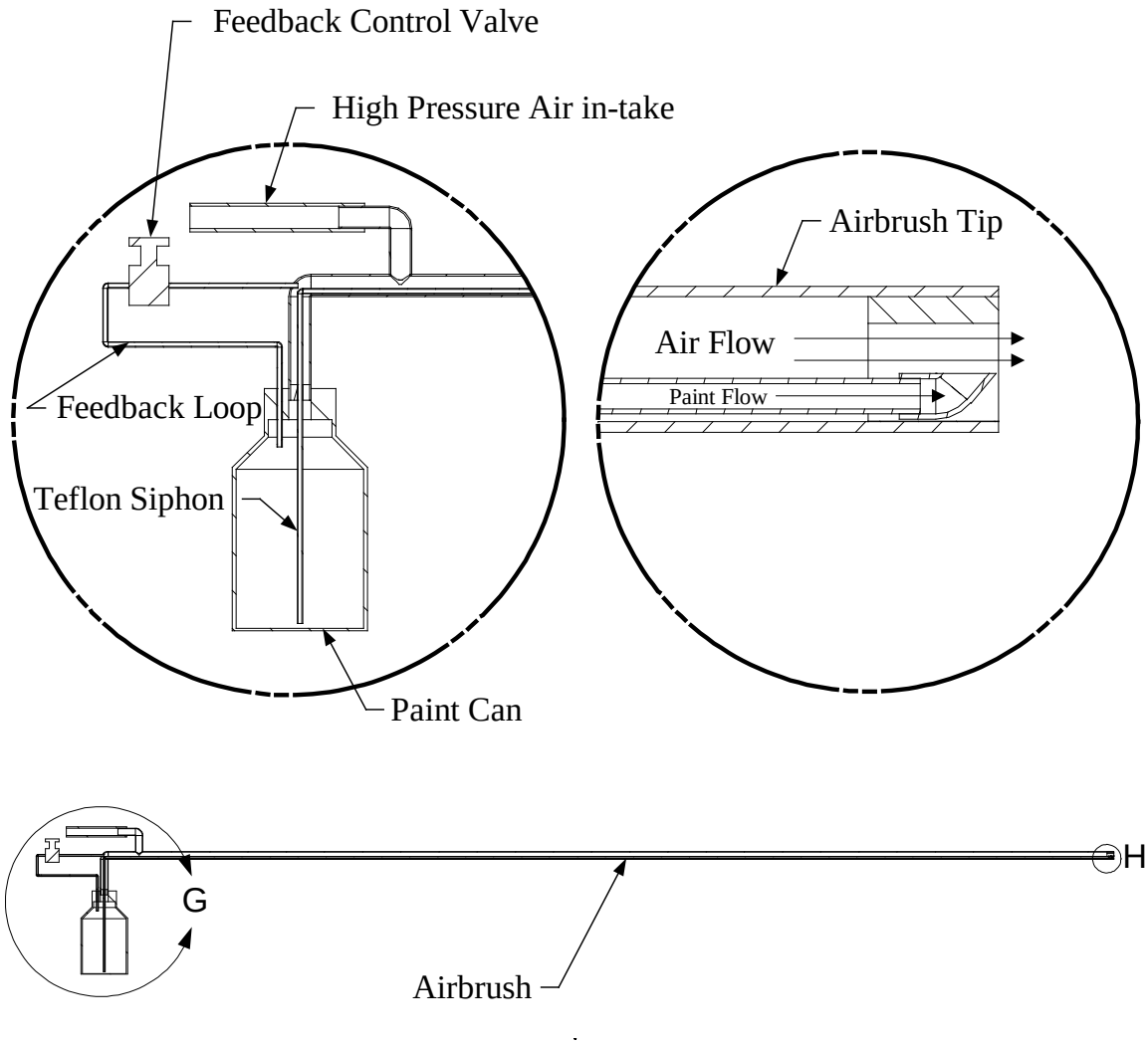

Figure 5.2: Schematic drawing of the cross-section of the final airbrush design based on Bernoulli's effect.

above the the tip at the end of the brass tube. This low pressure region causes the air to be sucked out of the teflon tube which in turn causes the paint to flow up the teflon tube towards the tip of the airbrush. When paint reaches the tip of teflon tube it mixes with the fast flowing air and is sprayed as a mist.

Feedback Loop

As with the first design, when is airbrush is used to spray water it works extremely well using only the Bernoulli effect. However, because of the high viscosity of the Eljen-520 the paint flows up the teflon tube to a certain point and then gets "stuck". To compensate for the high viscosity of the paint a feedback loop was incorporated into the airbrush design as can be seen in figure 5.2. This feedback loop diverts a portion of the high pressure air intake directly into the paint can. This process pressurizes the paint can and helps to "push" the paint through the teflon tube while the Bernoulli effect "pulls" the paint through. The

feedback loop is equipped with a valve so that the pressure diverted into the paint can be continuously adjusted from zero to some maximum value. Note that the maximum pressure inside is controlled by the diameter and length of the tube used to connect the paint can to the airflow. This strategy of incorporating a feedback loop proved to be extremely effective.

A digital photograph of the actual airbrush used to paint prototype detector cells is shown in Fig. 5.3.

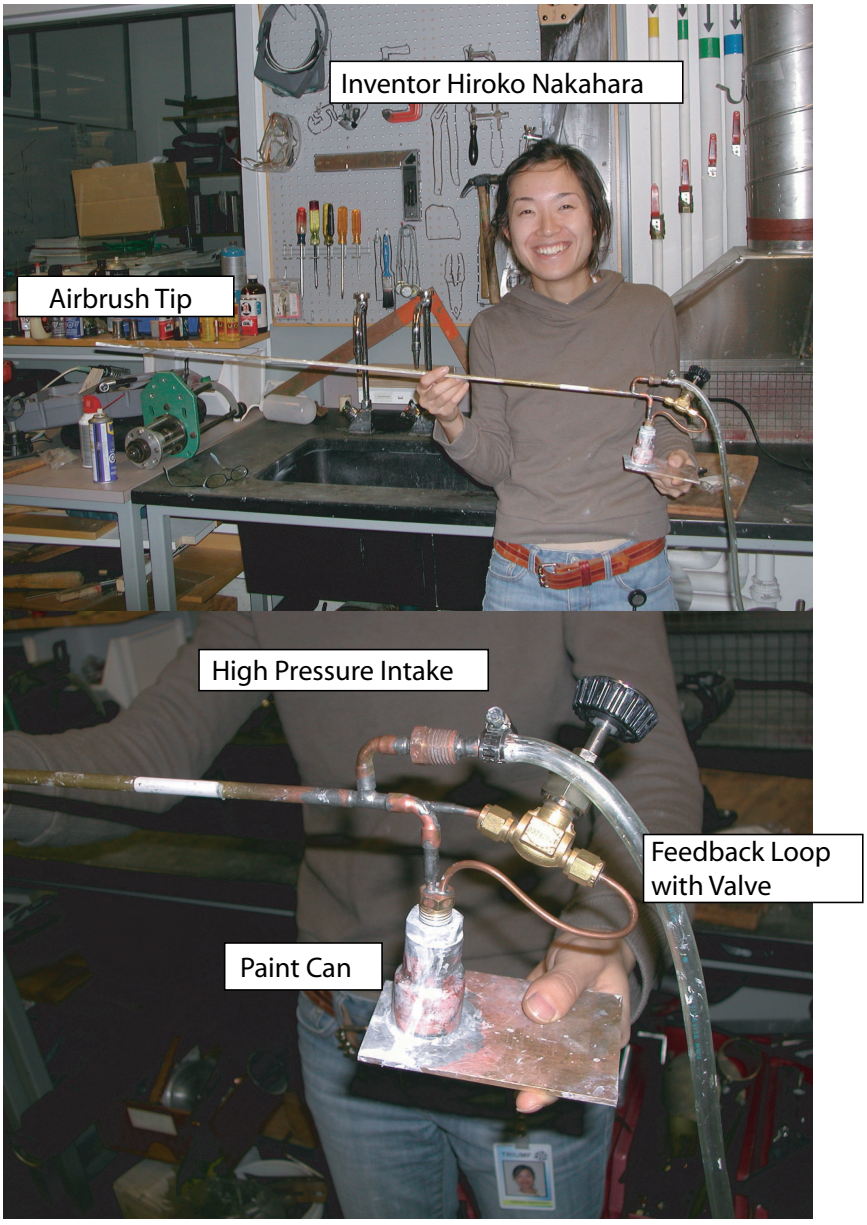

Figure 5.3: Digital photograph of inventor Hiroko Nakahara and the airbrush.

5.4 Painting with Eljen-520

Using the custom airbrush the inner walls of the polypropylene detector cells were coated. First the paint can was loaded with fresh Eljen-520 paint. The recipe for mixing the paint is two parts by weight of the white paint base (part A) and one part hardener (part B). Once mixed, the paint should be used within 30-60 minutes before the paint begins to harden. The long brass tube of the airbrush was inserted into the to 50 cm long detector cell. With the valve of the feedback loop fully opened the high pressure are supply was turned on. It takes about 15 seconds for the paint to flow up the long teflon tube. Once paint begins spraying out of the tip the airbrush is pulled through the detector cell at a constant speed. It was found that the optimal coating was applied when the airbrush was pulled through a 50 cm cell in 90 seconds. To ensure a uniform coat of paint a least three coats of paint are recommended. The cell should be left to dry at least 24 hours between coats. It is also a good idea to alternate the end of the cell that tip of the airbrush is inserted into for each coat. The cell can also be rotated by 180° along its long axis for consecutive coats. These procedures will promote a uniform coating. For example, if the airbrush sprays slightly upwards, then rotating the airbrush will prevent the "top" of the cell from having a thicker coating of paint.

It is essential that the paint can and teflon tube of the airbrush be cleaned after use well before the Eljen-520 paint has hardened. The paint readily dissolves in acetone so the recommended cleaning procedure is to spray acetone through the airbrush. First the paint can is emptied of excess paint and rinsed with acetone. Then the can is filled with acetone and reattached to the airbrush. The feedback valve is sealed off because acetone flows sufficiently well that the Bernoulli effect is enough to pull it through the teflon tube. Spraying two full cans of acetone through the airbrush will do a good job of cleaning out the Eljen-520.

5.5 Sanding

In general the coatings applied using the airbrush were found to be a great improvement when compared to the coatings from the previous technique using the sponges. However, it was found that the paint still tended to migrate away from the corners of the detector cell during the drying process. To solve this problem the inner surface of the detector cells were roughened and then cleaned prior to applying the first coat of paint. The inner surfaces roughed by taping sandpaper to a long (> 75 cm) square aluminum rod that can be inserted into the polypropylene cell. The two ends of the aluminum rod were clamped in vices and the cell was vigorously run back and forth over the sandpaper while applying pressure. All four sides were sanded and special effort was made to roughen the inner corners of the cell. It was found that 180 grit sandpaper gave the desired roughness. Figure 5.4 shows the surface of a cell before and after sanding with 180 grit sandpaper. After sanding the tubes were cleaned by repeatedly (4-5 times) pushing sponges soaked in ethonal or acetone through the cell using a long rod. The sanding and cleaning technique effectively stopped the paint from migrating from the cell corners during the drying process. After applying three coats of paint several detector cells were cut along their length using a Dremel tool with a cut-off wheel allowing for a detailed inspection of the coated surfaces of the cell. It was observed that the coatings were continuous and uniform, moreover, the paint was stuck

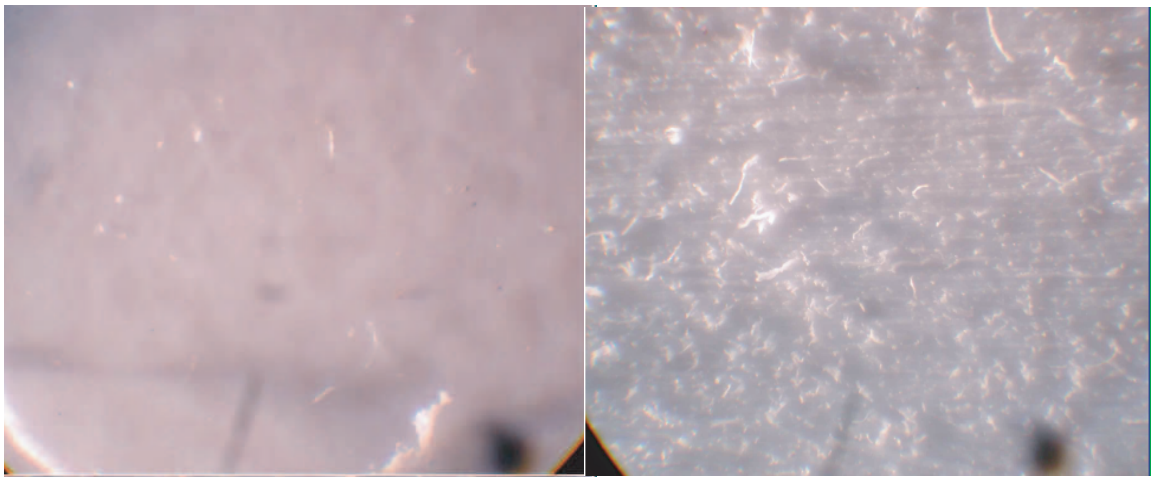

Figure 5.4: Digital photograph of the surfaces of polypropylene cell before (left) and after (right) sanding with 180 grit sandpaper.

to the surface of the cell extremely well.

The sanding procedure as describe above is probably not a reasonable option when building the FGD for the T2K project which will have approximately 6000 individual cells. One could imagine developing a sandblasting technique to roughen the inner surfaces of the cells prior to painting.

5.6 Light Output Measurement

The main purpose of painting the detector cell is to protect the polypropylene from chemical attack by the QSA in the liquid scintillator solution. To test the effectiveness of the paint the light output of prototype detectors made with cells with and without the protective coating must be tested over an extended period of time. Eight identical prototype detectors were constructed, four with three coats of Eljen-520 and four with no paint. All eight cells were filled with the same liquid scintillator solution (70% water, 25% QSA, 5% Triton-X 100 with biological inhibitors Germall Plus (0.5%) and zinc acetate (3000 ppm)).

The first light output measurement was performed as part of this thesis in November 2006 and the next is scheduled for April 2006. The results of the first light output measurement are shown in figure 5.5.

5.7 Conclusion

As can be seen the light output of the painted detectors increased by about 25%. Any other conclusions (a coat of paint protects the inner wall of the detector cell from the chemical attack from QSA) will have to wait for the results of the next light output measurements. As a final comment it is noted that coating the inner walls of the detectors with a reflective paint will also limit cross talk between neighbouring cells. That is, light produced in one

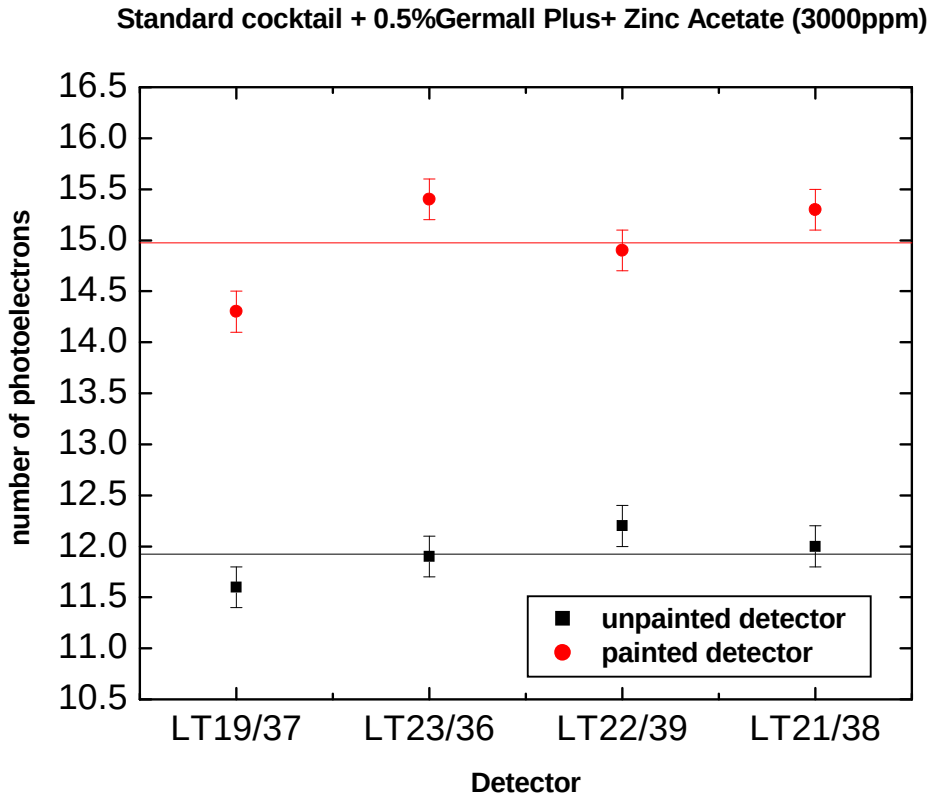

Figure 5.5: Light output of eight identical prototype detectors Four detector cell were given protective coatings of Eljen-520 (red points) and four detectors have no protective coatings (black points). The red (15.0) and black (11.9) lines are the average number of photoelectrons for the painted and unpainted light outputs respectively.

cell will more likely be reflected when incident on a cell wall rather than penetrating into the next cell.

Chapter 6

Outlook and Conclusions

In the first part of this thesis scintillator cocktails containing varying amounts of primary and secondary fluor were prepared and the light outputs of these solutions were measured. Using the analysis procedure outline in §3.5 the number of photoelectrons produced by the different solutions were extracted. It was determined that the maximum light output was obtained when the primary and secondary fluor concentrations found in the commercially available scintillator Quicksafe A are used.

The second part of this thesis was devoted to evaluating the suitability of adding various biological inhibitors to the liquid scintillator solution. A series of cloud point tests were carried out and it was found that adding 0.5% of the commercially available inhibitor Germall Plus did not reduce the cloud point temperature when compared to that of the standard solution. Solutions containing zinc compounds were also tested because zinc is a known fungicide. Adding 1000-3000 ppm by weight of zinc to the standard cocktail with Germall Plus using the zinc compounds zinc sulphate and zinc acetate did not noticeably reduce the cloud point temperature.

The light outputs of the solutions containing zinc and Germall Plus were also measured. It was found that adding just Germall Plus did not change the light output, however, adding high concentrations of zinc lowered the light output by up to 10%. If the zinc effectively prevents fungi growth in the liquid scintillator thereby extending the detectors lifetime a small reduction in light output may be acceptable. The solutions need to be watched over an extended period of time to look for any signs of biological growth. In addition the light outputs must be measured several more times to ensure the detector performance does not degrade with time.

In the third part of this project, an airbrush was built to coat the inner walls of the detector cells with a reflective paint to protect the cell from the chemical attack by the QSA. The light output of prototype detectors coated with paint were measured and was found to be 25% higher than unpainted detectors. Again, these light output measurements must be repeated in the future to ensure the detector performance does not deteriorate.

The current model of our airbrush was designed to paint prototype detector cells that are 50 cm long. However, the real fine grained detector used in T2K will be made of 30 sheets (1 cm $\times$ 200 cm $\times$ 200 cm) with 200 detector cells per sheet. A 2 m long version of the airbrush needs to be made and tested. Currently, when painting the inside of the 50 cm detector cell, the air brush is pulled through the detector by hand over a 90 second time interval. To paint approximately 6000 tubes, a method of automating this process is needed. The sanding procedure as described in §5.5 is probably not a reasonable option when building the FGD for the T2K project. Perhaps a sandblasting technique could be used to roughen the inner surfaces of the cells prior to painting.

Appendix A

Components of the Prototype Detector

A.1 Scintillation Detection

In particle physics scintillator detectors are common tools to observe charged particles such as protons and electrons, ultraviolet light, and other ionizing radiation. The scintillation detectors are composed of a scintillator and an amplifying device such as a photomultiplier tube (PMT). There are six different types of scintillator materials; organic crystals, organic liquids, plastics, inorganic crystals, gases, and glasses. [19, 24]

The two FGDs in the T2K near detector use two different scintillator materials. One uses a plastic material and the the other uses an organic liquid. The plastic scintillator is good because of its ease of use and flexibility. The shape and the size of the plastic material can be easily adapted from a thin film to very large sheets. Plastic scintillators are very common and commercially available from a number of distributors. The plastic FGD consists of polystyrene infused with the fluor PPO (1%) and POPOP (0.1%). [19, 22]

A liquid scintillator FGD was also included in the T2K near detector. This FGD has a high water content so that the neutrino interactions in this detector are the same as those in the Cherenkov far detector Super-Kamiokande. A liquid scintillator solution generally contains at least one type of organic solvent, a scintillator, and a fluor. [3].

In any scintillator detector the sequence of events that ultimately lead to detection are the same. As the radiation passes through the scintillator it excites the molecules of the scintillator. When the excited molecules return to the original state, the extra energy is transferred to a primary fluor as light. The primary fluor re-emits the light at a new wavelength compatible with the PMT and the light is detected. In some cases a secondary fluor is needed to further adjust the wavelength of the light emitted by the primary fluor. PPO is commonly used as a primary fluor and POPOP is a common secondary fluor. Quicksafe A (QSA), supplied by Zinsser Analytic, is the liquid scintillator used in this project which uses PPO as a primary fluor and bis-MSB as a secondary fluor. [19, 24]

A.2 Wavelength Shifting Fiber

In addition to a secondary fluor a wavelength shifting fiber (WSF) can also be used to further adjust the wavelength of the light prior to detection by the PMT. Once the light is emitted by the secondary fluor the light is collected by the WSF. The WSF fiber consists of three layers: a polystyrene core, a PMMA inner coat, and a fluorinated polymer as an outer coating. The outer coating of the WSF must resist chemical attack from the surrounding

liquid scintillator. The index of refractions of the three layers are 1.59, 1.49, and 1.42 with the innermost layer having the highest index of refraction and the outermost the lowest. Once inside the WSF the light is trapped and transferred to the PMT due to total internal reflection. Light that travels down the fibre away from the PMT is reflected back towards the PMT by a mylar reflector glued to the opposite end of the fibre. [22, 25]

A.3 Photomultiplier Tube (PMT)

In the prototype detectors tested in this thesis the light produced by the liquid scintillator is detected by a PMT. A schematic diagram of a PMT is given in Fig. A.1. The photomultiplier

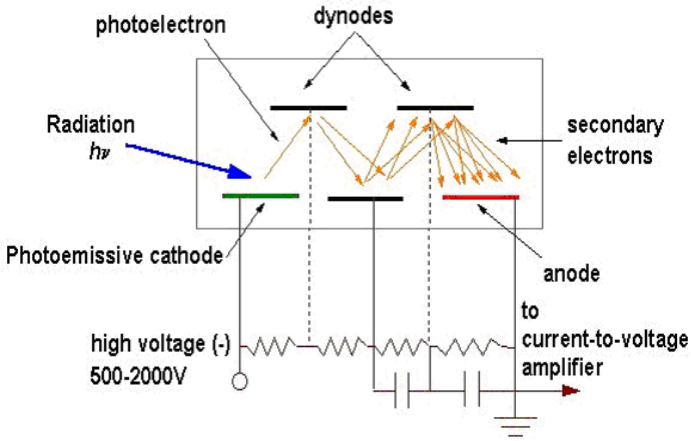

Figure A.1: Schematic diagram of a simple photomultiplier tube.

is a vacuum tube consisting of a photo-cathode, dynodes, and an anode. When light enters the tube and hits the photo-cathode electrons are liberated via the photoelectric effect. A potential difference is maintained across the cathode and first dynode that accelerates the liberated electron towards the dynode. When the energetic electron hits the dynode it liberates many additional electrons. These electrons are accelerated to the second dynode (all dynodes have a higher voltage relative to the dynode one step before) and each liberates many more electrons. In this way an avalanche of electrons is generated. When the electron avalanche reaches the anode a current is produced. The current is proportional to the intensity of the light impinging on the photo-cathode. If this anode current is passed through an anode resistor the light intensity is proportional to the voltage across that resistor. [9]

A.4 Matraplast

Matraplast is a white polypropylene sheet made up of 200 tubes of inner dimensions 8.5 mm $\times$ 8.5 mm $\times$ 2455 mm and a wall thickness of 0.75 mm. A drawing of matarplast sheets can be found in Fig. 2.3. The Matraplast boards are inexpensive and commercially produced and are commonly used as a billboard signs at construction sites. [proposal]. The polypropylene resists chemical attack by the QSA in the liquid scintillator solution relatively well, however, over long periods of time the water-base scintillator solution was observed to change from

clear to a yellowish colour and is thought to be due to chemical reactions between the polypropylene and an ingredient of QSA. Over coming this problem is the topic of chapter 5 of this thesis. [22]

Appendix B

Table with Errors

Please find attached printouts of the tables shown in table 3.1 and 3.2 that include the error estimates that were omitted in the main text of the report.

Run #	Amount of Fluor (%) (Standard QSA = 100)	Pedestal(ch)	error (ch)	1 p.e.peak (ch)	error (ch)	1 p.e peak (ch/p.e)	error (ch/p.e)	Muon centroid (ch)	error (ch)	Unconrrected Muon (p.e.#)	error (p.e.#)	Conrrected Muon (p.e.#)	error (p.e.#)
711	100	125.9	0.10	153	3	27	3	589	2	15.1	0.33	15.1	0.3
712	~	~	~	~	~	~	~	~	~	~	~	~	~
713	50	126.0	0.2	155.9	0.3	29.9	0.4	517.8	0.6	12.76	0.28	12.80	0.3
714	80	126.0	0.3	160.6	0.7	34.5	0.8	572	2	14.5	0.32	14.5	0.3
715	90	125.9	0.2	153	3	27	3	464	1.9	11.0	0.25	14.7	0.4
716	unknown												
717	90	108.9	0.2	155	3	46	3	428	1.9	10.39	0.24	13.9	0.3
718	~	~	~	~	~	~	~	~	~	~	~	~	~
719	100	110.5	0.2	141	1.2	31	1.3	462	3	11.5	0.26	15.3	0.4
720	100	110.8	0.2	144	1.0	33	1.0	451	2	11.1	0.25	14.8	0.4
721	80	112.6	0.2	143.1	0.4	30.5	0.4	417.9	0.5	9.95	0.22	13.3	0.3
722	90	112.7	0.2	143.2	0.4	30.5	0.5	429.1	0.5	10.31	0.23	13.8	0.3
723	150	113.3	0.3	144.1	0.4	30.8	0.5	455.0	0.5	11.13	0.24	14.9	0.3
724	125	112.9	0.2	145	1.2	31.6	1.2	457	1.1	11.20	0.25	14.9	0.4
725	100 (H.M. QSA)	112.8	0.3	144.9	0.3	32.0	0.4	370.9	0.7	8.41	0.18	11.2	0.3
726	nanosuspension	~	~	~	~	~	~	~	~	~	~	~	~
727	200	113.5	0.3	147.6	0.5	34.1	0.5	446	1.2	10.85	0.24	14.5	0.3
728	100 (H.M. QSA)	113.2	0.3	142	3	29	3	454	1.3	11.11	0.25	14.8	0.4
730	90	112.4	0.2	144	1.0	32	1.0	447	1.3	10.90	0.24	14.6	0.3

Run #	amount of bis-MSB (the amount of MSB in Standard QSA = normal bis-MSB)	Pedestal(ch)	Pedestal error (ch)	1 p.e.peak (ch)	1 p.e.peak error (ch)	1 p.e peak (ch/p.e)	1 p.e peak error (ch/p.e)	Muon centroid (ch)	Muon centroid error (ch)	Unconrrected Muon (p.e.#)	Unconrrected Muon error(p.e.#)	Conrrected Muon (p.e.#)	Conrrected Muon error(p.e.#)
711	1 x normal bis-MSB	125.9	0.1	153.2	3.3	27.4	3.3	588.5	1.5	15.07	0.11	15.1	0.1
729	2 x normal bis-MSB	112.9	0.2	144.9	1.6	32.0	1.7	461.2	1.9	11.35	0.10	15.1	0.2
731	3 x normal bis-MSB	113.1	0.2	144.6	0.3	31.5	0.4	464.3	0.5	11.44	0.08	15.3	0.2

Table B.1: Measured number of photoelectrons with errors from muon centroid peaks for standard (70/25/5) cocktail solutions with varying concentrations of primary fluor. The solutions tested in this table were prepared by mixing standard cocktails of homemade QSA (no fluor) with standard cocktails made with commercial QSA. For solutions with greater than 100% fluor appropriate amounts of primary and secondary fluor were added to the cocktail made with commercial QSA.

Appendix C

Table with Errors

Please find attached printouts of table 4.9 from §4.2.3 that include the error estimates that were omitted in the main text of the report.

Run #	Type of Soluton	Cell	Reflector	Pedestal(ch)	error	1 p.e. peak (ch)	error	1 p.e. peak (ch/p.e.)	error	Muon centroid (ch)	error	Uncorrect ed Muon (p.e. #)	error	Correced Muon (p.e. #)	error
756	Control (no inhibitor)	Painted	On	103.1	0.2	128.5	0.7	25.4	0.8	457.6	0.8	14.0	0.2	14.0	0.2
757	Control + Germall Plus(0.5%)	Painted	On												0.0
758	Control + Germall Plus(0.5%)	Painted	On	102.6	0.3	125.9	0.6	23.3	0.6	443.5	0.6	14.6	0.2	14.6	0.2
759	Control	Unpainted	On	102.5	0.2	125.0	0.6	22.5	0.7	501.9	1.0	18.6	0.3	18.6	0.3
760	Control	Unpainted	On	102.7	0.2	125.6	0.5	23.0	0.5	491.3	1.1	18.1	0.3	18.1	0.3
761	Control	Unpainted	On	102.7	0.2	124.9	1.6	22.2	1.6	485.7	1.0	17.8	0.3	17.8	0.3
762	Control	Unpainted	On	102.6	0.4	125.5	1.4	22.9	1.4	486.9	1.0	17.9	0.3	17.9	0.3
763	Control + Germall Plus(0.5%)	Unpainted	On	102.3	0.3	127.5	1.0	25.2	1.0	501.5	0.7	18.6	0.3	18.6	0.3
764	Control + ZnAc	Unpainted	On	101.9	0.3	124.6	1.1	22.7	1.1	496.3	0.7	18.3	0.3	18.3	0.3
765	Control + ZnAc + Germall Plus(0.5%)	Unpainted	On	102.3	0.3	126.2	1.1	23.8	1.1	502.9	1.0	18.6	0.3	18.6	0.3
766	Control + ZnAc + Germall Plus(0.5%)	Unpainted	Off	102.5	0.3	128.1	1.3	25.6	1.3	365.6	2.4	12.2	0.2	18.6	0.5
767	Control + ZnAc + Germall Plus(0.5%)	Unpainted	Off	101.7	0.2	125.1	1.4	23.3	1.5	358.6	1.0	11.9	0.2	18.2	0.5
768	Control + ZnCl2	Unpainted	Off	103.0	0.4	125.1	0.8	22.1	0.9	371.4	0.7	12.5	0.2	19.0	0.5
769	Control + ZnCl2 + Germall Plus(0.5%)	Unpainted	Off	102.7	0.3	123.7	1.2	21.0	1.3	364.4	0.9	12.2	0.2	18.5	0.5
770	Control + ZnSO4	Unpainted	Off	102.5	0.3	123.6	1.2	21.1	1.2	375.0	1.1	12.7	0.2	19.3	0.5
771	Control + ZnSO4 + Germall Plus(0.5%)	Unpainted	Off	102.5	0.3	123.2	0.6	20.6	0.7	354.9	0.6	11.7	0.2	17.9	0.5
772	Distilled water	Unpainted	Off	102.0	0.1	123.5	0.3	21.5	0.3						
773	Control	Unpainted	Off	102.0	0.3	122.6	2.4	20.5	2.5	348.4	0.8	11.5	0.2	17.4	0.5
774	Control	Unpainted	Off	101.9	0.4	123.1	0.6	21.2	0.7	354.2	0.6	11.7	0.2	17.9	0.5
775	Control + ZnSO4	Unpainted	Off	101.5	0.3	125.0	1.2	23.6	1.2	355.5	1.0	11.8	0.2	18.0	0.5
776	Control + ZnSO4 + Germall Plus(0.5%)	Unpainted	Off	101.5	0.3	123.1	1.1	21.5	1.1	353.6	0.8	11.7	0.2	17.9	0.5

Table C.1: This full table with error bars includes the results of the light output measurements the standard 70/25/5 cocktail without or with zinc compounds (100 ppm) and Germall Plus (0.5%) (G) as biological inhibitors. The zinc compounds added into this standard 70/25/5 cocktail, used as a control solution (C), are zinc acetate(ZA), zinc chloride (ZC), and zinc sulfate(ZS).

Appendix D

Mathematica Analysis of Light Output Data

Please find attached a printout of the Mathematica notebook used to analysis the muon light output data set shown in Fig. 3.3.

```
Clear["Global`*"]
Needs["Statistics`NonlinearFit`"]
Needs["Statistics`LinearRegression`"]
Needs["Statistics`ContinuousDistributions`"]
Needs["Statistics`DescriptiveStatistics`"]
Needs["Graphics`Graphics`"]
Date[]
```

```
{2006, 1, 11, 13, 14, 7}
```

Weighted fit of pedestal (gauss1), 1 p.e. peak (gauss2), and muon centroid (gauss3) to estimate peaks of both pedestal and muon centroid

Set the directory and import the data

```
SetDirectory["c:/Sapphire/hiro/T2K/hiro data"]
```

```
c:\Sapphire\hiro\T2K\hiro data
```

```
rawdata = Import["run713_adc3mu.dat"];
```

```
xaxis = Transpose[rawdata][[1]];
```

```
yaxis = Transpose[rawdata][[2]];
```

Set the error as the squareroot of the number of counts

```
error = Sqrt[yaxis];
```

```
data = Transpose[{xaxis, yaxis}];
```

```
datawerr = Transpose[{xaxis, yaxis, error}];
```

Plot the raw data

```
ErrorListPlot[datawerr, PlotRange → All, Axes → False, Frame → True]
```

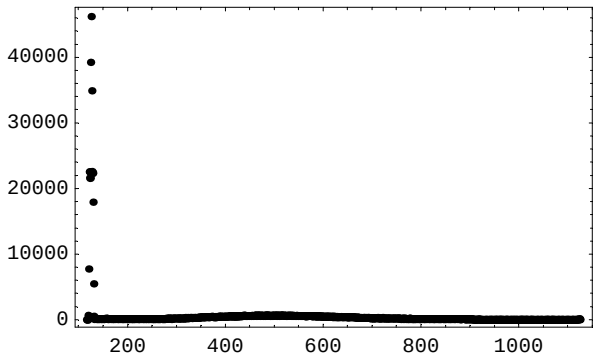


```
- Graphics -
```

Create three guassian distributions

```
gauss1 = Sqrt[A1^2] / (Sqrt[w1^2] Sqrt[π / 2]) Exp[-2 (x - xc1)^2 / w1^2]
```

$$\frac{\sqrt{A1^2}\ e^{-\frac{2\,(x-xc1)^2}{w1^2}}\ \sqrt{\frac{2}{\pi}}}{\sqrt{w1^2}}$$

```
gauss2 = Sqrt[A2^2] / (Sqrt[w2^2] Sqrt[π / 2]) Exp[-2 (x - xc2)^2 / w2^2]
```

$$\frac{\sqrt{A2^2}\ e^{-\frac{2\,(x-xc2)^2}{w2^2}}\ \sqrt{\frac{2}{\pi}}}{\sqrt{w2^2}}$$

```
gauss3 = Sqrt[A3^2] / (Sqrt[w3^2] Sqrt[π / 2]) Exp[-2 (x - xc3)^2 / w3^2]
```

$$\frac{\sqrt{A3^2}\ e^{-\frac{2\,(x-xc3)^2}{w3^2}}\ \sqrt{\frac{2}{\pi}}}{\sqrt{w3^2}}$$

Create a model that is the sum of three Gaussians. This model will be used to obtain initial estimates for the parameters of the three Gaussian peaks to be used later in the fitting routine.

```
model = gauss1 + gauss2 + gauss3 + Sqrt[offset^2]
```

$$\sqrt{offset^2} + \frac{\sqrt{A1^2}\ e^{-\frac{2\,(x-xc1)^2}{w1^2}}\ \sqrt{\frac{2}{\pi}}}{\sqrt{w1^2}} + \frac{\sqrt{A2^2}\ e^{-\frac{2\,(x-xc2)^2}{w2^2}}\ \sqrt{\frac{2}{\pi}}}{\sqrt{w2^2}} + \frac{\sqrt{A3^2}\ e^{-\frac{2\,(x-xc3)^2}{w3^2}}\ \sqrt{\frac{2}{\pi}}}{\sqrt{w3^2}}$$

Perform the weighted fit and plot the data with the result. The estimates came from ORIGIN (fit using origin to get these numbers).

```
fit1 = NonlinearRegress[data, model, x,
  {{A1, 3*^5}, {xc1, 126}, {w1, 6}, {A2, 1200}, {xc2, 156}, {w2, 13}, {A3, 1.8*^5},
   {xc3, 510}, {w3, 260}, {offset, 0.1}}, ShowProgress → True, Weights → 1 / error^2,
  RegressionReport → {BestFit, BestFitParameters, ParameterTable}]
```

```
Iteration:1 ChiSquared:1.8585986918234325`*^6
  Parameters:{300000., 126., 6., 1200., 156., 13., 180000., 510., 260., 0.1}

Iteration:2 ChiSquared:187785.67215784904` Parameters:
  {224735., 125.949, 5.16755, 2250.94, 155.658, 21.6496, 201701., 516.11, 280.945, 5.70063}

Iteration:3 ChiSquared:41786.20095694978` Parameters:
  {238480., 125.971, 4.47173, 2486.32, 154.956, 21.9395, 202702., 517.687, 281.903, 4.70303}

Iteration:4 ChiSquared:35855.34593578374` Parameters:
  {233281., 126.078, 4.24102, 2410.58, 156.003, 18.9152, 202735., 518.671, 280.24, 3.98146}

Iteration:5 ChiSquared:35789.6474492641` Parameters:
  {232050., 126.08, 4.29193, 2493.46, 155.81, 20.0869, 202710., 519.121, 279.042, 3.54984}

Iteration:6 ChiSquared:35773.03977581551` Parameters:
  {231965., 126.087, 4.26602, 2476.21, 155.842, 19.8071, 202732., 518.906, 279.342, 3.61206}

Iteration:7 ChiSquared:35769.023713444345` Parameters:
  {231994., 126.084, 4.2806, 2482.27, 155.845, 19.8597, 202722., 518.988, 279.173, 3.57689}

Iteration:8 ChiSquared:35767.57452919262` Parameters:
  {231971., 126.086, 4.27228, 2481.08, 155.834, 19.878, 202725., 518.945, 279.251, 3.59643}

Iteration:9 ChiSquared:35767.14582926985` Parameters:
  {231982., 126.085, 4.27696, 2480.87, 155.845, 19.8462, 202724., 518.967, 279.208, 3.58535}

Iteration:10 ChiSquared:35767.00174852761` Parameters:
  {231975., 126.085, 4.27429, 2481.39, 155.837, 19.8736, 202724., 518.955, 279.231, 3.59151}

Iteration:11 ChiSquared:35766.95637443325` Parameters:
  {231979., 126.085, 4.27581, 2480.93, 155.842, 19.854, 202724., 518.962, 279.218, 3.58802}
```

$$\{\text{BestFit} \to 3.58998 + 579.284\, e^{-0.000025652\,(-518.958+x)^2} + 99.6513\, e^{-0.0050672\,(-155.839+x)^2} + 43296.6\, e^{-0.109438\,(-126.085+x)^2},\ \text{BestFitParameters} \to \{A1 \to 231977.,\ xc1 \to 126.085,\ w1 \to 4.27495,\ A2 \to 2481.27,\ xc2 \to 155.839,\ w2 \to 19.8669,\ A3 \to 202724.,\ xc3 \to 518.958,\ w3 \to 279.225,\ \text{offset} \to 3.58998\},\ \text{ParameterTable} \to$$

	Estimate	Asymp. SE	TStat	PValue
A1	231977.	2893.47	80.1726	$9.99691521551 \times 10^{-437}$
xc1	126.085	0.0276137	4566.03	$4.21491317554 \times 10^{-2154}$
w1	4.27495	0.0303042	141.068	$1.42569713435 \times 10^{-660}$
A2	2481.27	388.367	6.38898	2.55951×10^{-10}
xc2	155.839	1.72472	90.3559	$3.40819867716 \times 10^{-482}$
w2	19.8669	3.4027	5.83858	7.11967×10^{-9}
A3	202724.	2845.94	71.2329	$3.48635465561 \times 10^{-393}$
xc3	518.958	1.97329	262.992	$1.52940703843 \times 10^{-922}$
w3	279.225	3.43056	81.3935	$2.12263933182 \times 10^{-442}$
offset	3.58998	0.948896	3.78333	0.000163973

}

```
plot1 = DisplayTogether[ErrorListPlot[datawerr], Plot[BestFit /. fit1, {x, 0, 1200},
    PlotStyle → {RGBColor[1, 0, 0], Thickness[.002]}], PlotRange → All]
```

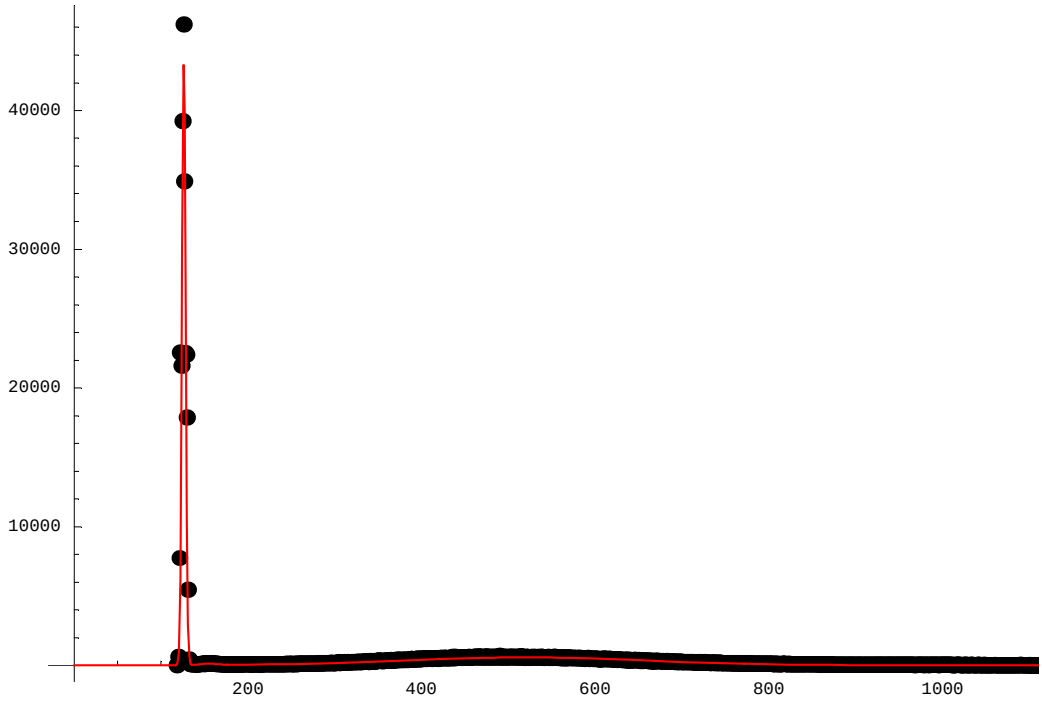


```
- Graphics -
```

Weighted fit of pedestal (gauss 1)

This is just plotting pedestal with error to see where we should cut a pedestal from other data.

```
ErrorListPlot[datawerr,
 PlotRange → {{115, 140}, {0, 50000}}, Axes → False, Frame → True]
```

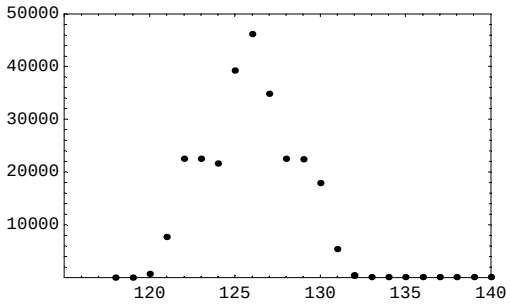


```
- Graphics -
```

We counted the number of points in pedestal and take those data in x and y. "pedestal" is for fitting and "pedestalwerr" is for plotting with error.

```
points = 13;
pedestal = Transpose[{Take[xaxis, points], Take[yaxis, points]}];
pedestalwerr =
  Transpose[{Take[xaxis, points], Take[yaxis, points], Take[error, points]}];
errorg1 = Take[error, points];
```

```
gauss1 = Sqrt[A1^2] / (Sqrt[w1^2] Sqrt[π / 2]) Exp[-2 (x - xc1)^2 / w1^2]
```

$$\frac{\sqrt{A1^2}\ e^{-\frac{2\,(x-xc1)^2}{w1^2}}\ \sqrt{\frac{2}{\pi}}}{\sqrt{w1^2}}$$

This is the model for fitting the pedestal peak to a single Gaussian with an offset. Note that Sqrt[A^2], etc. assures that the area is always a positive number.

```
modelg1 = gauss1 + Sqrt[offset^2]
```

$$\sqrt{offset^2} + \frac{\sqrt{A1^2}\ e^{-\frac{2\,(x-xc1)^2}{w1^2}}\ \sqrt{\frac{2}{\pi}}}{\sqrt{w1^2}}$$

These are the results (parameters) from first fitting for three peaks.

```
results1 = ParameterTable /. fit1
```

	Estimate	Asymp. SE	TStat	PValue
A1	231977.	2893.47	80.1726	$9.99691521551 \times 10^{-437}$
xc1	126.085	0.0276137	4566.03	$4.21491317554 \times 10^{-2154}$
w1	4.27495	0.0303042	141.068	$1.42569713435 \times 10^{-660}$
A2	2481.27	388.367	6.38898	2.55951×10^{-10}
xc2	155.839	1.72472	90.3559	$3.40819867716 \times 10^{-482}$
w2	19.8669	3.4027	5.83858	7.11967×10^{-9}
A3	202724.	2845.94	71.2329	$3.48635465561 \times 10^{-393}$
xc3	518.958	1.97329	262.992	$1.52940703843 \times 10^{-922}$
w3	279.225	3.43056	81.3935	$2.12263933182 \times 10^{-442}$
offset	3.58998	0.948896	3.78333	0.000163973

Use the results from the first fit as estimates in this fit.

```
EstA1 = results1[[1, 1, 1]];
Estxc1 = results1[[1, 2, 1]];
Estw1 = results1[[1, 3, 1]];
Estoff1 = results1[[1, 10, 1]];
```

This is the weighted fit for the pedestal.

```
fit1g1 = NonlinearRegress[pedestal, modelg1, x,
  {{A1, EstA1}, {xc1, Estxc1}, {w1, Estw1}, {offset, Estoff1}},
  ShowProgress → True, Weights → 1 / errorg1^2,
  RegressionReport → {BestFit, BestFitParameters, ParameterTable}]
```

```
Iteration:1 ChiSquared:29905.913434497365` Parameters:{231977., 126.085, 4.27495, 3.58998}

Iteration:2 ChiSquared:29501.778098703136` Parameters:{233725., 126.111, 4.37732, -0.24469}

Iteration:3 ChiSquared:29452.506717925236` Parameters:{233649., 126.125, 4.33736, 0.392917}

Iteration:4 ChiSquared:29433.749539672568` Parameters:{233719., 126.125, 4.36048, -0.244311}

Iteration:5 ChiSquared:29412.40797909899` Parameters:{233676., 126.126, 4.3484, 0.0631234}

Iteration:6 ChiSquared:29409.52055057482` Parameters:{233681., 126.126, 4.3547, -0.0388191}

Iteration:7 ChiSquared:29405.953935572335` Parameters:{233679., 126.126, 4.35145, 0.00396812}

Iteration:8 ChiSquared:29405.825941889965` Parameters:{233678., 126.126, 4.3528, -0.00326679}

Iteration:9 ChiSquared:29405.54109492481` Parameters:{233678., 126.126, 4.35244, 0.000345756}

Iteration:10 ChiSquared:29405.530437871374` Parameters:{233678., 126.126, 4.35247, -0.000236116}
```

$$\{\text{BestFit} \to 0.0000561635 + 42837.2\, e^{-0.105574\,(-126.126+x)^2},\ \text{BestFitParameters} \to \{A1 \to 233678.,\ xc1 \to 126.126,\ w1 \to 4.35248,\ \text{offset} \to 0.0000561635\},\ \text{ParameterTable} \to$$

	Estimate	Asymp. SE	TStat	PValue
A1	233678.	29014.5	8.05384	0.000020979
xc1	126.126	0.315646	399.581	0.
w1	4.35248	0.481712	9.03544	8.26781×10^{-6}
offset	0.0000561635	86.2035	6.51522×10^{-7}	0.999999

$\}$

Plot the pedestal data with the fit

```
plotg1 = DisplayTogether[ErrorListPlot[pedestalwerr], Plot[BestFit /. fit1g1,
    {x, 115, 140}, PlotStyle → {RGBColor[1, 0, 0], Thickness[.002]}], PlotRange → All]
```

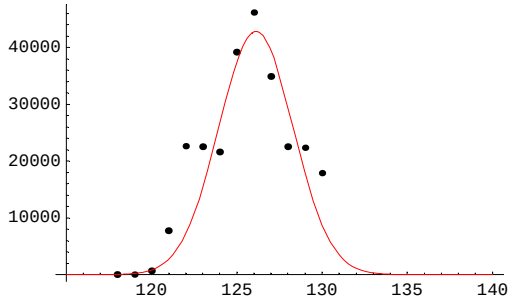


```
- Graphics -
```

Weighted fit of muon centroid (gauss 3)

Plot the 1 p.e. and centroid peaks together and cut the data

```
ErrorListPlot[datawerr, PlotRange → {{100, 1200}, {0, 750}}, Axes → False, Frame → True]
```

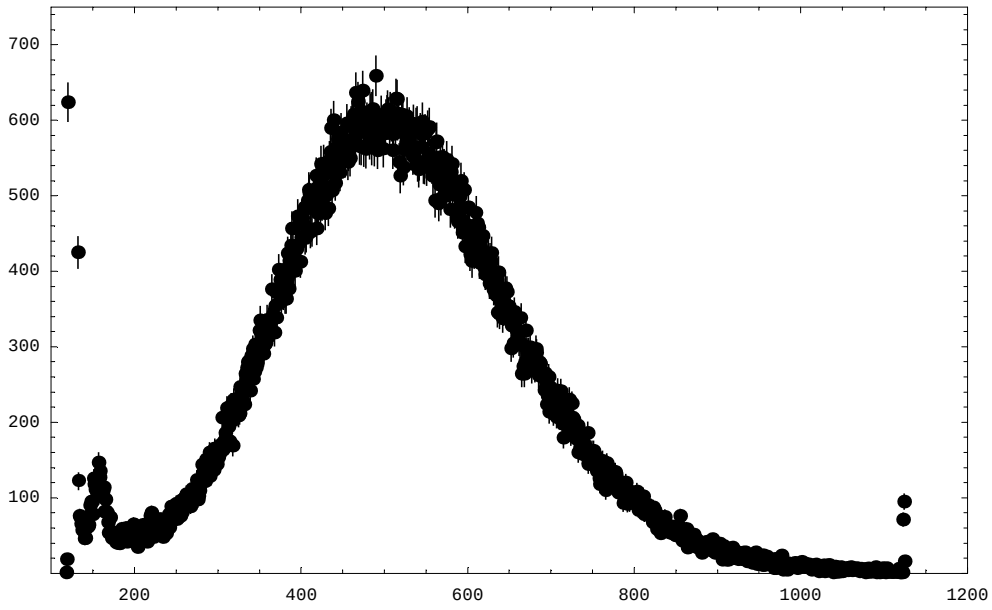


```
- Graphics -
```

```
data[[90]]
data[[700]]
```

```
{207, 53}
```

```
{817, 88}
```

This block of code makes a list of data that is just the centroid peak

```
points = 90;
point2 = 700;
muon = Transpose[{Take[xaxis, {points, point2}], Take[yaxis, {points, point2}]}];
muonwerr = Transpose[{Take[xaxis, {points, point2}],
    Take[yaxis, {points, point2}], Take[error, {points, point2}]}];
errorg3 = Take[error, {points, point2}];
```

Plot the centroid peak

```
ErrorListPlot[muonwerr, PlotRange → All, Axes → False, Frame → True]
```

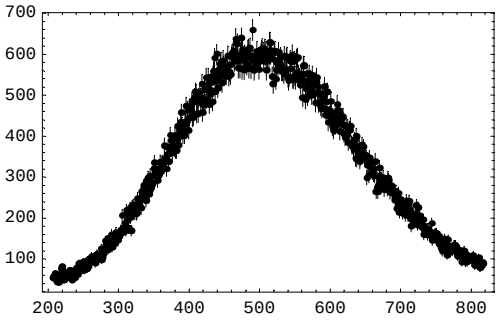


```
- Graphics -
```

Here is the model for the centroid peak

```
A3 =.
w3 =.
xc3 =.
gauss3 = Sqrt[A3^2] / (Sqrt[w3^2] Sqrt[π / 2]) Exp[-2 (x - xc3)^2 / w3^2]
```

$$\frac{\sqrt{A3^2}\ e^{-\frac{2\,(x-xc3)^2}{w3^2}}\ \sqrt{\frac{2}{\pi}}}{\sqrt{w3^2}}$$

```
modelg3 = gauss3 + Sqrt[offset^2]
```

$$\sqrt{offset^2} + \frac{\sqrt{A3^2}\ e^{-\frac{2\,(x-xc3)^2}{w3^2}}\ \sqrt{\frac{2}{\pi}}}{\sqrt{w3^2}}$$

Again use parameters from the first fit as starting points for this fit

```
results1 = ParameterTable /. fit1
```

	Estimate	Asymp. SE	TStat	PValue
A1	231977.	2893.47	80.1726	$9.99691521551 \times 10^{-437}$
xc1	126.085	0.0276137	4566.03	$4.21491317554 \times 10^{-2154}$
w1	4.27495	0.0303042	141.068	$1.42569713435 \times 10^{-660}$
A2	2481.27	388.367	6.38898	2.55951×10^{-10}
xc2	155.839	1.72472	90.3559	$3.40819867716 \times 10^{-482}$
w2	19.8669	3.4027	5.83858	7.11967×10^{-9}
A3	202724.	2845.94	71.2329	$3.48635465561 \times 10^{-393}$
xc3	518.958	1.97329	262.992	$1.52940703843 \times 10^{-922}$
w3	279.225	3.43056	81.3935	$2.12263933182 \times 10^{-442}$
offset	3.58998	0.948896	3.78333	0.000163973

```
EstA3 = results1[[1, 7, 1]];
Estxc3 = results1[[1, 8, 1]];
Estw3 = results1[[1, 9, 1]];
Estoff = results1[[1, 10, 1]];
```

```
fit1g3 = NonlinearRegress[muon, modelg3, x,
  {{A3, EstA3}, {xc3, Estxc3}, {w3, Estw3}, {offset, Estoff}},
  ShowProgress → True, Weights → 1 / errorg3^2,
  RegressionReport → {BestFit, BestFitParameters, ParameterTable}]
```

```
Iteration:1 ChiSquared:1678.267166704289` Parameters:{202724., 518.958, 279.225, 3.58998}

Iteration:2 ChiSquared:1505.508055800472` Parameters:{197415., 515.612, 270.751, 9.43939}

Iteration:3 ChiSquared:1499.0562762109203` Parameters:{194294., 515.278, 267.193, 13.9951}

Iteration:4 ChiSquared:1498.7386140470417` Parameters:{194133., 515.105, 266.945, 14.2356}

Iteration:5 ChiSquared:1498.7222333087211` Parameters:{193955., 515.095, 266.751, 14.49}

{BestFit → 14.4968 + 580.143 e^(-0.0000281087 (-515.085+x)^2), BestFitParameters →
  {A3 → 193950., xc3 → 515.085, w3 → 266.744, offset → 14.4968}, ParameterTable →
```

	Estimate	Asymp. SE	TStat	PValue
A3	193950.	2664.51	72.7902	0.
xc3	515.085	0.544315	946.299	$4.67089325690 \times 10^{-964}$
w3	266.744	2.60646	102.339	$4.98910437105 \times 10^{-385}$
offset	14.4968	3.73729	3.87897	0.000116363

}

Plot the centroid data with the new fit

```
plot1g3 = DisplayTogether[ErrorListPlot[muonwerr], Plot[BestFit /. fit1g3,
   {x, 180, 900}, PlotStyle → {RGBColor[1, 0, 0], Thickness[.002]}], PlotRange → All]
```

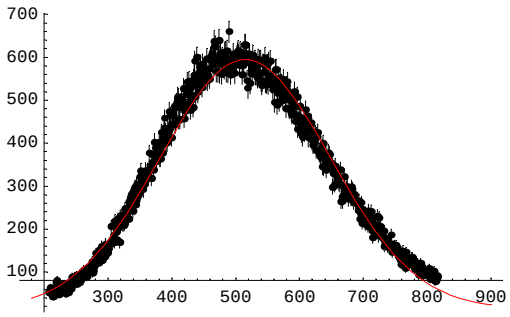


```
- Graphics -
```

Weighted fit of 1 photoelectron peak by using the weighted fit of muon centroid

Plot the 1 p.e. peak

```
ErrorListPlot[datawerr, PlotRange → {{130, 185}, {0, 200}}, Axes → False, Frame → True]
```

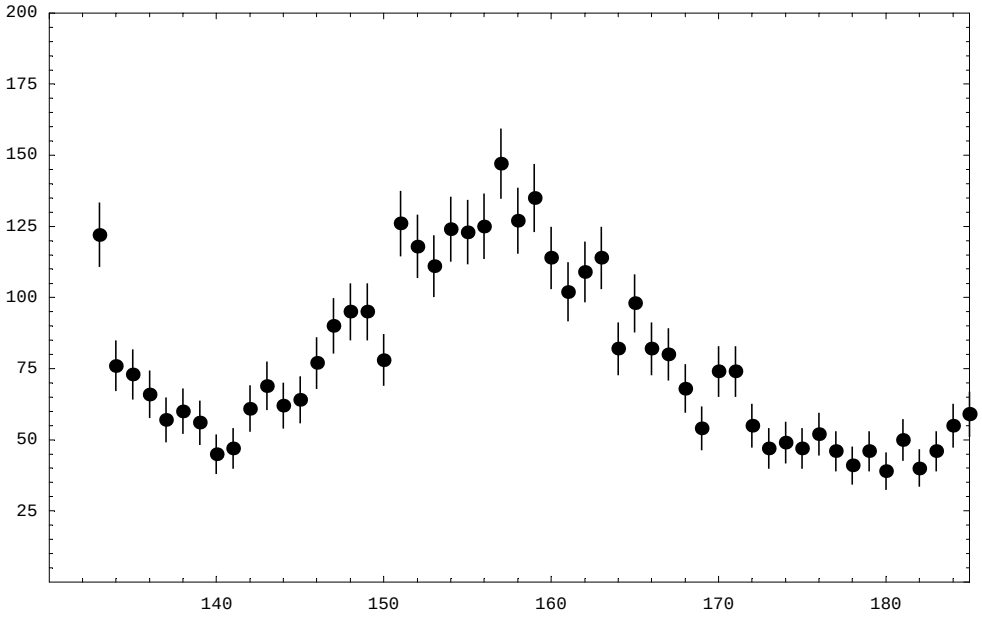


```
- Graphics -
```

Cut the data and make a data list of just the 1 p.e. peak

```
data[[23]]
data[[58]]
```

```
{140, 45}
```

```
{175, 47}
```

```
point1 = 23;
point2 = 58;
pepeak = Transpose[{Take[xaxis, {point1, point2}], Take[yaxis, {point1, point2}]}];
pepeakerr = Transpose[{Take[xaxis, {point1, point2}],
    Take[yaxis, {point1, point2}], Take[error, {point1, point2}]}];
errorg2 = Take[error, {point1, point2}];
```

plot the 1 p.e. peak

```
ErrorListPlot[pepeakerr, PlotRange → All, Axes → False, Frame → True]
```

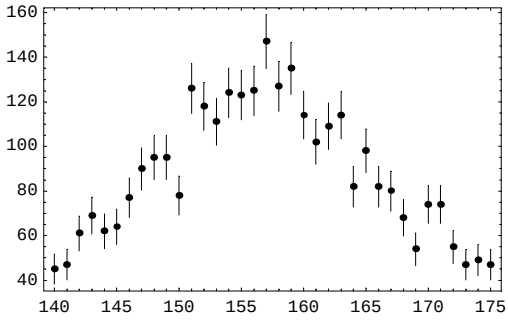


```
- Graphics -
```

Using the parameters from the centroid peak fit subtract the contribution of the centroid tail from the 1 p.e. peak
First calculate the propagation of error in gauss3,
then get the results from the centriod fit and set the appropriate parameter values

Calculate the error in gauss3

```
Δgauss3 =
 Simplify[Sqrt[(D[gauss3, A3] ΔA3)^2 + (D[gauss3, xc3] Δxc3)^2 + (D[gauss3, w3] Δw3)^2]]
```

$$\sqrt{\frac{2}{\pi}}\ \sqrt{\left(\frac{1}{w3^8}\left(e^{-\frac{4\,(x-xc3)^2}{w3^2}}\right.\right.$$
$$\left.\left.(w3^6\,\Delta A3^2 + A3^2\,w3^4\,\Delta w3^2 + 16\,A3^2\,(x-xc3)^4\,\Delta w3^2 - 8\,A3^2\,w3^2\,(x-xc3)^2\,(\Delta w3^2 - 2\,\Delta xc3^2))\right)\right)}$$

```
results3 = ParameterTable /. fit1g3
```

	Estimate	Asymp. SE	TStat	PValue
A3	193950.	2664.51	72.7902	0.
xc3	515.085	0.544315	946.299	$4.67089325690 \times 10^{-964}$
w3	266.744	2.60646	102.339	$4.98910437105 \times 10^{-385}$
offset	14.4968	3.73729	3.87897	0.000116363

```
A3 = results3[[1, 1, 1]];
ΔA3 = results3[[1, 1, 2]];
xc3 = results3[[1, 2, 1]];
Δxc3 = results3[[1, 2, 2]];
w3 = results3[[1, 3, 1]];
Δw3 = results3[[1, 3, 2]];
gauss3
Δgauss3
```

$$580.143\, e^{-0.0000281087\,(-515.085+x)^2}$$

$$1.57602 \times 10^{-10} \sqrt{\left(e^{-0.0000562174\,(-515.085+x)^2}\right.}$$
$$\left.(3.8512 \times 10^{21} - 1.32778 \times 10^{17}\,(-515.085+x)^2 + 4.08886 \times 10^{12}\,(-515.085+x)^4)\right)$$

This do loop subracts the contribution of the centroid peak from the 1 p.e. peak

```
pepeakcorr = {};
Do[{x = pepeak[[i, 1]],
  pepeakcorr = Append[pepeakcorr, {pepeak[[i, 1]], pepeak[[i, 2]] - gauss3}]},
 {i, 1, Length[pepeak]}]
pepeakcorr
```

```
{{140, 33.8805}, {141, 35.6439}, {142, 49.4029}, {143, 57.1574},
 {144, 49.9074}, {145, 51.6528}, {146, 64.3936}, {147, 77.1297},
 {148, 81.8609}, {149, 81.5874}, {150, 64.3089}, {151, 112.025},
 {152, 103.737}, {153, 96.443}, {154, 109.144}, {155, 107.84}, {156, 109.53},
 {157, 131.215}, {158, 110.895}, {159, 118.569}, {160, 97.2369},
 {161, 84.8994}, {162, 91.5561}, {163, 96.2069}, {164, 63.8517}, {165, 79.4904},
 {166, 63.1231}, {167, 60.7495}, {168, 48.3697}, {169, 33.9834}, {170, 53.5907},
 {171, 53.1915}, {172, 33.7857}, {173, 25.3732}, {174, 26.9538}, {175, 24.5277}}
```

This next do loop calculates the error delta gauss3 at each x-value for the 1 p.e. peak

```
ErrGauss3 = {};
Do[{x = pepeak[[i, 1]], ErrGauss3 = Append[ErrGauss3, {pepeak[[i, 1]], Δgauss3}]},
 {i, 1, Length[pepeak]}]
ErrGauss3
```

```
{{140, 0.776642}, {141, 0.788596}, {142, 0.800676}, {143, 0.812882},
 {144, 0.825214}, {145, 0.837672}, {146, 0.850255}, {147, 0.862965},
 {148, 0.8758}, {149, 0.888761}, {150, 0.901847}, {151, 0.915059},
 {152, 0.928396}, {153, 0.941858}, {154, 0.955445}, {155, 0.969156},
 {156, 0.982991}, {157, 0.99695}, {158, 1.01103}, {159, 1.02524}, {160, 1.03957},
 {161, 1.05402}, {162, 1.06859}, {163, 1.08328}, {164, 1.09809}, {165, 1.11302},
 {166, 1.12807}, {167, 1.14324}, {168, 1.15852}, {169, 1.17392}, {170, 1.18944},
 {171, 1.20507}, {172, 1.22082}, {173, 1.23667}, {174, 1.25264}, {175, 1.26872}}
```

Finally this third do loop combines the error in gauss3 with the error in the 1 p.e. peak data in quadrature.

```
Errpepeakcorr = {};
Do[Errpepeakcorr = Append[Errpepeakcorr, Sqrt[ErrGauss3[[i, 2]]^2 + errorg2[[i]]^2]],
 {i, 1, Length[pepeak]}]
Errpepeakcorr
```

```
{6.75301, 6.90086, 7.85118, 8.3463, 7.91713, 8.04374, 8.81606, 9.526, 9.78606,
 9.78723, 8.87769, 11.2622, 10.9024, 10.5777, 11.1764, 11.1328, 11.2235, 12.1653,
 11.3147, 11.6641, 10.7276, 10.1544, 10.4948, 10.7319, 9.12172, 9.96187, 9.12538,
 9.01704, 8.32719, 7.44165, 8.68417, 8.68632, 7.51601, 6.9663, 7.1112, 6.97206}
```

Combine these errors with the corrected 1 p.e. peak data

```
CorrectedPePeakData = {};
Do[CorrectedPePeakData = Append[CorrectedPePeakData,
   Append[pepeakcorr[[i]], Errpepeakcorr[[i]]]], {i, 1, Length[pepeak]}]
CorrectedPePeakData
```

```
{{140, 33.8805, 6.75301}, {141, 35.6439, 6.90086}, {142, 49.4029, 7.85118},
 {143, 57.1574, 8.3463}, {144, 49.9074, 7.91713}, {145, 51.6528, 8.04374},
 {146, 64.3936, 8.81606}, {147, 77.1297, 9.526}, {148, 81.8609, 9.78606},
 {149, 81.5874, 9.78723}, {150, 64.3089, 8.87769}, {151, 112.025, 11.2622},
 {152, 103.737, 10.9024}, {153, 96.443, 10.5777}, {154, 109.144, 11.1764},
 {155, 107.84, 11.1328}, {156, 109.53, 11.2235}, {157, 131.215, 12.1653},
 {158, 110.895, 11.3147}, {159, 118.569, 11.6641}, {160, 97.2369, 10.7276},
 {161, 84.8994, 10.1544}, {162, 91.5561, 10.4948}, {163, 96.2069, 10.7319},
 {164, 63.8517, 9.12172}, {165, 79.4904, 9.96187}, {166, 63.1231, 9.12538},
 {167, 60.7495, 9.01704}, {168, 48.3697, 8.32719}, {169, 33.9834, 7.44165},
 {170, 53.5907, 8.68417}, {171, 53.1915, 8.68632}, {172, 33.7857, 7.51601},
 {173, 25.3732, 6.9663}, {174, 26.9538, 7.1112}, {175, 24.5277, 6.97206}}
```

Now fit the corrected 1 p.e. peak data to a gaussian, again use the parameters from the first fit as initial estimates

```
x =.
model = gauss2 + offset
```

$$\text{offset} + \frac{\sqrt{A2^2}\; e^{-\frac{2\,(x-xc2)^2}{w2^2}}\sqrt{\frac{2}{\pi}}}{\sqrt{w2^2}}$$

```
results1 = ParameterTable /. fit1
```

	Estimate	Asymp. SE	TStat	PValue
A1	231977.	2893.47	80.1726	$9.99691521551\times10^{-437}$
xc1	126.085	0.0276137	4566.03	$4.21491317554\times10^{-2154}$
w1	4.27495	0.0303042	141.068	$1.42569713435\times10^{-660}$
A2	2481.27	388.367	6.38898	2.55951×10^{-10}
xc2	155.839	1.72472	90.3559	$3.40819867716\times10^{-482}$
w2	19.8669	3.4027	5.83858	7.11967×10^{-9}
193950.	202724.	2845.94	71.2329	$3.48635465561\times10^{-393}$
515.085	518.958	1.97329	262.992	$1.52940703843\times10^{-922}$
266.744	279.225	3.43056	81.3935	$2.12263933182\times10^{-442}$
offset	3.58998	0.948896	3.78333	0.000163973

```
EstA2 = results1[[1, 4, 1]];
Estxc2 = results1[[1, 5, 1]];
Estw2 = results1[[1, 6, 1]];
Estoff = results1[[1, 10, 1]];
```

```
fit1g2 = NonlinearRegress[pepeakcorr, model, x,
  {{A2, EstA2}, {xc2, Estxc2}, {w2, Estw2}, {offset, Estoff}},
  ShowProgress → True, Weights → 1 / Errpepeakcorr^2,
  RegressionReport → {BestFit, BestFitParameters, ParameterTable}]
```

```
Iteration:1 ChiSquared:41.40644300710722` Parameters:{2481.27, 155.839, 19.8669, 3.58998}

Iteration:2 ChiSquared:35.6843868124105` Parameters:{1738.97, 155.997, 16.3043, 22.5513}

Iteration:3 ChiSquared:34.19628328147043` Parameters:{1885.68, 156.036, 16.5708, 20.1344}

Iteration:4 ChiSquared:34.194849036803376` Parameters:{1889.15, 156.03, 16.5727, 20.055}
```

$$\{\text{BestFit} \to 20.0427 + 90.9606\, e^{-0.0072792\,(-156.03+x)^2},$$

$$\text{BestFitParameters} \to \{A2 \to 1889.67,\ xc2 \to 156.03,\ w2 \to 16.5758,\ \text{offset} \to 20.0427\},$$

$$\text{ParameterTable} \to$$

	Estimate	Asymp. SE	TStat	PValue
A2	1889.67	317.071	5.95978	1.21947×10^{-6}
xc2	156.03	0.322302	484.109	0.
w2	16.5758	1.74742	9.48586	8.1152×10^{-11}
offset	20.0427	7.65922	2.6168	0.0134378

$\}$

```
plot1g2 = DisplayTogether[ErrorListPlot[CorrectedPePeakData], Plot[BestFit /. fit1g2,
    {x, 140, 175}, PlotStyle → {RGBColor[1, 0, 0], Thickness[.002]}], PlotRange → All]
```

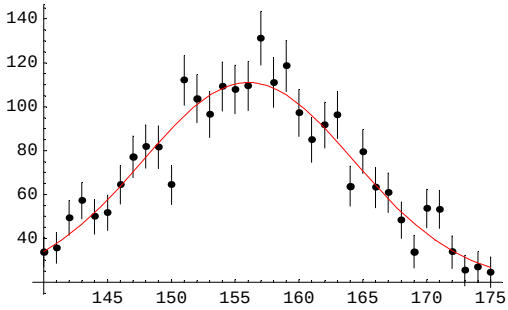


```
- Graphics -
```

Bibliography

[1] T. J. Bowles and R. G. Hamish Robertson. Tritium Beta Decay and the Search for Neutrino Mass. *Los Alamos Science*, 25:6, 1997.

[2] R. Slansky, S. Raby, T. Goldman, and G. Garvey. The Oscillating Neutrino: An introduction to neutrino masses and mixings. *Los Alamos Science*, 25:8, 1997.

[3] Internal documents.

[4] D. Griffiths. *Introduction to Elementary Particles.* John Wiley & Sons, Inc., USA, 1987.

[5] C. L. Cowan jr., F. Reines, F. B. Harrison, H. W. Kruse, and A. D. McGuire. Detection of the Free Neutrino: A Confirmation. *Science*, 124:103, 1956.

[6] KATRIN neutrino experiment.
`www-ik.fzk.de/ katrin/index.html` .

[7] B. Ryden. *Introduction to Cosmology.* Addison-Wesley Publishing Company, San Francisco, 2003.

[8] Project on government secrecy.
`www.fas.org/sgp/othergov/doe/lan/pubs/00326609.pdf` .

[9] Super-kamiokande at the university of california, irvine .
`www.ps.uci.edu/~superk/neutrino.html/`.

[10] Super-kamiokande collaboration. Super-Kamiokande Collaboration, Y. Fukuda et al., hep-ex/9803006.

[11] Presentation slide of evidence for oscillation of atmosphreric neutinos by erika prime.
`www.physics.ubc.ca/ waltham/p400/presentation/prime.pdf`.

[12] Super-kamiokande official home page.
`www-sk.icrr.u-tokyo.ac.jp/doc/sk/index1.html`.

[13] The Super-Kamiokande Collaboration. Evidence for Oscillation of Atmospheric Neutrinos. *Phys. Rev. Lett*, 81:1562, 1998.

[14] The SNO Collaboration. Measurement of Day and Night Neutrino Energy Spectra at SNO and Constraints on Neutrino Mixing Parameters,. *Phys. Rev. Lett*, 89(1):1301, 2002.

[15] QSA. Zinsser Analytic - Zinsser North America Inc. 19145 Parthenia Street Suite C Northridge, CA. 91324, USA, `www.zinsser-analytic.com/137.asp`.

[16] Private communication with Mareike Navin and Dr. Lee Thompson from Sheffield university.

[17] Adam D. Schneider. Neutrino detector r&d, January 2004. Work Term Report.

[18] G. L. Squires. *Practical Physics*. McGraw-Hill, Maidenhead, Berkshire, England, 1968.

[19] William R. Leo. *Techniques for Nuclear and Particle Physics Experiments*. Springer-Verlag, Berlin Heidelberg New York London Paris Tokyo, 1987.

[20] Joanna Duniewska. Reaction of Fungi of Trichoderma Genus To Selected Abioic Factors. *Electronic Journal of Polish Agricultural Universities, Agronomy*, 6:Issue 2, 2003. `www.ejpau.media.pl/series/volume6/issue2/agronomy/art-04.html`.

[21] Eljen-520. APACE Sicence, Inc. Mitomo-Bldg.#2-6F, 2-8, Ebisu-nishi 2-Chome, Shibuya-Ku, Tokyo 150-0021, `www.apace-science.com/eljen/ej-520.htm`.

[22] Patrick Bonnick. Liquid scintillator research for the 280 m near detector to be used in the t2k neutrino oscillation experiment, 2004. Work Term Report.

[23] T.R.Sandin A. Lewis Ford Hugh D. Young, Roger A. Freedman. *Sears and Zemansky's University Physics*. Addison Wesley Publishing Company, San Francisco, 1999.

[24] Jenna M. King. Progress and development of t2k's 280 m near detector, 2004. Work Term Report.

[25] Catalog of Kuraray Scintillation Material. Optical Products Company, Kuraray Nihonbashi Building, 1-6, 3-Chome, Nihonbashi, Chou-ku, Tokyo 102-8254 JAPAN, `www.kuraray-am.com/`.